Transformation of Tracking Error in Parallel Kinematic Machining

Vom Fachbereich Produktionstechnik

der

Universität Bremen

Zur Erlangung des Grades

Doktor- Ingenieur

genehmigte

Dissertation

von

M.Sc. Ghasem Amirian

Gutachter: Prof. Dr.-Ing. Bernd Kuhfuss

Prof. Dr.-Ing. Gert Goch

Tag der mündlichen Prüfung: 28. November 2008

Acknowledgements

I would like to express my deepest sense of gratitude to my advisor Prof. Dr.-Ing. Bernd Kuhfuss, for the patient guidance, valuable advices and moral support. In addition, I would like to thank him for his support during my Ph.D. studies.

I also wish to express my deep appreciation to Prof. Dr.-Ing. Gert Goch for serving on my dissertation and Prof. Dr.-Ing. habil. Reinhold Kienzler for serving on my candidacy exam and dissertation committee.

Especially, I would like to thank Dr.-Ing. Christian Schenck for introducing me to the new area of PKM. His ideas and inspirations have greatly helped the development of my dissertation.

I would also like to acknowledge my colleagues at the Machine Tools Institute in University of Bremen, especially, Mrs. Birgit Taeger, Dipl.-Ing. Sebastian Allers, Dipl.-Ing. Frank Lichthorn, Dipl.-Ing. Stephan Schädlich and Dipl.-Ing. Linghan Li.

I am indebted to my friend, Dr.-Ing. Mostafa Mehrafza, for the valuable discussions and help.

Special thanks are due to Mrs. Tatjana Evas for their warm friendship and help.

Thanks to Miss. Özlem Yilmaz for the support. I also wish to express my appreciation to Dipl.-Ing. Seyed Jafar Tavakkoli and M.Sc. Reza Malek Mohammadi Nourifar.

Finally, I can never thank enough for my parents for their love and encouragement. I always owe my wife, a lot for her support and understanding. She has always been a smart consultant of mine in my life and work. The words are too little to describe my thanks to my wife and dearest daughter, Alae, for their patience and endless support.

Contents

List of abbreviations

AFLC	Adaptive Fuzzy Logic Controller
CAD	Computrized Aided Design
CCC	Cross Coupling Controller
CNC	Computer Numerical Control
D	Dimension
DBB	Double Ball Bar
DOF	Degree Of Freedom
FK	Forward Kinematic
G.R	Gear Ratio
HSM	High Speed Machining
IK	Inverse Kinematic
IKF	Inverse Compensation Filter
LVDT	Linear Variable Displacement Transformer
MITF	Modified Inverse Transfer Function
NN	Neural Network
P	Proportional
PC	Personal Computer
PI	Proportional and Integration
PID	Proportional, Integration and Deviation
PKM	Parallel Kinematics Machining
PTP	Point To Point
SKM	Serial Kinematics Machining
TCP	Tool Center Point
ZPETC	Zero Phase Error Tracking Controller

List of symbols

A_i	mm	platforms displacement
B_i	mm	base plates displacement
C_x	-	cross coupling gain
C_y	-	cross coupling gain
c	mm	compensated contour error
D	-	coefficients of the denominator

E	-	geometric error matrix
e_{ss}	-	steady state error
f	Hz	frequency
G_a	-	actual transfer function
G_a^{-1}	-	inverse actual transfer function
G_c	-	servo controller transfer function
G_m	-	mechanical transfer function
i	-	index number
J	-	Jacobian matrix
J_e	kgm^2	motor shaft inertia
j	-	imaginary unit
K_1	$^{rad}/_{mm}$	transmission ratio
K_2	$^{mm}/_{rev}$	transmission ratio
K_c	-	cross coupled controller
K_m	$^{Nm}/_{A}$	motor constant
K_{nV}	-	feed forward control factor
K_p	$^{As}/_{rad}$	velocity loop proportional gain
K_{pi}	$^{V}/_{A}$	current regulator proportional gain
K_V	s^{-1}, $^{m/min}/_{mm}$	velocity gain in closed loop control in Cartesian coordinate
K_{Vx}	s^{-1}, $^{m/min}/_{mm}$	velocity gain of x axis in Cartesian coordinates
K_{Vy}	s^{-1}, $^{m/min}/_{mm}$	velocity gain of y axis in Cartesian coordinates
K_{V_X}	s^{-1}, $^{m/min}/_{mm}$	velocity gain in Cartesian coordinates
K_{V_U}	s^{-1}, $^{m/min}/_{mm}$	velocity gain in machine axes
$K_{V\ -\ rel}$	-	relative velocity gain
L	mm	length of strut
L_a	H	armature inductance
N	-	coefficients of the numerator
n	-	number of samples
p	$^{mm}/_{rev}$	pitch of ball screw
p_a	mm	actual position
p_{ax}	mm	x-component of p_a
p_{ay}	mm	y-component of p_a
p_s	mm	setpoint position
p'_s	mm	position on the setpoint contour, close to actual position

R_a	mm	actual radius
R_b	mm	radius of base plate
R_e	Ω	armature resistance
R_p	mm	radius of platform
R_s	mm	setpoint radius
R_{sx}	mm	x-component of R_s
R_{sy}	mm	y-component of R_s
r_x	mm	position feedback variable
T_d	s	derivative time
T_{En}	s	equivalent delay time
T_{Gn}	s	velocity setpoint delay time
T_i	s	integral time
T_m	Nm	motor torque
T_p	s	velocity loop integral action time
T_{pi}	s	current regulator integral action time
T_s	Nm	static disturbance torque
t	s	time
t_d	s	delay time
t_p	s	peak time
t_r	s	rise time
t_s	s	settling time
$\vec{U}_a$	mm	actual position vector on machine coordinate
$\vec{U}_s$	mm	setpoint position vector on machine coordinate
$\dot{\vec{U}}$	$^{mm}/_{s}$	velocity vector in machine coordinate
u(t)	-	unit step signal
$\vec{u}$	-	unit vector
v	$^{mm}/_{s}$	contour velocity
v_a	$^{mm}/_{s}$	actual velocity
v_x	$^{mm}/_{s}$	x-component of contour velocity
v_y	$^{mm}/_{s}$	y-component of contour velocity
w_{Vn}	-	feed forward control variable of velocity control loop
w_x	-	commond variable of position control loop
$\vec{X}_a$	mm	actual position vector on Cartesian coordinate
$\vec{X}s$	mm	setpoint position vector on Cartesian coordinate

$\dot{\vec{X}}$	$^{mm}/_{s}$	velocity vector on Cartesian coordinate
$x_a(t)$	mm	actual signal
$x_{a\text{-}tr}(t)$	mm	transient response
$x_{a\text{-}ss}(t)$	mm	steady state response
Δt	s	delay time
$_{\Delta}\vec{U}$	mm	tracking error vector on machine coordinate
$_{\Delta}\vec{X}$	mm	tracking error vector on Cartesian coordinate
Δx	mm	tracking errors in x-direction
Δy	mm	tracking errors in y-direction
α	°	angle of circular trajectory
β	°	angle of strut
θ	°	angle of star contour
γ	°	angle deviation
δR	mm	radial error
ε	mm	contour error

Transformation der Schleppfehler in Parallelkinematischen Maschinen

Zusammenfassung

Parallelkinematische Systeme werden unter anderen als numerisch gesteuerte Werkzeugmaschinen eingesetzt. Die Bewegungseigenschaften der konventionellen Werkzeugmaschinen wie Geschwindigkeit und Beschleunigung der einzelnen Antriebe werden direkt auf den Wirkpunkt übertragen. Bei Parallelkinematiken werden im Allgemeinen Bewegungen der Achsen durch eine nichtlineare Transformationsfunktion beschrieben.

Ziel dieser Arbeit ist die Untersuchung der Übertragung dynamischer Eigenschaften der parallelkinematischen Werkzeugmaschinen von Maschinen- in Werkstückkoordinaten. Die Transformation der Schleppfehler und der Geschwindigkeitsverstärkung von den Antriebskoordinaten zu den Werkstückkoordinaten im Arbeitsraum wird zunächst an einem einachsigen Modell (Monopod) untersucht. Dabei ist das Verhalten der Parallelkinematiken examplarisch auf ein Bewegungssystem mit einem Freiheitsgrad reduziert.

Der Prüfstand (Monopod) wird basierend auf der Methode der Neuronalen Netze kalibriert. Parallel zu den Messungen wird das Regelverhalten simuliert. Um die Untersuchung der reinen Schleppfehler-Effekte zu vereinfachen, werden mechanische Effekte wie Trägheit, Reibung und Elastizität vernachlässigt. Die Untersuchungen zeigen eine relative Geschwindigkeitsverstärkung zwischen der Antriebsachse und dem Wirkpunkt.

Die Betrachtungen werden dann auf Parallelkinematiken mit mehreren Achsen (Bipod und Tripod) erweitert und der Einfluss der Schleppfehlerübertragung auf die Bahngenauigkeit untersucht. Bei der Simulation werden ausschließlich Modelle mit konstanten Streben eingesetzt. Ein Algorithmus zur Berechnung des Bahnfehlers auf Basis der Jakobi Matrix und der Schleppfehler in den Antrieben wird vorgestellt und mit einem Tripod verifiziert. Die experimentellen Ergebnisse stammen sowohl von Stern-Tests, die aus Bewegungen entlang gerader Linien mit unterschiedlichen Orientierungen bestehen, als auch von Kreisformtests.

Eine genaue Bahnregelung ist eine fundamentale Anforderung an eine numerisch gesteuerte Maschine. Zur Reduzierung der Bahnfehler wird eine Methode zur Kompensierung der Fehler vorgestellt, die eine Soll-Bahn in Gegenrichtung zu auftretenden Bahnfehlern mit gleicher Fehlergröße definiert. Die reale Transformationsfunktion die, das Übertragungsverhalten der Regler und der Regelstrecke beschreibt, kann mit der Methode der Neuronalen Netze ermittelt werden.

Transformation of Tracking Error in Parallel Kinematic Machining

Abstract

One emerging application of Parallel Kinematic Mechanisms (PKM) is in the computerized numerical control (CNC) machine tools and, recently, several prototypes of such CNC machines have been developed.

In Cartesian machine tools, motion properties like velocity and acceleration of the individual drives are directly transferred to the tool center point (TCP). With PKM, the axes motions are transformed by nonlinear transfer functions as a general rule. The goal of the present study is to study the transformation of dynamic properties in PKM based machine tools.

Transformation of tracking error and velocity gain from machine coordinates to Cartesian coordinates in workspace is, initially, investigated by a one axis mechanism (Monopod). In this study, the PKM behavior is simplified to a single degree of freedom (DOF) motion system with a nonlinear transformation of dynamic properties like position and velocity. The test bench of Monopod is calibrated by a neural network (NN) method and the model is simulated in the Matlab/Simulink environment. The results of transformation illustrate the relative velocity gain between TCP and drive axis, and are developed to multi axis PKM such as Bipod and Tripod. The effect on trace accuracy is discussed in light of these mechanisms. In the simulation phase, models are performed with constant length of strut, and the mechanical effects like inertia, flexibility, friction and backlash are neglected. This ensures to study uncoupled closed loop controller effects.

A contour error algorithm is developed and verified by the Bipod and the Tripod to predict the contour error of a generalized machine tool by the Jacobian matrix and estimated tracking errors in the drives.

The experimental results are obtained using a method for star contouring test that consists of straight lines in the workspace with varying orientations and the double ball bar in circular trajectory.

An accurate trajectory control is a fundamental requirement for CNC machine tools. To eliminate the contour error, a compensated path method is introduced that generates a setpoint path, with a programmed deviation equal in amount but negative in direction to the calculated contour error. The real transfer function can be identified by the NN approach.

1 Introduction

Increasing demands on manufacturing processes for higher productivity and improved accuracy have motivated the development of high speed machining (HSM). High speed and high accuracy machining is required for short lead times, high productivity, and complicated workpieces. With this background, the development of parallel kinematic machines to increase dynamic parameters can be seen. The PKM has the conceptual high potential for high speed machining because of the closed loop structure, and its lightweight and no error accumulation characteristics [CHE06].

In general, there are three types of control systems in CNC machine tools; positioning control systems, which make the CNC machine tools move from point to point (PTP), line and contouring control systems, which make the CNC machine tools move in direction of a machine axis or along a continuous contour [RAM05]. Most CNC machine controllers are organized in a cascade structure, comprising the position, velocity and current loops. PID types of servo controllers generate tracking errors in each axis. Tracking errors are a significant factor on machining accuracy, besides geometric machine errors, vibrations, tool errors and temperature changes, due to the proportional position control loop [WEC 90]. It involves a divergence of the target and actual profile and causes contour error. In general, contour error sources in machining processes may be listed into three categories: mechanical hardware deficiencies, cutting process effects and controller and drive dynamics. The first and second sets of error sources can only be reduced by improving the mechanical hardware or utilizing compensation techniques. The third set of error sources can be eliminated or reduced by improving servo controllers and dynamics.

In Cartesian machine interpolation, the velocities of the drives are translated directly to TCP, being the resultant of the two perpendicular velocity components. Drive velocities in PKM, however, are not orthogonal and are different in comparison with a Cartesian machine.

The kinematics of a PKM can be described by the Jacobian matrix that is the relation between partial deviations of a position vector in Cartesian coordinates with respect to joint coordinates.

The development of machine tools based on PKM leads to new challenges in the control system in comparison to serial kinematic machines (SKM). The transformation behavior becomes important in independently controlled drives due to the parallel setup [AST06]. This transformation causes differences of the dynamic characteristics in joint space and workspace with unexpected consequences leading to the contour error.

The research work being discussed in the thesis applies a new subject of CNC machine tools based on PKM. This thesis addresses the tracking problem for the feed drives of parallel kinematic machines.

2 State of the art

2.1 Parallel Kinematic Machines

2.1.1 Introduction

"A general development trend of machine tools aims at the reduction of primary processing times by increased cutting speeds and at reduction of secondary processing times by enhanced rapid feeds and accelerations. With respect to an increase of dynamic parameters the development of parallel kinematic and hybrid kinematic machines has to be seen [KUH04-1]." Here, the advantages and limitations of PKM versus traditional machining centres are discussed.

2.1.2 High Speed Machining

The diversity of available definitions of high speed machining points to the various critical considerations relevant to the process of transition from conventional to the HSM. The benefits of HSM have been confirmed in variety of manufacturing aspects. The major advantage of HSM is the increased material removal rate. Moreover, the application of a HSM leads to the increased quality of the machined parts and thus, changes not only the machine design but also and most importantly the substance and quality of the manufacturing process. The success of HSM is conditioned by the significant developments in relevant techniques and elements such as machine tools, spindles, feed drives, modeling and control techniques, tools as well as CNC technologies [STE02, WAN04, WEC03].

The adoptation of machine tools from conventional machining to HSM requires re-consideration of the static and dynamic behavior of the machine tool structure. To minimize structural deformation, the static and dynamic stiffness has to be sufficiently high. Furthermore, the lightweight of moving structures and, consequently, their low inertia allows high feed rates and accelerations.

A number of scientific studies have analyzed the application of modern machine tool structures to HSM. Traditional machine tools have a serial kinematic structure. Each axis has to be built on top of another axis or base. Thus, each axis has to carry the axes on top of it, including their actuators, guideways and joints. This structure results in higher inertia load at the lower axis that is not suitable for the HSM application. The classical structure may result in decreased machine rigidity and worse positioning accuracy as well as additional demands

on design for particular axes. The suggested solution for an application of modern machine tools to HSM is the machine tools with parallel kinematics structure [MAR06, WAN04].

2.1.3 Parallel mechanisms

There are two categories of mechanisms: serial and parallel. Serial mechanisms are open chain mechanisms made up of consecutive links connected by revolute or translate joints connected from a base to an end effector [CAM06, KRA04]. A parallel mechanism is composed of two or more closed loop kinematic chains in which the end effector (mobile platform) is connected to the base platform by at least two independent kinematics chains [WEC02]. In PKM, the moving mass is connected to the base through several kinematics chains or legs that are mounted in parallel. It has been convincingly argued that compared to the serial machine a parallel kinematic machine tool for HSM is stiffer, has lower moving mass and allows higher acceleration [EST06, NEU06, WAN04]. The PKM machine tools use actuators to produce multi axis motion at the table (or spindle) of the machine. The application of PKMs has a potential to develop the manufacturing methods used in the production of aircraft and aerospace components of complex geometry. Most current research on PKMs has focused on fully parallel mechanisms and its variants [HEI06]. A base platform is a link fixed to the ground and connected to the limbs and an end effector platform is a link connected to the limbs.

Despite the wide range of PKM that have been developed, they can be divided into two main groups: machines with constant length struts and machines with variable length telescopic struts, [CHE04, PRI00] as provided in Figure 2-1 below.

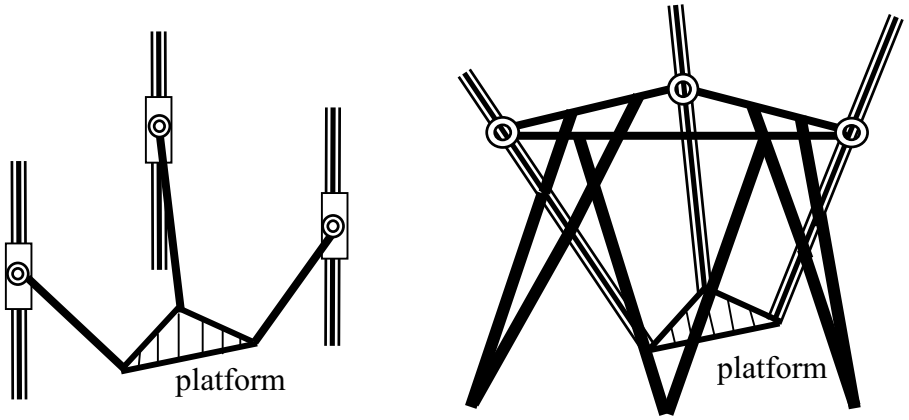

a: fixed length struts b: variable length struts

Figure 2-1: Parallel kinematic machining [CHE04]

In contrast to PKM with telescopic drives, in fixed length struts the strut base point is movable. The choice between fixed length and variable length struts determines the behaviour of the machine. In machines with variable length struts, actuators have to be mounted on the struts to increase moved masses. The telescopic variable length struts compared to the fixed struts have advantages in terms of better machine size, driving stroke and Cartesian velocity. However, fixed struts considered to be more advantageous in terms of the static stiffness and first natural frequency [CHE04].

Limitation of PKMs

The previous section of this chapter has summarized the main characteristics and advantages of the PKM. However, PKM also possess some inherent limitations and disadvantages discussed in this section. The defining characteristics of PKM are low moving mass, simple frame design and use of repetition parts [BRE06-1, SAE02]. This characteristics contribute to the disadvantages of PKM that include limited dexterity, high susceptibility to thermal load, low workspace size, more singular configurations than serial mechanisms and complex kinematic and dynamic characteristics that make their control difficult [BRU02, COL04, GRE04, GRO02, SAE02, VAL02, WEC02]. Furthermore, kinematic models complexity of PKM as compared to the serial kinematic machines (SKM) makes calibration of PKMs complicated [COB02, KRA04].

Here, we have discussed three main groups of characteristics and conditions that contribute to the major disadvantages of the PKM [DON04]. First, variable kinematics and dynamics. In parallel kinematic mechanisms, the Jacobian matrix changes across Cartesian coordinates. This variation gives rise to nonlinear behavior across the workspace producing variations in resolution, accuracy and stiffness across the workspace of the machine [COB02]. This varying stiffness may cause highly changing dynamic and actuator loads across the workspace of the HSM and, thus, making it difficult to achieve high contouring performance [PRI00].

Second, difficult forward kinematics and dynamic problems. The forward kinematics problem of a fully parallel mechanism makes it impossible to close the control loop around the kinematics of the machine. This limitation, coupled with the previously discussed nonlinear kinematics of PKMs, makes high contouring performance very difficult to achieve [GRE04, WEC02]. Further, because the forward dynamics problem embeds the forward kinematics problem, control strategies that involve computing forces and torque and applications, involving force feedback, also become extremely difficult to implement.

Third**,** small usable workspaces and long structural members. Singularities reduce the usable workspace of PKM systems. This leads to a poor workspace volume to machine volume ratios [WEC02, PRI00]. More importantly, it leads to long flexural members compared to the dimensions of workspace. This results in larger moving masses and lower structural rigidity of individual members. These again contribute negatively on the performance of machining with HSM [DON04, SAE02].

Design requirements of PKM for HSM

Therefore, building on the main characteristics, advantages and disadvantages of PKM as discussed above, a development of a PKM applicable for HSM requires consideration of mechanical structure, kinematic topology and controller behavior [DON04].

A part of mechanical structure of PKM and its important design consideration is minimal mass of moving parts [BRU02, EST06]. In HSM, especially along nonlinear trajectories, a very large fraction of the load on the drive system is inertial. Additionally, to achieve the desired speeds of HSM, direct drives are often required. Therefore, relatively large loads with high frequency content are transmitted through the structural components of the machine. Thus, the application of PKM for HSM requires the small structural loop between the drives and the TCP.

The second element that is necessary to address in developing PKM for HSM is kinematic topology. The nonlinear effects are difficult to deal with in the context of high speeds and high accuracies expected from HSM. At the same time, nonlinear effects not only cause stability problemes, but also require additional computations that slow the servo cycle rate.

The kinematic conditioning relates the magnitude of the joint space displacement vector to that of the workspace. The variations in this mechanical characteristics will produce variable performance across the workspace [BRE06-1, DON04].

The third element is the controller behavior. For these above reasons, for high accuracies the control loop should receive feedback from the displacements of the TCP in direct measurement system, rather than those of the joints [FLE06-2, MUN06]. The matching of the dynamic characteristics of each workspace axes becomes important to decrease contouring errors.

2.1.4 Hybrid mechanisms

A hybrid mechanism is a combination of open loop and closed loop kinematic chains. Thus, hybrid kinematic machines are a combination of a parallel kinematic structure with additional serial mechanisms [CAM06, HEI04].

One recent study [GRE04] compared the applications of parallel mechanisms and hybrid mechanisms in machine tools, material handling and assembly machines. The sduty shows the industrial acceptance of the trade off between the serial and parallel mechanisms. It is interesting to note that parallel mechanisms are mostly used in machine tool applications in 1998 and hybrid mechanisms are developed for these applications in 2002.

Machining of three dimensional curves impose high demands on the machine kinematics and design with respect to accuracy, acceleration and workspace size. PKM meet the first two requirements, but are limited regarding workspace size and tilting abilities. HKM, through combination of serial and parallel machine axes and integration of machining capabilities into one machine structure, is able to eliminate this disadvantage [BRE06-1, FLE06-1, HES02, MAR06]. However, “underlaid serial links with long tracking can carry a PKM and thus spread the local advantages over a wide range [KUH07]”.

2.2 Servo Motion Control

2.2.1 Introduction

Generally the CNC machine tools are divided into two main parts: the mechanical parts with servo drive systems and the servo controllers that control the multi axis motion of mechanical parts [YEU06]. The machining of a workpiece using a machine tool to create a desired shape requires that the tool and workpiece move in relation to each other. In order to accomplish this, the individual feed drives must be adjustable in their position. Predominantly, the position controls with velocity controlled electrical drives are used to adjust the position of feed drives. Based on the location where, in the machine tool, the data is measured, the direct and indirect position measurements are distinguished [GRO01]. This section addresses to servo motion control elements.

2.2.2 Step and impulse response of a system

Commonly, to test the input signals, step functions, impulse functions and the likes are used. The signals are functions of time, thus, analyses of the control systems with these test signals can be carried out. The time domain response of a control system consists of transient and

steady state response. The transient response goes from the initial to final state. The steady state response shows the manner in which the system output behaves as t approaches infinity [OGA02], Figure 2-2.

Thus the system response $x_a(t)$ may be written as

$$x_a(t) = x_{a\text{-}tr}(t) + x_{a\text{-}ss}(t) \tag{2-1}$$

Where the first term on the right side of the equation is the transient response and the second term is the steady state response [OGA02].

A unit step signal is defined as

$$u(t) = \begin{pmatrix} 0 & t < 0 \\ 1 & t \geq 0 \end{pmatrix} \tag{2-2}$$

If the setpoint value is a scalar A, then the signal can be written as Au(t). The response $x_a(t)$ to the unit step signal u(t) is called the step response of the system. Figure 2-2 shows a typical step response.

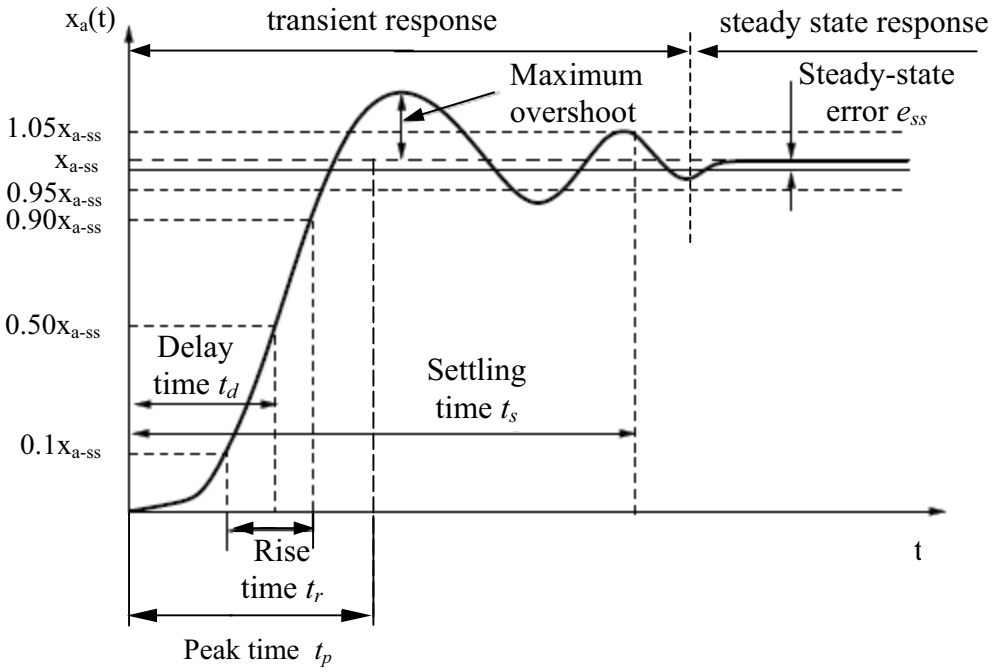

Figure 2-2: Typical step response of a control system [OGA02]

There are several interesting characteristics of a system that can be derived from its step response, namely, steady state error e_{ss}, maximum overshoot, delay time t_d, rise time t_r, settling time t_s and peak time t_p.

For the unit impulse input, the output of the first order system is shown in Figure 2-3-a. t_d is the delay time or time constant. As t approaches infinity, e^{-t/t_d} approaches zero and the response approaches zero [OGA02].

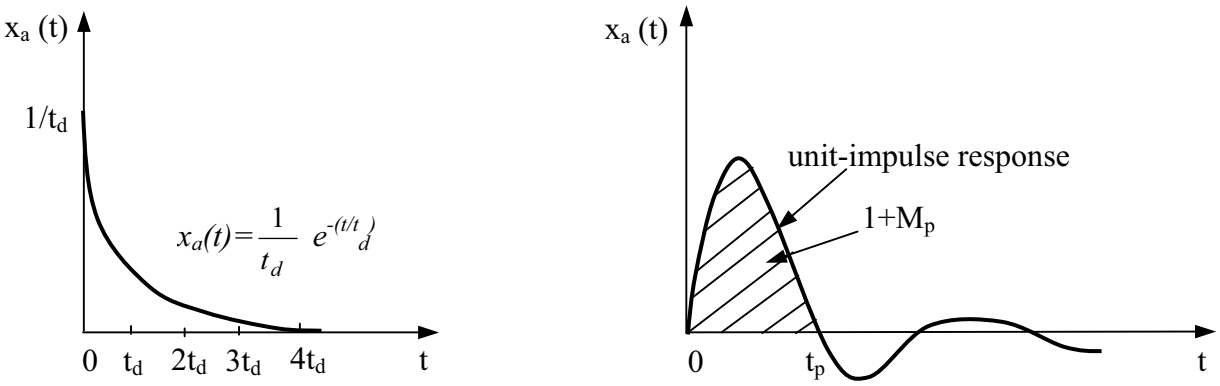

a: The first order system b:Second order system

Figure 2-3: Unit impulse response [OGA02]

The unit impulse response of the second order system oscillates about zero and takes both positive and negative values. Since the unit impulse response function is the time derivative of the unit step response function, the maximum overshoot M_p for the unit step response can be found from the corresponding unit impulse response. This is the area under the unit impulse response curve from t=0 to t_p, as shown in Figure 2-3-b, is which equal to $1+M_p$, where M_p is the maximum overshoot for the unit step response. The peak time t_p for the unit step response corresponds to the time where the unit impulse response first crosses the time axis [OGA02].

2.2.3 PID control algorithm

PID type controllers are widely used in industry because of their simplicity and successful industrial applications. Basically, according to Figure 2-4, a PID controller generates actual signal $x_a(t)$ according to the tracking error signal $\Delta x(t)$.

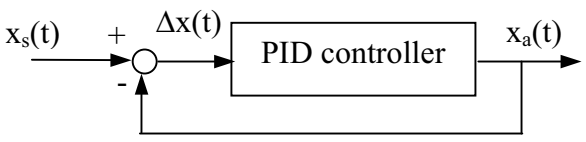

Figure 2-4: A schematic of PID control system

It consists of the proportional part generates a control action, which is proportional to the error signal, the integral part on the integral of the error signals, and the derivative part on the changing rate of the error signal.

Table 2-1: PID control algorithm

response type	element	differential equation	transfer function	
proportional	P-element	$x_a(t)=K_p \cdot \Delta x(t)$	$\frac{X_a(s)}{\Delta X(s)} = K_p$	K_p: proportional gain
integral	I-element	$x_a(t) = \frac{1}{T_i}\int_0^t \Delta x(t)dt$	$\frac{X_a(s)}{\Delta X(s)} = \frac{1}{T_i s}$	T_i: integral time
derivative	D-element	$x_a(t) = T_d \frac{d\Delta x(t)}{dt}$	$\frac{X_a(s)}{\Delta X(s)} = T_d s$	T_d: derivative time

For a controller with proportional control action, the relationships between the output of the controller $x_a(t)$ and the actuating error signal $\Delta x(t)$ and the Laplace transformed quantities are listed in Table 2-1.

The proportional controller is essentially an amplifier with an adjustable gain. Each controller manufacturer uses different implementations of the PID control algorithm [WAN04]. The most common implementations are:

• Ideal algorithm

$$x_a(t) = K_p [\, \Delta x(t) + 1/ T_i \int \Delta x(t)\, dt + T_d \, d\Delta x(t) / dt] \quad (2\text{-}3)$$

• Parallel algorithm

$$x_a(t) = K_p \, \Delta x(t) + 1 / T_i \int \Delta x(t)\, dt + T_d \, d\Delta x(t) / dt \quad (2\text{-}4)$$

• Serial algorithm

$$x_a(t) = K_p [\Delta x(t) + 1/ T_i \int \Delta x(t)\, dt\,][1 + T_d \, d\Delta x(t) / dt] \quad (2\text{-}5)$$

Currently, most of the PID controllers are implemented digitally and based on the ideal algorithm.

Increasing K_p increases the bandwidth (faster response) of the closed loop system, and reduces the steady state error. However, the steady state error cannot be reduced to zero, and with high proportional gain K_p, the closed loop system tends to be unstable. In order to reach a minimal steady state error, an integral term must be included [WAN04].

2.2.4 Cascade tracking controller structure

The cascade controller structures are used in most of the servo motion control systems instead of a single control loop. A simplified cascade controller structure for motion control is illustrated in Figure 2-5. The cascade controller structure consists of several control loops including the innermost current torque control loop that is enclosed by a velocity control loop, which is further enclosed by the position control loop.

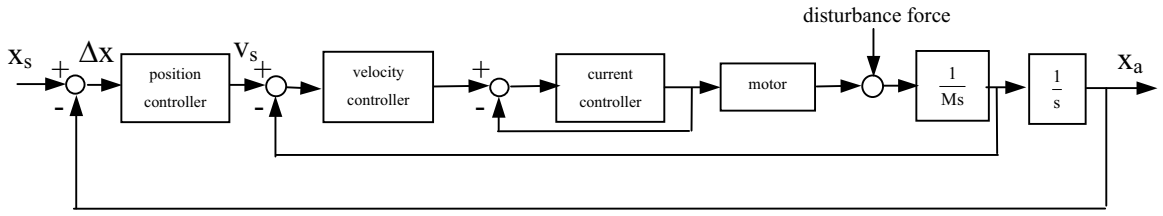

Figure 2-5: Cascade control structure [WAN04]

With a cascade control structure, there may be more tuning parameters than that with a single loop control structure. However, to ensure a safe start up of the entire system, the cascade control structure is usually tuned step by step starting from the innermost loop to the outermost loop. The effects of nonlinearity and disturbance input in the inner loop are dealt with in the inner loop. In this way, the nonlinearity and disturbance can be eliminated with less influence to the outer loop. Cascade controller structure requires that the bandwidth of each loop increases from an outer loop to an inner loop so that the dynamic delay caused in the inner loop could be ignored by the outer loop. As in the case of cascade motion control structure, the current control loop usually has the highest bandwidth, and the position control loop has the lowest bandwidth. Velocity feed forward and acceleration feed forward are commonly applied [ERK01-2].

The first inner element of the cascade structure is a current loop. The current control loop for the servo motion control system is some times also referred as the torque control loop [WAN04]. This reference is based on the fact that the current in the windings of the motors is usually proportional to the generated torque. Based on the torque generation characteristics of the motor it is then possible to build a torque control loop in cooperation with the current control loop. The current loop is usually realized with an ideal algorithm of PID controller [ERK06-2].

The second element of the cascade structure, velocity control loop, is built up on the top of the current loop. The friction force is nonlinear in nature and can be related to the velocity and position. The disturbance in velocity loop will cause error in the output velocity. The velocity

loop is usually designed as a PID controller in order to eliminate the steady state velocity error. The performance of the velocity loop is very important for the motion control system, because almost all the disturbance force of the system enters in this loop. A good velocity feedback signal, which contains less noise and phase error, is critical to increase the velocity control loop gain [ERK01-2, WAN04,YEU06].

Because there is an integrator in the position loop, it is sufficient to use a proportional controller for the position control loop. The integration of the velocity signal gives the position signal. This integrator in the position loop will reduce the steady state position error of a step response. Position controllers in closed loop servo systems define the machining accuracy. The proportional response of the controlling device is indicated by the proportional coefficient of the controller [ERK06-2, WEC01]. This value, the velocity gain K_V, also called the K_V factor, is calculated as the ratio between the setpoint velocity v_s and the position control deviation Δx:

$$K_V = v_s / \Delta x \tag{2-6}$$

For a straight line motion with constant velocity the position control deviation, that named tracking error is based on this correlation [GRO01]:

$$\Delta x = v_s / K_V \tag{2-7}$$

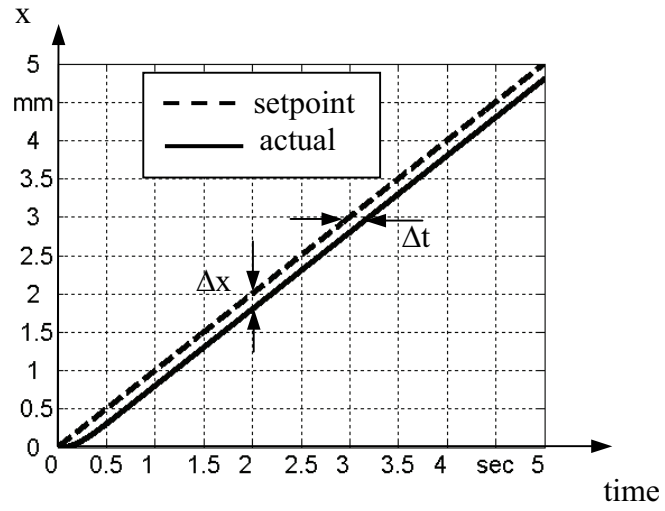

Figure 2-6: Tracking error in straight line path

The tracking error indicates how much the actual position value lags behind the position setpoint value, Figure 2-6. Tracking error is defined as the difference between setpoint position and actual position.

Requirement of the optimum position control loop is that the programmed position must be followed with minimum time delay and minimum tracking error during the motion [SCH99].

The most popular algorithm to control PKMs is a linear PID controller at joint space, and inverse kinematics algorithm on top of the control loop, Figure 2-7.

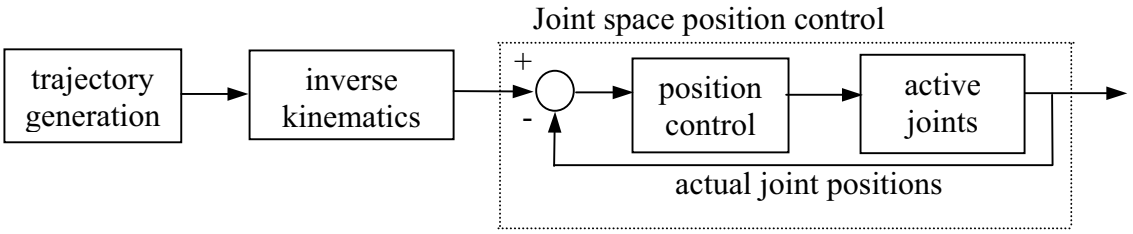

Figure 2-7: Basic control scheme for PKM

In [KRÜ00, BLE03] velocity gain in PKM are presented as following formula. Allow $\dot{\vec{U}}$ to be the velocity vector in machine coordinate and $\dot{\vec{X}}$ to be the velocity vector in Cartesian coordinate. $\overrightarrow{\Delta U}$ denotes the tracking error vector on the joint space, $\overrightarrow{\Delta X}$ denotes the tracking error vector on the platform and J presents the Jacobian matrix. $K_{V\text{-}U}$ and $K_{V\text{-}X}$ are velocity gain factor in closed loop control system and virtually in Cartesian coordinates respectively.

$$\dot{\vec{U}} = J . \dot{\vec{X}} \tag{2-8}$$

$$\overrightarrow{\Delta U} = \frac{\dot{\vec{U}}}{K_{V\text{-}U}} \tag{2-9}$$

$$J^{1} . \overrightarrow{\Delta U} = J^{1} \frac{\dot{\vec{U}}}{K_{V\text{-}U}} \quad \text{and} \quad \overrightarrow{\Delta X} = J^{1} . \overrightarrow{\Delta U} \tag{2-10}$$

$$\overrightarrow{\Delta X} = \frac{J^{-1} . J . \dot{\vec{X}}}{K_{V\text{-}U}} = \frac{\dot{\vec{X}}}{K_{V\text{-}X}} \quad \Rightarrow \quad K_{V\text{-}U} = K_{V\text{-}X} \tag{2-11}$$

In consequence of these formula the velocity gain factors in the TCP and in the drives are proved to be equal not only in conventional serial kinematic machine, but also in parallel kinematic machine. The estimation and linearization are valid in low value of tracking error which occurs in low velocity and not in high feed rate and high precision machining, because in high speed machining, tracking error is higher. Here the global linearization of the transfer function is too rough for a precise control and high velocity machining.

2.2.5 Contour error model originated from servo tracking errors in SKM

The contour errors are defined as the deviations of the cutting tool of a CNC machine tool from the programmed contour during the machining process [RAM00].

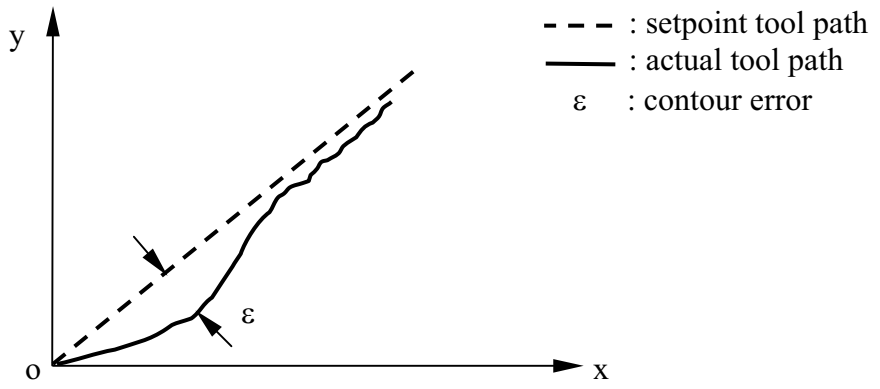

Figure 2-8: contour errors of biaxial system for linear trajectory [XIU98]

They are measured as the distances between the cutting points and the setpoint trajectory in the normal direction of the setpoint trajectory. Those contour errors contribute on the finished parts to the parts geometry inaccuracy. Figure 2-8 shows the principle of contour error for a straight line for a biaxial system during a machining process.

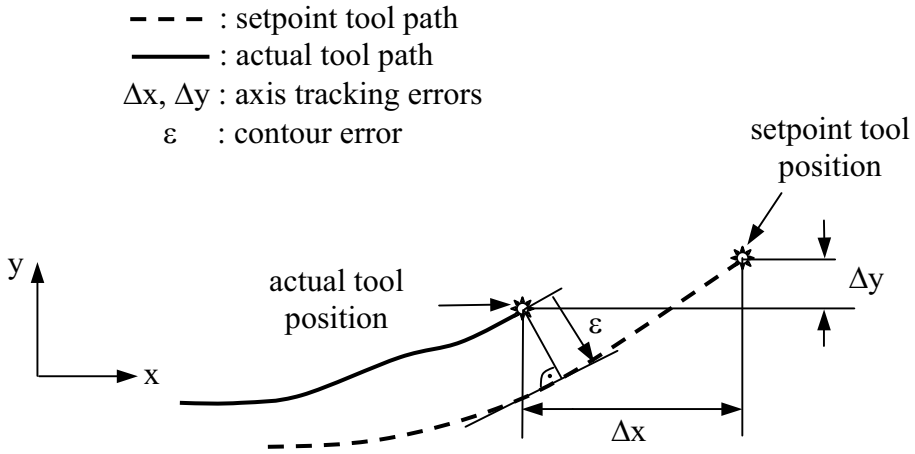

Figure 2-9: Contour error originating from servo tracking errors [ERK06-1]

There are multiple error sources including geometric, static and dynamic loading, thermal deviations and mismatches between servo loop gains [MER06, PRI02, WEI04]. All these origins affect positioning accuracy at the tool tip in a complex way.

Figure 2-9 shows contour errors originating from servo tracking errors in the individual axes, which become prevalent when tracking reference trajectories.

In the following, the contour errors originating from servo tracking errors are modeled to give an entire description of the accuracy of conventional serial machine tools.

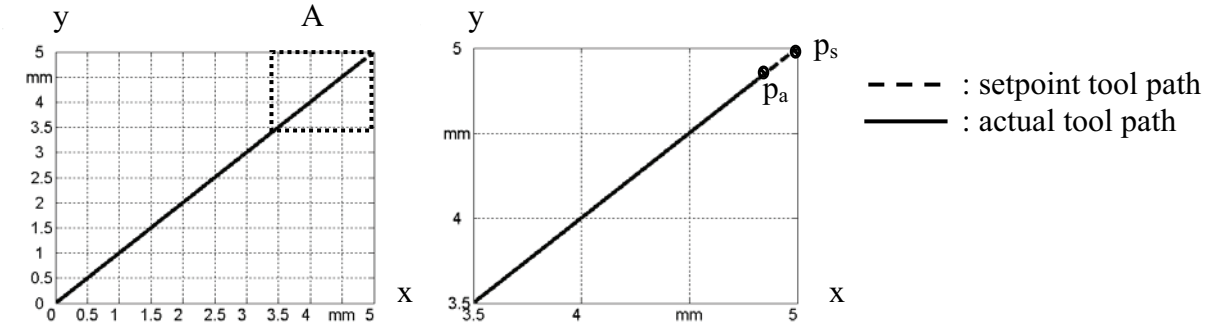

a: y-axis over x-axis b: zoom of view A

Figure 2-10: Linear trajectory in biaxial SKM system, $K_{Vx}=K_{Vy}$ a) y-axis over x-axis b) zoom of view A

In straight line motions the tracking error does not cause contouring errors, Figure 2-10, when the velocity gains in all position control loops generating the contouring path are identical [GRO01].

Allow in the Figure, setpoint and actual point on the paths are p_s and p_a. Although the contour error is zero the actual path occurs later than the setpoint path due to delay time in the system. Normally for straight line motions the pose deviation caused by tracking errors of the axes should follow delayed but exactly on the linear path for a constant pose velocity and equal dynamics characteristics.

The machining of a circular contour as well as any other curve path in space involves at least two linear feed axes. The position of linear feed axes setpoints is computed by the interpolator of the CNC. The computing is conducted according to the selected type of interpolation and applied to the feed drives.

As illustrated in Figure 2-11, the circular interpolation at a constant feed rate by two linear axes in SKM requires the injection of a sinusoidal signal on each axis. A radial error, δR and delay time Δt and the effect of transient response in start and stop points are indicated in the Figure 2-11. In a circular test path the contouring error is easy to measure by the radial deviation.

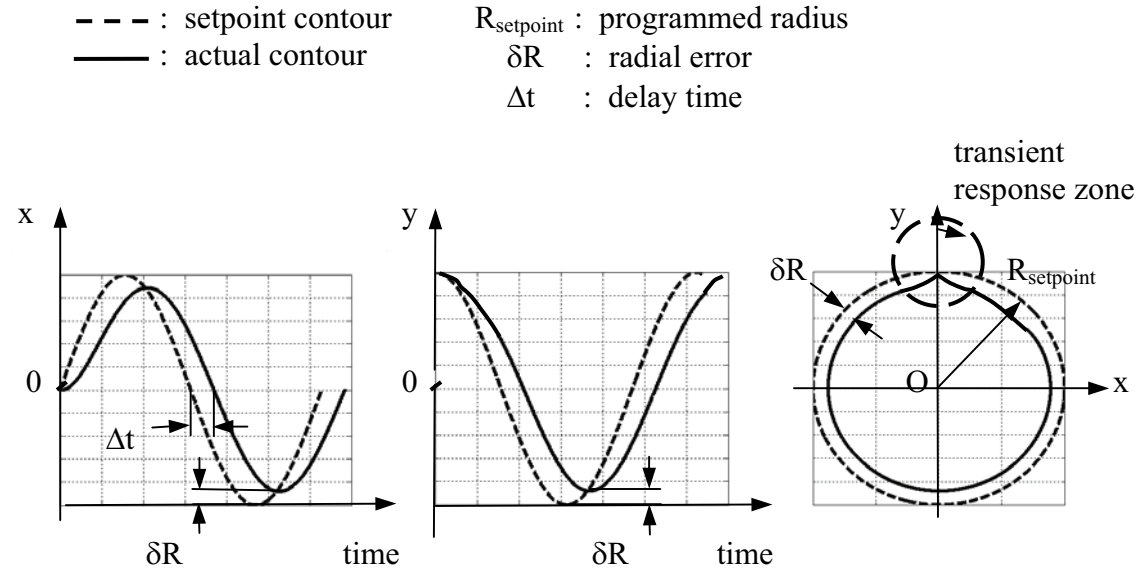

a: path in x- direction b: path in y- direction c: circular trajectory

Figure 2-11: 2-D circular trajectory in SKM [WEC01]

Formula (2-12) gives the radial error in circular trajectory in a 2-D Cartesian machine. Radial error δR is dominated by a term proportional to the square of feedrate v, inversely proportional to the programmed radius of circle, R_s and inversely proportional to the square of velocity gain factor, K_V [PRI96, WEC01].

$$\delta R = \frac{1}{2R_s}\left(\frac{\mathbf{v}}{K_V}\right)^2 \tag{2-12}$$

In the case of circular contours, a perfect circle (except in the start and stop) is generated with a radius smaller than the setpoint radius, depending upon the amount of K_V and feedrate. Here assuming that K_V is equal for both drive controllers and is constant for constant velocity.

Figure 2-12 shows the effect of K_V mismatch in axis of two dimensional serial kinematic machine tools in straight line and circle trajectory.

In multi axes interpolation CNC servo control system must be properly tuned. The mismatching of position loop gain between two simultaneously drive axes causes contouring error. In straight line motion a parallel offset occures in trajectory. If position loop gain for the y-axis is higher than the position loop gain of the x-axis in circular trajectory, it causes an elliptical shape on the x-y plane and Eq. (2-12) is not valid [GRO01, WEC01]. This type of contouring errors can be minimized through adjustment of servo parameters in CNC controllers.

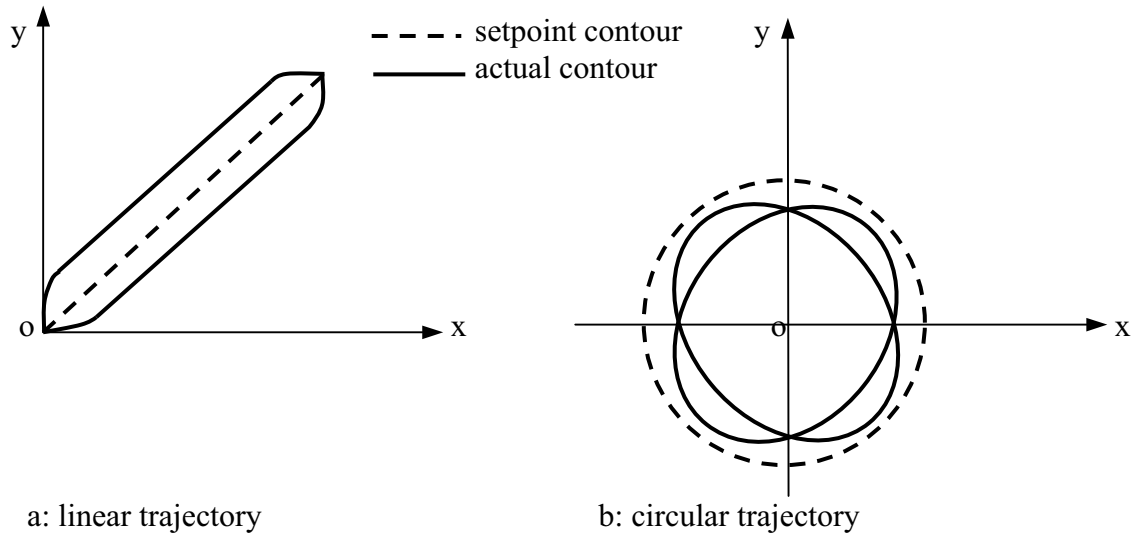

Figure 2-12: The effect of mismatch in K_V ($K_{Vx} \neq K_{Vy}$) [WEC01]

Feed rate is resultant of two perpendicular velocity components. Drive velocities in PKM are not orthogonal and different in comparison to Cartesian machine. PKMs are characterised by their transmission of movements from joint to workspace. These transmission characteristics are influenced by the kinematic topology of the mechanism and its geometric configuration.
Many devices can be used for circular tests, however most of them are not suitable for measuring parallel kinematic machines [LIU05]. For example, a cross grid encoder has very high resolution, flexibility in measuring path, absolute radius and circle center position, but the measuring area is small and it needs strict orientation of measuring head against the scale plate. Thus, it is difficult to be used for PKM. Another common method well suited for checking PKM is the magnetic double ball bar (DBB). In high feed rates with a circular path, transients may occur at the start and end of the test. Angular overshoot is an arc travelled by the tip of the measuring system before and after the data sample arc**,** Figure 2-13. The purpose of the arc is to allow the machine to accelerate to the required feed rate before the ball bar passes through the data sample arc, and to decelerate before the feed out movement is performed [REN--].

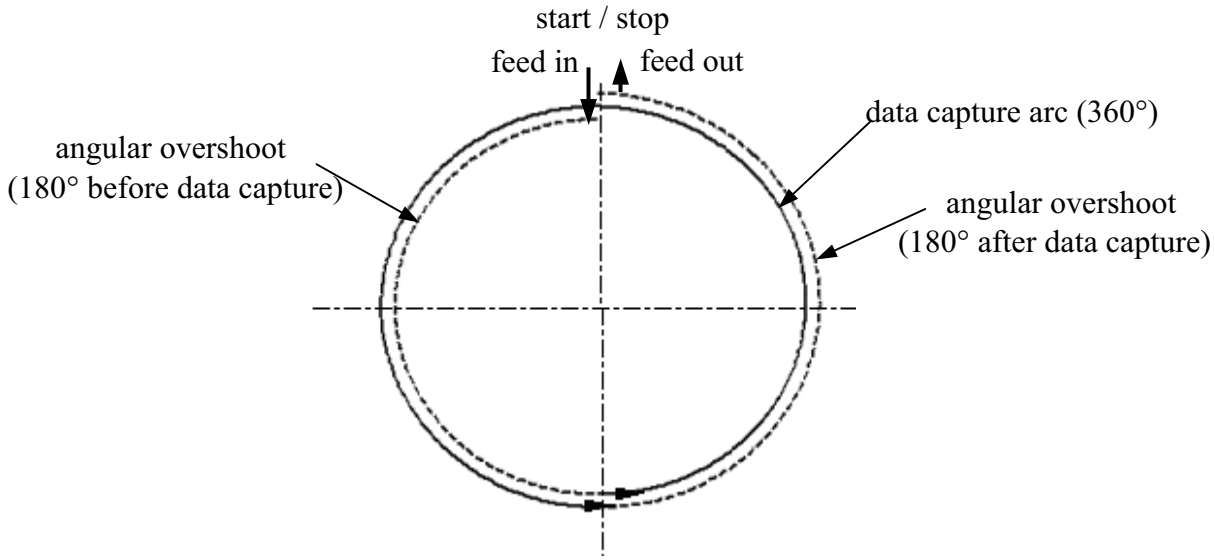

Figure 2-13: Schematic of the measuring path with double ball bar [REN--]

The software samples data from the ball bar transducer while it moves through an angular overshoot arc, but it discards this data after the data sample run is complete.

2.2.6 Tracking and contour error control

The contour error is the orthogonal deviation from the setpoint tool path that can be arises due to the tracking errors in the individual axes. There are two main approaches for reducing the contour error in high velocity drive systems: tracking control and contouring control. The tracking control approach concentrates on reducing the tracking error in each axis and thus indirectly contributes to the reduction of the contour error. The contouring control algorithm for reducing contour error estimates the contour error in real time and uses this estimation in the feedback control law [RAM05]. The research on techniques of error compensation may be classified on two broad categories: static and dynamic error compensation. The research on static error compensation techniques concentrates on the identification and correction of the basic machine errors. The research on dynamic error compensation techniques, also called a real time error compensation, is focused on the correction of the controller error, the thermal and cutting force induced errors. The real time error compensation technique is used continuously during an operation of a machine to constantly correct the inaccuracies.

The high accuracy advanced control algorithms are necessary to purpose high accuracy in spite of the conventional PID controllers that are commonly used on CNC systems [KOR92]. The use of high feedback gain to increase the tracking bandwidth is not sufficient. This approach has important negative limitations including instability, noise and undesirable

oscillations. The tracking accuracy may be improved by use of reference points that are possible to identify through the reference trajectory of the CNC systems known in advance.
In principle there are several ways established to reduce the contour distortions, either the controller gains are increased [PRI96, PRI99-1], or a feed forward branch is introduced in drive control, or look-ahead algorithms are applied by inverse modeling of the control path [ERK01-2]. The circular patch accuracy is improved through K_V value according to the square relation. Furthermore, PI path controller is used to reduce the settling time to zero inversely proportional to the K_V value. It was observed that a completely new quality of dynamic accuracy, difficult to achieve with conventional axes, could be reached through the use of direct drives on account of the extraordinary influence of the K_V value on path accuracy [PRI96, PRI99-1].
Feed forward control can be used to reduce tracking error with a cascaded configuration of the control loops and consequently increases the accuracy. The dynamic delay can also be compensated with proper feed forward action. Figure 2-14 shows a simplified configuration of a velocity feed forward control [GRO01].

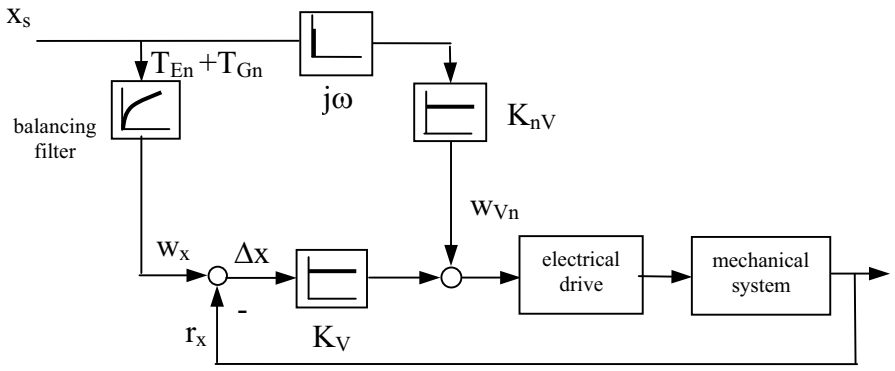

Figure 2-14: Simplified block diagram of a position control loop with velocity feed forward control [GRO01]

Variable w_{Vn} is obtained from a command variable model with differentiation in the motion guidance of the CNC velocity feed forward control. Variable w_{Vn} multiplied within the clock pattern of the velocity control loop with the feed forward control factor K_{nV} adds to the output of the position controller. To prevent the position controller to counter this applied signal a simulated model of the position controller system must be introduced into the path of the position command variable w_x. This is done with the balancing filter that simulates the equivalent delay time T_{En} of the velocity control loop, including the velocity setpoint delay T_{Gn}. Depending on the simulation accuracy of the controlled system the position will be

controlled by the velocity feed forward control variable w_{Vn} without intervention by the position controller. However the tracking error cannot be compensated completely due to the fact that a simple filter is not sufficient to simulate the velocity control loop [GRO01].

The performance of machine axes cannot be considerably increased by the feed forward control [PRI92]. Although [ERK01-2] addressed tracking accuracy of feed forward control there are also some disadvantages of generating high frequency components in the control signal as well as being very sensitive to parameter changes and disturbances due to its open loop nature.

Many researchers have worked on the position loop controller design of motion control system in conventional serial machine tools using PID control, Cross Coupling Controller (CCC), zero phase error tracking control (ZPETC), preview control, inverse compensation filter (IKF), and predictive control [CHE02, ERK01-2, KOR91, LO02, TAR99, WEC90, ZHO02].

Traditional algorithms are based on the feedback principle and in order to improve the tracking performance, feed forward control algorithms have been established.

A significant contribution in this field has been made by Tomizuka who proposed a zero phase error tracking controller (ZPETC). To achieve superior tracking performance in addition to the feedback controller also a feed forward controller is required. Assuming that the feedback controller already exists to compensate the delay in the closed loop transfer function and thus to utilize the desired output a feed forward controller is introduced. Consequently, as long as all the initial conditions are zero (i.e. all the closed loop zeros are inside the unit circle in the z-plane) the controller provides a perfect tracking . However, the system becames highly unstable if any of the zeros are outside, on the unit circle or even on the negative real axis and close to –1 [RAM05, YE92]. To address a zero phase error the the ZPETC system was developed. Based on the ZPETC method various accessory or variational algorithms are proposed. In conclusion, although ZPETC method has a potential to significantly improve the tracking performance of each individual axis the overall control performance for the multi axis machine tool is not always guaranteed [LO02].

The Cross Coupling Controller is aimed at the reduction of the contour error based on the controller objective, rather than the reduction of the individual axial tracking errors. Therefore, the CCC concept calls for the construction of a contour error model in real time and performing it in the determination of a control law that decreases the contour error [LAC00, SHI02, TAR99, ZHO02]. The simplified block diagram of CCC shows in Figure 2-15.

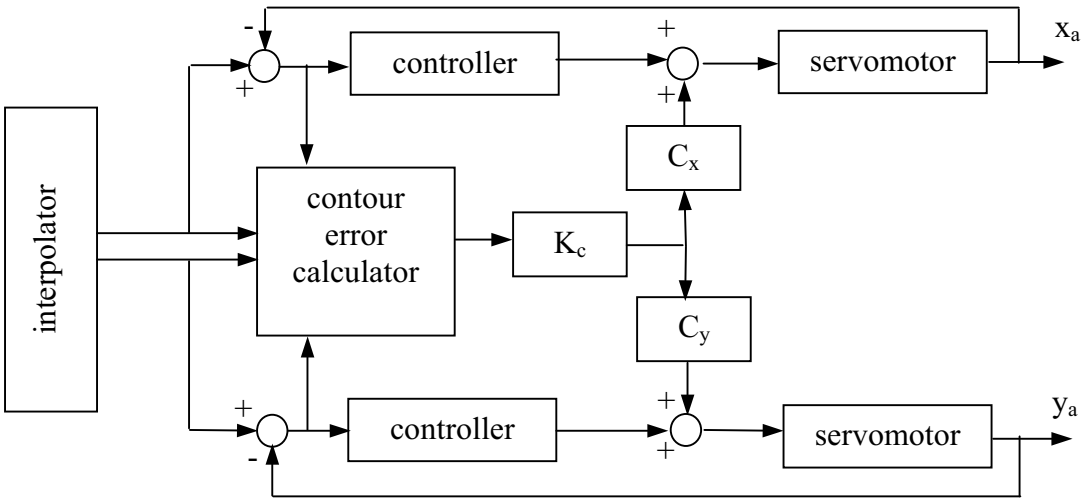

Figure 2-15: Biaxial motion control system with CCC [LAC00]

In the figure C_x and C_y are cross coupling gains and K_c is the cross coupled controller. It consists of two main parts: the contour error mathematical model and the control law, which can be a P, PI, PID or another type of controller.

Many control laws such as traditional PID control, adaptive control and fuzzy logic control have been proposed to implement the CCC. Later extending the contour error estimation to circular and parabolic tool paths, the performance of CCC has been modified [KOR91]. It is performed in a CCC scheme with feed forward axis dynamics compensation. This approach increases the accuracy of the machine [YEH02]. In spite of the intuitive simplicity and performance improvement provided by CCC there are also a number of disadvantages. A cross coupling control requires the axis controllers to be coupled among themselves in accordance with the kinematic configuration of the machine tool that has to be accurately known. In the context of the current machine tool design trend that is based on the production of standard feed drive modules with digital motors adaptable to various production arrangements the CCC solution requiring accurate knowledge of machine configuration is not practical. The major drawback of the cross coupling controller is low effectiveness in dealing with nonlinear contours. Furthermore, in linear contours when the steady state error goes to zero the contour error oscillates.

In addition to the methods discussed in previous paragraphs Weck and Ye [WEC90] designed a compensation method for tracking errors using the inverse compensation filter (IKF) control strategy. The IKF works according to the feed forward principle. There main idea is based on effects of feed forward controller on the transfer error of the proportional controlled position

control loop with a suitable command variable distortion. In detail, with an ideal low pass filter the IKF achieves the smoothing and compensation of the tracking error.

The use of look-ahead and velocity and acceleration feed forward gains are standard features in controller systems. To obtain high performance in contouring involves algorithms for dynamically scheduling feed rates based on the contouring capabilities of the machine and the geometry of the path [REN00].

To achieve precision contour machining that sets input and output membership functions simultaneously, an adaptive fuzzy logic controller (AFLC) is presented in [SUN04]. According to a continuous measurement of the performance of the controller and estimated disturbance values, the parameters of the controller are tuned.

Each individual axis has good positioning capability and a good tracking performance. However, this control approach may lead to degradation of contouring performance due to a mismatch of axial dynamics and axial loop gains.

The limitations of the existing solutions as discussed above triggered active research in the area of feed forward controller design. The basic philosophy of a feed forward controller design is to close the servo loop with a high feedback gain for disturbance and parameter variation robustness and then to cascade the closed loop dynamics with a prefilter that reduces most of its stable components. Based on this design philosophy, the Zero Phase Error Tracking Controller is addressed in [RAM05] and the Modified Inverse Transfer Function is presented in [PRI92]. Because of its high tracking accuracy, feed forward control must generate high frequency components in the control signal and must be very sensitive to parameter changes and disturbances because of its open loop nature.

To address the high frequency content of the control signal limitation it was suggested to use before a ZPETC a low pass filter with zero phase characteristic [WEC90].

Feed forward controllers are based on an experimentally identified model of closed loop axis dynamics. They identified by frequency weighted least squares algorithm. This strategy resulted in successful sharp corner. The parameter sensitivity issue is addressed in [PRI92] and adaptive solutions are proposed in [TSA87] as well as in [PRI97-1]. The studies show that the performance of feed forward controllers can degrade in the presence of parameter mismatch, therefore, the axis parameters have to be accurately known.

The possibility to measure the deviations caused by dynamic and process forces directly by means of a force free add-on position measurement device is useful to improve the accuracy of a PKM. In [VER06] a force free add-on position measurement device is suggested to improve the position accuracy of the TCP. Dynamic errors are eliminated in the position

control loops of the drives by using the control variable for the position measurement system. In symmetric design of the supporting structure the integration on the add-on signals into the position control loops is without difficulties.

To improve the accuracy of a PKM force forward control methods are studied in [BRE06] and a concept with an inverse model is introduced in [DEN04, DEN06]. The considerable force between the actuators of a planar PKM was proven with an experiment setup. The effect of the motor forces on the other actuators is reduced by the feed forward controller [BRE06].

Learning controls in PKM have been proposed and used in [ABD06]. To implement linear iterative learning algorithms on parallel and highly coupled system, a centralized control architecture has to be provided, i.e. feed forward or feedback computed force control. The consideration of inertia which varies over time can be used for decoupling control of the system. Furthermore the decoupling allows the application of linear controllers such as state control to improve the dynamic accuracy considering stability.

To increase accuracy without compensation a method with the concept of direct measurement system is presented in [FLE06-2]. This means, that the measurement system of the PKM has to be arranged directly at the TCP. The measurement system is suitable to decrease error, but reduces the dynamics of parallel kinematic machines.

Static calibration of a Tripod by neural network (NN) is addressed in [KUH06]. The proposed method is based on identifying the actual geometry of an hybrid kinematic milling machine by means of neural networks. Positioning deviations are the input and geometric errors are the output data. One of the most important properties of a NN is the ability to learn from its environment. A suitable training phase should attempt to collect data representing the most common operating modes. Since the reliability of the NN model depends on the learning condition, appropriate input patterns of the input layer must be suitable to the characteristics of machine. In order to give the network good prediction capability, it has to go through a training phase in which a learning algorithm is used. After training by simulated data, in a second step NN is fed with unknown data in the application phase. Within this process, the parameters of the network are adapted through optimization schemes by comparing the network output to the target.

3 Description of problem

In recent years parallel kinematic machine tools were in focus of intensive research due to their predicted prospective features, but early hopes are still hard to realize. Especially, the accuracy of the dynamic performance is yet not sufficient. One of the principal reasons is the uneven controller gain transform from drive space to workspace discussed in this thesis.

As some prerequisites for high speed machining, faster feed motion is considered. In industrial CNC machine tools, PID servo controllers are mostly used. Due to the limited bandwidth in these controllers, there exist tracking errors in each axis. The justification is that the closed loop control system is not able to track the rapidly varying setpoint positions [ERK01-2].

In serial kinematic machine tools the motion of the machine axes and, especially, their drive dynamics are directly translated to the tool center point, but in most parallel kinematic machines the motion is transformed to the TCP nonlinearly.

When the actual position in joint space is transformed to the TCP in Cartesian coordinates, the tracking errors lead to contouring errors in work coordinates.

Enhanced accuracy in parallel kinematic machining requires high performances both in the mechanical parts, especially in the joints with multiple degree of freedom, and in the machine controller. In the thesis, servo control behavior is studied.

Although the reviewed contour error controllers could not be implemented in standard control systems, they can be integrated with some modifications in the hardware of the drive systems.

In principle, there are several ways established to reduce the contour errors, either the setpoint velocity as input to closed velocity loop instead of setpoint position or online adapted velocity gain parameters or pre-compensated contour error. The first method can only be realized in high communication rates that are not applicable.

K_V factor in a closed loop position control is a constant value and must ensure stability in the most critical position in nonlinear systems. Nonlinear effects are difficult to deal with at high speeds and high accuracies. K_V values must be equal for all interpolating drives in SKM as a basic rule but this is not granted with PKM, when the gains are constant parameters in the axes controllers. Thus an online adjustable K_V is demanded in machine controllers. It could equalize the error in the Cartesian space. This algorithm is not possible in conventional control systems as well as in non commerical solution.

The pre-compensated contour deviation requires an actual model. It is possible to obtain the exact model with advanced methods such as neural network approach. This method is a fast approximation for real time application, simple and useful in conventional control systems.
The goal of the thesis is to find an efficient algorithm to predict contour errors in parallel kinematic machining when identically available position controllers are applied.
Investigation on the new challenge in accuracy of PKM in comparison to SKM is addressed. To simplify tracking error transformation principles first a 1-DOF mechanism is studied. To investigate contour errors, transformation principles are developed to 2-DOF setup and the tracking error transformation principles to 3-DOF. To study trace accuracy and transformed tracking error effects an experimental milling machine is used. Simulation effects are performed to ensure uncoupled closed loop controller. The pure closed loop controllers are based on servo control system and kinematics transformation, neglecting the mechanical effects.

4 Principle of Tracking Error Transformation in a Simplified Test Bench

4.1 Introduction

This chapter describes the transformation of controller gain in a parallel kinematic machine. PKM behavior is simplified to one axis transform of position and velocity, the so called Monopod. For this subject, a mechanism is investigated for the dynamic characteristics in active platform and their translate to TCP. Positions and velocities are transformed from joint to work coordinates. Based on experiment with a test bench and simulation model the behavior of dynamic characteristics in active platform and TCP has been studied.

4.2 Structure of Monopod

A general functional representation of the Monopod system is depicted in Figure 4-1. The theoretical path of TCP is inversely transformed into the active platform trajectory, and then transmitted to the Computer Numerical Control in the form of a program. The trajectory generation algorithm identifies the distance to be traveled.

The conventional cascaded controller includes P and PI where the first is used for position closed loop control and the latter is used for velocity and current closed loop control, respectively.

The main task of the servo system consists of controlling the machine axis in order to ensure the geometry of motion, which is described by the program. The system is moved via setpoint position, with the required path accuracy.

The mechanical structure consists of two main platforms (active platform and passive one) and the connection strut. Control system would be directly completed in a closed loop by interacting on references and the feedback from the servo control units and the measurement systems.

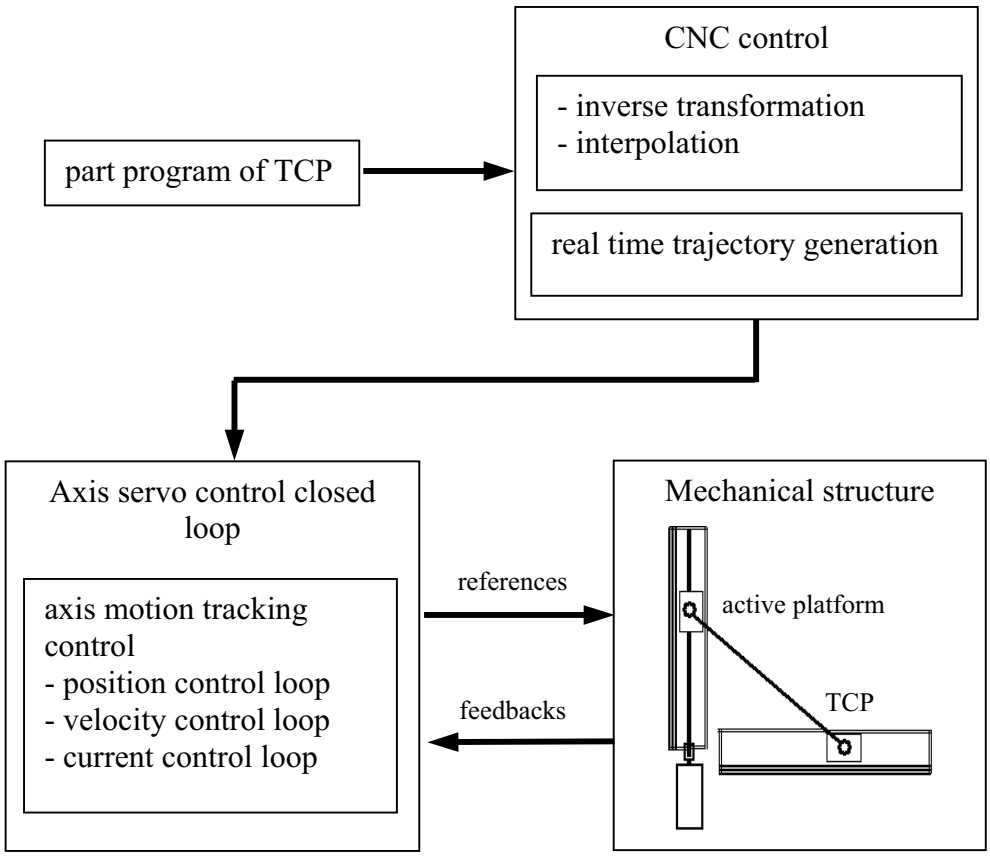

Figure 4-1: Functional representation of the Monopod mechanism

4.2.1 Mechanical and measuring system

The simple PKM of the 1-DOF Monopod is based on fixed length strut and moving base point in straight line direction.

Figure 4-2 shows the Monopod consisting of two sliders, two rotary joints, two guideways, one strut and one servo motor. According to the figure, the servo motor is coupled to a conventional ball screw to drive the Monopod. The active platform and ball screw are connected via screw joint and translated in u-direction with a transmission ratio of 10 $^{mm}/_{rev}$. The active platform and TCP are connected to the strut via rotary joints. The revolute joints allow the strut to rotate to the platform and the TCP.

The tool center point is represented by a linear guideway carriage moving in x-direction.

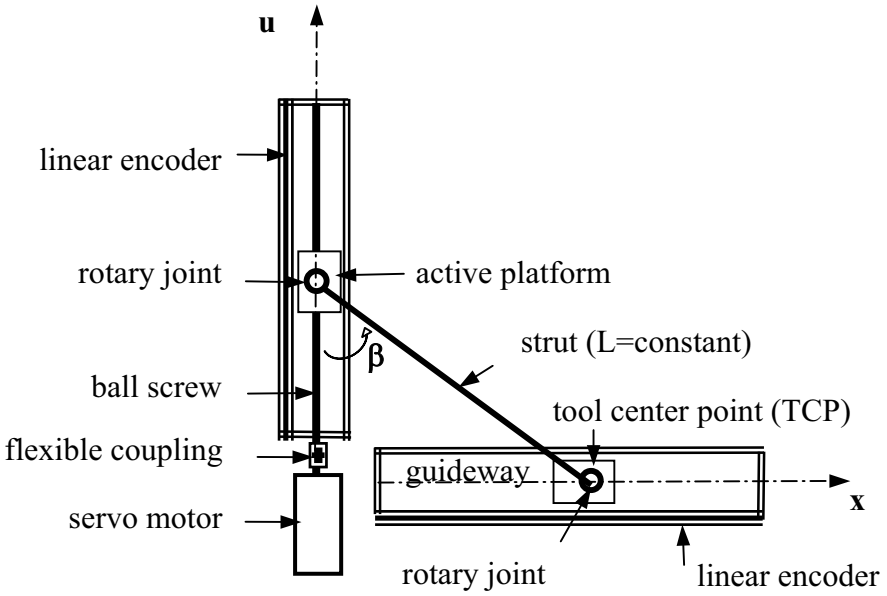

Figure 4-2: Schematic of Monopod

In the experiment, various values for angle β between u-axis and strut in the range from 35° - 60° are tested.

The position function is obtained as follows:

$$u^2 + x^2 - L^2 = 0 \tag{4-1}$$

Inverse kinematic (IK):

$$u = \pm\sqrt{L^2 - x^2} \tag{4-2}$$

Forward kinematic (FK):

$$x = \pm\sqrt{L^2 - u^2} \tag{4-3}$$

The position of the active platform can be measured with a direct measuring system in high accuracy for closed loop control. In x-direction, the displacement of the TCP is also measured with a linear encoder. The encoder body is mounted to the fixed base, and the moving reading head is attached to the slider.

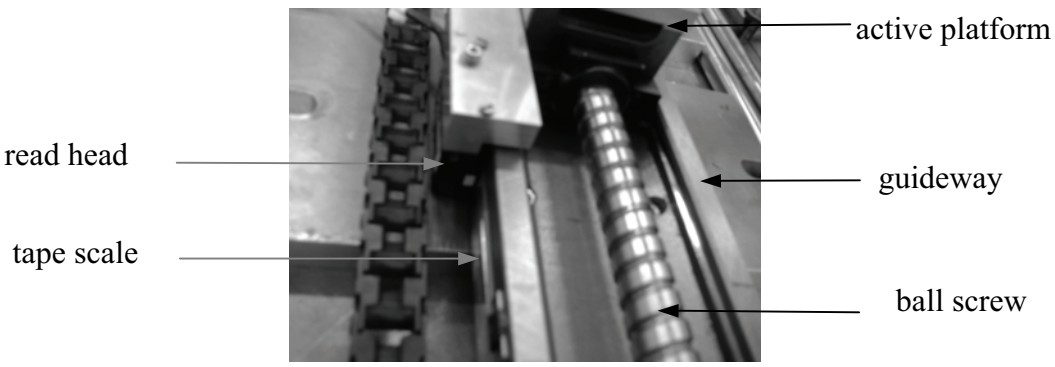

Figure 4-3: Schematic of positioning measuring system in Monopod

4.2.2 Geometric calibration of Monopod by NN method

Uncertainities of the production and tolerances of the assembly cause positioning errors in the motion of TCP. In production and assembly of the machined parts, there is an acceptable of tolerance to the finished parts, that is not avoidable with reasonable costs. To realise a good correlation between the results of measurements and simulations, the mechanism must be calibrated.

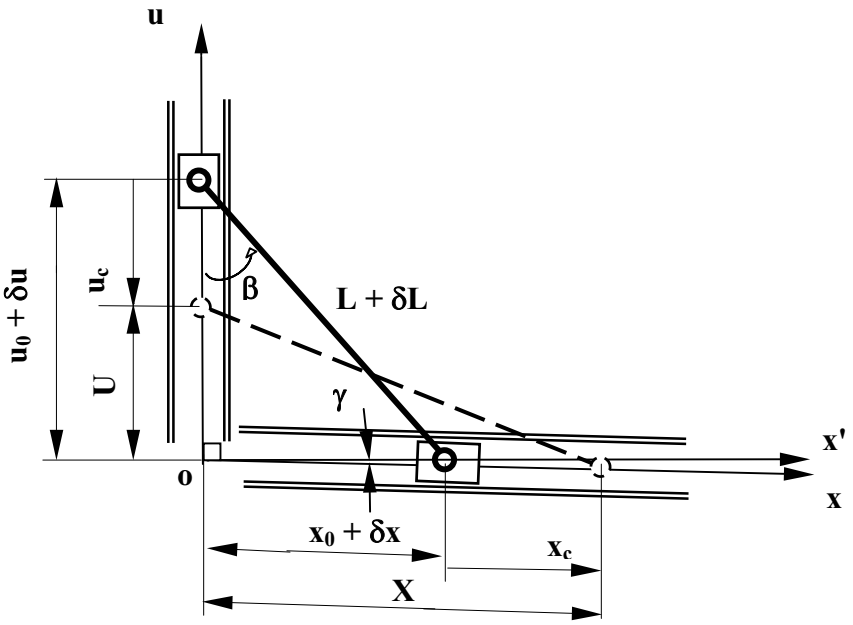

$x_0 + \delta x$: start point in TCP (position of zero point in TCP)

$u_0 + \delta u$: start point in active platform (position of zero point in nut)

x_c : path of movement in TCP in CNC program

u_c : path of movement in active platform in CNC program

X : position of TCP in xou coordinate

U : position of active platform in xou coordinate

xou : test bench coordinate

x'ou : perpendicular coordinate

γ : angle deviation between xou coordinate and x'ou coordinate (out of perpendicularity)

β : angle between strut and driver axis

L + δL : actual length of strut

Figure 4-4: Geometric model of Monopod

The static calibration technique is usually employed for evaluating the positioning accuracy of any mechanism. The important values in positioning accuracy are actual length of strut (L + δL), real value of start point in TCP (x_0+δx), start point in the active platform (u_0+δu) and perpendicularity deviation between two axes (γ), Figure 4-4.

Accuracy of Monopod can be achieved through calibration, which is the estimation of the parameters of the kinematic model that is implemented in the kinematic transformations.

The test bench is calibrated with the neural network based procedure, described in [KUH06], here without the need of external sensors.

For Monopod calibration, a mathematical model is needed to describe the geometric values. To achieve well converging results with NN applications the parameters must be independent. As length of strut is function of x_0 +δx, u_0 +δu and γ, this parameter is eliminated here. Then, for Monopod calibration, a geometric error matrix E is defined to describe the independent parameters of δx, δu and γ value, Equation 4-4.

$$E = \begin{pmatrix} \gamma \\ \delta x \\ \delta u \end{pmatrix} \tag{4-4}$$

Calibration of Monopod is realized in three consecutive steps of each iteration. For each value, the first NN is trained by the simulated values, where γ, x_0 and u_0 are filled with a variety of arbitrary values. A set of 300 training vectors proves to be sufficient. Every iteration is performed with estimated parameter separately.

In a first step, γ is specified by first application of NN in the workspace in each iteration. In a second and third step, a further NN is created to specify x_0 and u_0, respectively. After every step a new set of training data is created. Iteration of steps 1, 2 and 3 improves the results.

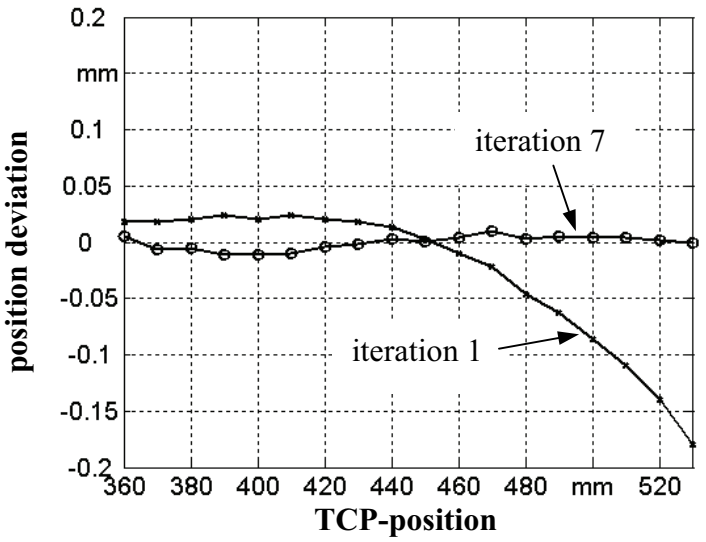

Figure 4-5: Position deviation after 7 iteration loops

Position deviations are calculated by actual positions of measurement devices and setpoint values. Figure 4-5 shows the static position error in start and after 7 iteration loops of the calibration procedure.

Table 4-1 compares the statistical characteristics of static position measurement before and after calibration. The important conclusion from these test series is that the static calibration increased accuracy with reduction uncertainty of position from 265 micrometer to 44 micrometer. The values of reversal error and standard deviation are almost constant.

Table 4-1: Comparison of statistic characteristics before and after calibration

	before calibration	after calibration
uncertainty	265	44
reversal error	12	11.6
standard deviation	5.3	5

data in micrometer

4.2.3 Kinematics transformation

In a serial mechanism, the velocity transmission ratios are constant in the workspace. In contrast, in a parallel mechanism these ratios may vary significantly in the workspace because the displacement of the tool is not linearly related to the displacement of the actuators. PKM exhibit inherently nonlinear dynamics over the whole workspace. The transfer function in Monopod between u- and x-axis is nonlinear, as shown in Figure 4-6. In this model, the set position value and the actual position value of active platform and the analytically calculated value for the TCP are used.

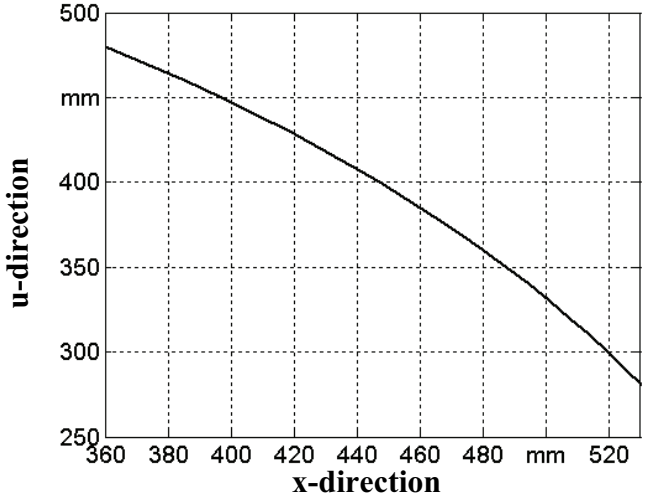

Figure 4-6: Nonlinearity between driver and TCP in Monopod

From the geometric model of Monopod shown in Figure 4-4, we obtain:

$$U = u_0 + \delta u + u_c \tag{4-5}$$

$$X = x_0 + \delta x + x_c \tag{4-6}$$

and using vector loop approach, the position equation is obtained as follows:

$$U^2 - 2 \cdot U \cdot X \cdot \cos(90° + \gamma) + X^2 - (L + \delta L)^2 = 0 \tag{4-7}$$

or

$$U^2 + 2 \cdot U \cdot X \cdot \sin\gamma + X^2 - (L + \delta L)^2 = 0 \tag{4-8}$$

Inverse kinematics:

$$U = -X \cdot \sin\gamma + \sqrt{X^2 \cdot \sin^2\gamma - X^2 + (L + \delta L)^2} \tag{4-9}$$

Forward kinematics:

$$X = -U \cdot \sin\gamma + \sqrt{U^2 \cdot \sin^2\gamma - U^2 + (L + \delta L)^2} \tag{4-10}$$

Equation for velocity of active platform and TCP are:

$$\dot{U} = \frac{-(2 \cdot X + 2 \cdot U \cdot \sin\gamma)}{(2 \cdot U + 2 \cdot X \cdot \sin\gamma)} \dot{X} \tag{4-11}$$

$$\dot{X} = \frac{-(2 \cdot U + 2 \cdot X \cdot \sin\gamma)}{(2 \cdot X + 2 \cdot U \cdot \sin\gamma)} \dot{U} \tag{4-12}$$

A translation factor between velocities of active platform and TCP, the so called gear ratio (G.R), is defined by:

$$G.R = \frac{\dot{U}}{\dot{X}} = \frac{-(2 \cdot X + 2 \cdot U \cdot \sin\gamma)}{(2 \cdot U + 2 \cdot X \cdot \sin\gamma)} \tag{4-13}$$

This formula shows that the gear ratio is a function of position of active platform and TCP in workspace. This relationship clearly indicates that the dynamic characteristic cannot be the same in machine coordinates and Cartesian coordinates.

Inverse transformation of tracking error

In detail the relationships shown in Figure 4-7, whereby the movable base point lies in the u-direction and the end of the strut lies together with the TCP in the x-axis.

The dominant nonlinear position transmission between the drive motion in the u-direction and the motion of the TCP in the x-direction is very obvious:

$\Delta x_{1\_left} = \Delta x_{1\_right} = \Delta x_{2\_left} = \Delta x_{2\_right}$

but

$\Delta u_{1\_left} < \Delta u_{1\_right}$ *and* $\Delta u_{1\_left} / \Delta u_{1\_right} \neq \Delta u_{2\_left} / \Delta u_{2\_right}$

This transmission ratio also describes the velocity and acceleration transmission in the u-direction. Given large value of x, the velocity transmission ratio between x and u greatly increases and can be calculated by formula 4-13.

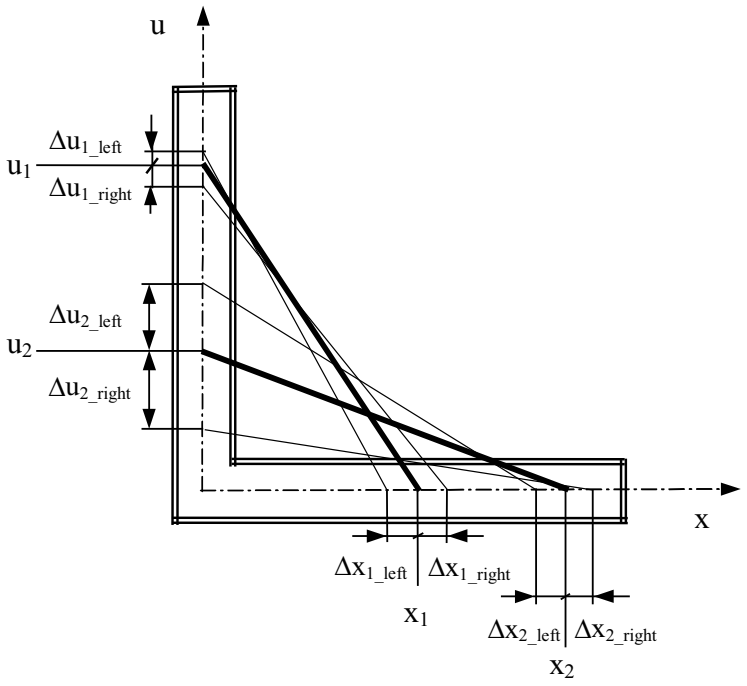

Figure 4-7: Geometric transform in Monopod workspace

When a feed rate v =10,000 $^{mm}/_{min}$ and a velocity gain K_V=3 $^{1000}/_{min}$ is considered, according to the formula $\Delta x_{estimate} = v_{setpoint} / K_V$, a tracking error of Δx=3.333 mm is obtained.

For the Monopod setup, a constant deviation Δx is transformed by inverse kinematics to joint space, Figure 4-8. The magnitudes of the resulting deviations Δu depend on the position. According the Figure, the deviations depend not only on absolute position but also on the relative position. In Figure 4-8, the quotients $\Delta u_{i\_rel} = \Delta u_{i\_left} / \Delta u_{i\_right}$ and $\Delta x_{i\_rel} = \Delta x_{i\_left} / \Delta x_{i\_right} = 1$ are estimated with Δx = 3.333 mm as a function of TCP position. The graph indicates, that the relative tracking error in active platform cannot be linearized and is a nonlinear function of TCP-position. Although TCP with constant velocity in work coordinates behaves isotropic, the tracking error behavior in active platform is unisotropic.

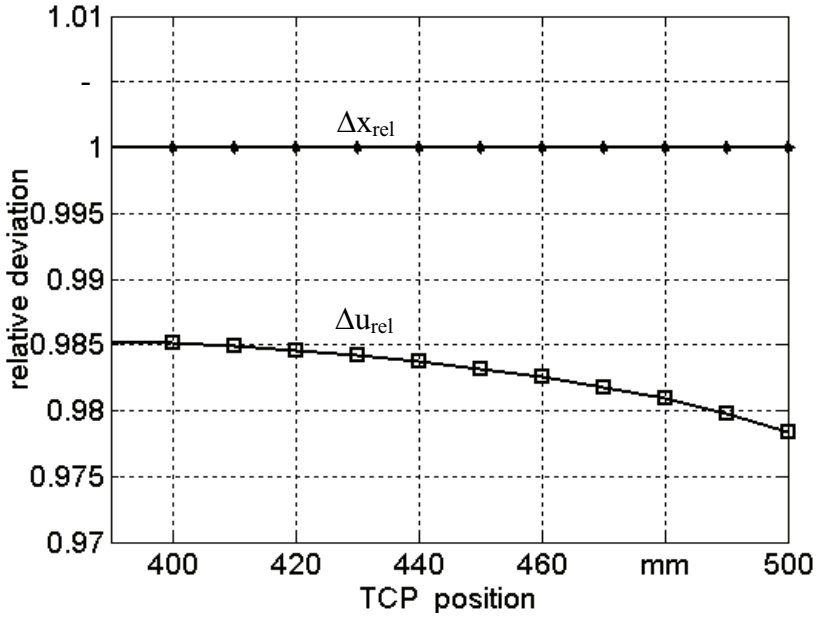

Figure 4-8: Nonlinear transform of virtual tracking errors in work coordinates

4.2.4 Controller gain settings

The most important position control system parameters influencing the tool path behavior are the velocity gain and a time constant. When the velocity gain is too high, an overshoot from desired path occurs. With low values, rise time to the desired path is long; it is, therefore, necessary to select optimal values of these parameters with consideration of stability.

In conventional closed loop control systems, the nonlinear transform controller settings must be adjusted to the most critical positions. Here, two areas of Monopod are studied, station-1 with minimum TCP-position and station-2 with more horizontal strut, Figure 4-9-a. In the Monopod, the most critical position is the region of minimum TCP-position according to station-1 in Figure 4-9-b.

a: Monopod working range

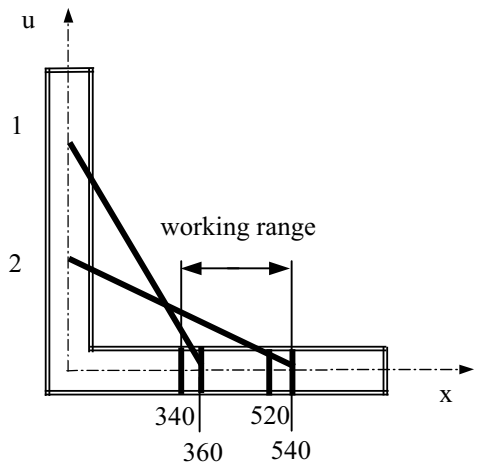

b: station-1

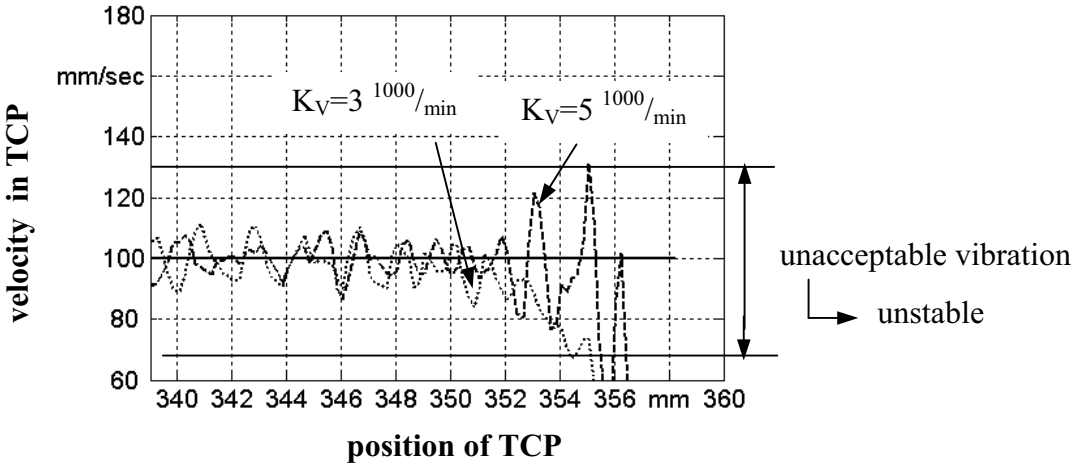

c: station-2

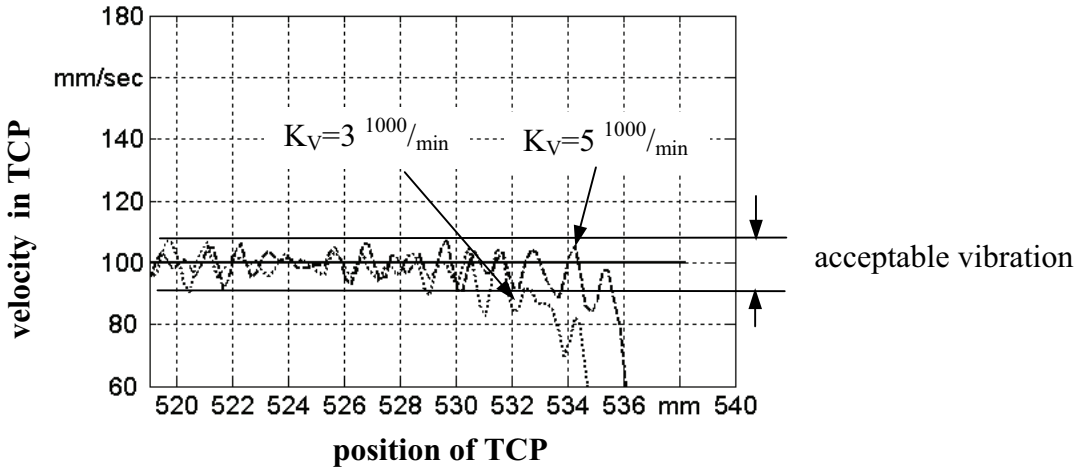

Figure 4-9: Response of TCP in different position of TCP and K_V

(solid line: setpoint velocity; dashed line: response with $K_V = 5\ ^{1000}/_{min}$; dotted line: response with $K_V = 3\ ^{1000}/_{min}$)

For a more horizontal strut position (station-2 in Figure 4-9-c), a higher gain is possible in the controller concerning stability in the TCP. The critical position of the Monopod is the region of minimum β.

It implies that the setting K_V in machine controller cannot be constant and should be online re-adjusted over position. That means adaptable K_V could equalize the error and to keep it equal in the Cartesian space, K_V must be adapted in process in the drives.

In station-1, small deviations in u are transformed to large deviations in x and tiny vibrations in the drive cause unacceptable vibrations in the TCP.

Figure 4-10 shows the maximum available setting K_V in conventional and adaptive control system. In conventional control system setting the value of K_V is based on critical area (x_s) and during motion is constant but according to Figure 4-10, the maximum available setting K_V in control system depends on TCP-position considering stability.

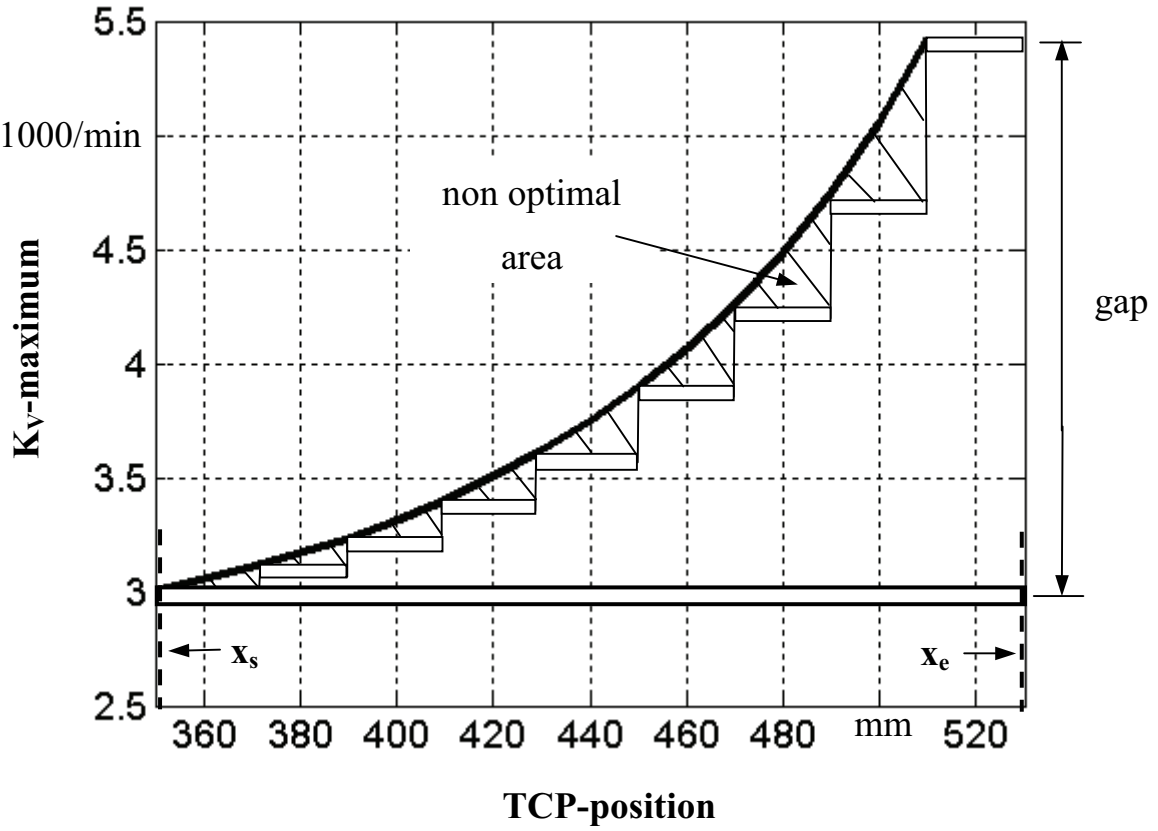

Figure 4-10: K_V-maximum over position of TCP

In the setup the difference between K_V in critical area (x_s) and that one in the position x_e is about two times. The difference is considerable and affects the performance of the system significantly. Setting the value in different areas reduces the tracking error. Although this method improves the system, there are drawbacks. This algorithm is a non continuous method

and not satisfying, because there are non optimal areas. The best solution is adaptive control that varies velocity gain continuously.

4.3 Simulation model

In simulation phase, two models are investigated. First model is based on a simple estimated correlation between the setpoint velocity and the position control deviation

$$\Delta x \cdot K_V = v_{setpoint} \quad \text{with} \quad \Delta x = x_{setpoint} - x_{actual} \tag{4-14}$$

In case of stable controller conditions and for a straight line motion with constant velocity, the position deviation, called the tracking error, can be estimated by

$$\Delta x_{estimate} = v_{setpoint} / K_V \tag{4-15}$$

giving a simple but rough method for axes interpolation. These constraints are also taken into account and compared with experiment and simulated model for the study later on.

The second model to study the dynamic effects of servo drive is illustrated in Figure 4-11. It contains the inverse and forward kinematics and a cascade controller that is modeled in Matlab/Simulink with several distinct control loops using position and velocity feedback.

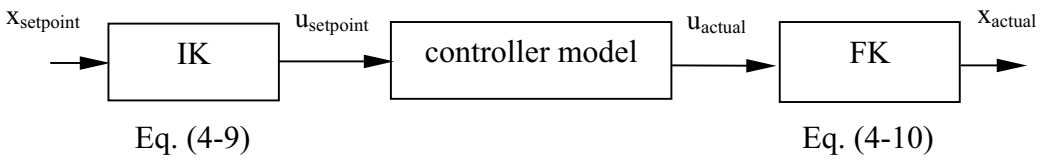

Figure 4-11: Schematic of simulation model

The simulation values are achieved by numerical calcuations of setpoint path, the Monopod specification and setting parameters in servo controller.

Mechanical parts are modeled as rigid bodies without friction and backlash. Servo tracking controller involves servo controller model of active axis. CNC program in TCP inverted to trace in active platform $u_{setpoint}$ as setpoint path and the activated actual path u_{actual} is translated to actual path in the Cartesian coordinate x_{actual}.

4.4 Results

Kinematic characteristics relate the magnitude of the joint space displacement vector to that of the workspace. Variations in these mechanical characteristics will produce variable performance across the workspace.

In experimental setup, trace of TCP is input and transformed to position of active platform inversely. Motion with the trajectory of drive is controlled and the actual position of both axes are measured by the direct measurement systems.

The response of linear position control loops can be determined mathematically. In position control loops with nonlinearities, as they exist in practical system applications, this is complex. In order to obtain the main parameters acting on the system, the transformation is shown in rate of actual velocity gain by position, velocity and tracking error variation.

To investigate the transformation of velocity gain, the relative actual velocity gain, defined as actual K_V in TCP to actual K_V in active platform, is studied.

$$K_{V\text{ - }rel} = K_{V\text{ -}TCP} \;/\; K_{V\text{ - }active\ platform} \tag{4-16}$$

With substitution of (4-11), (4-12) and (4-15) into (4-16) and consideration of geometry of test bench, $K_{V\text{ - rel}}$ is defined as:

$$K_{V-rel} = \frac{\Delta u \cdot (u_s - \Delta u\ )}{\sqrt{L^2 - (u_s - \Delta u)^2} \cdot \left[\sqrt{L^2 - (u_s - \Delta u\ )^2} - \sqrt{L^2 - {u_s}^2}\right]} \tag{4-17-a}$$

assuming γ equals 0. Taking γ into account, we get:

$$K_{V-rel} = \frac{\Delta u \cdot \left[(u_s - \Delta u).\cos^2\gamma + \sqrt{L^2 - (u_s - \Delta u)^2.\cos^2\gamma} \cdot \sin\gamma\right]}{\sqrt{L^2 - (u_s - \Delta u)^2.\cos^2\gamma} \cdot \left[\Delta u.\sin\gamma + \sqrt{L^2 - (u_s - \Delta u)^2.\cos^2\gamma} - \sqrt{L^2 - {u_s}^2.\cos^2\gamma}\right]} \tag{4-17-b}$$

The resulting data can be calculated according to the setpoint data and values measured by the two linear encoders. Relevant results are condensed in Figure 4-12 with the relative velocity gain $K_{V\text{ - rel}}$.

According to [KUH04], the drives in PKM are usually accelerating and a constant feed rate is unlikely in joint space. As in closed loop position control in consequence K_V cannot be considered constant in workspace coordinates.

4.4.1 Effect of position

As shown in Figure 4-12, $K_{V\text{ - rel}}$ is not constant and this means the $K_{V\text{ - rel}}$ depends on workspace position. The $K_{V\text{ - rel}} \neq 1$ that means this factor in active platform and transformed value in TCP are not the same behavior [KUH08].

4.4.2 Effect of velocity

In the following, tests are carried out with different velocities in TCP. Constant velocity in TCP requires a permanent change of velocity in the active platform. An increase of constant

velocity in TCP causes high velocity in active platform. As velocity and tracking error are correlated together, higher velocity results in higher tracking error.

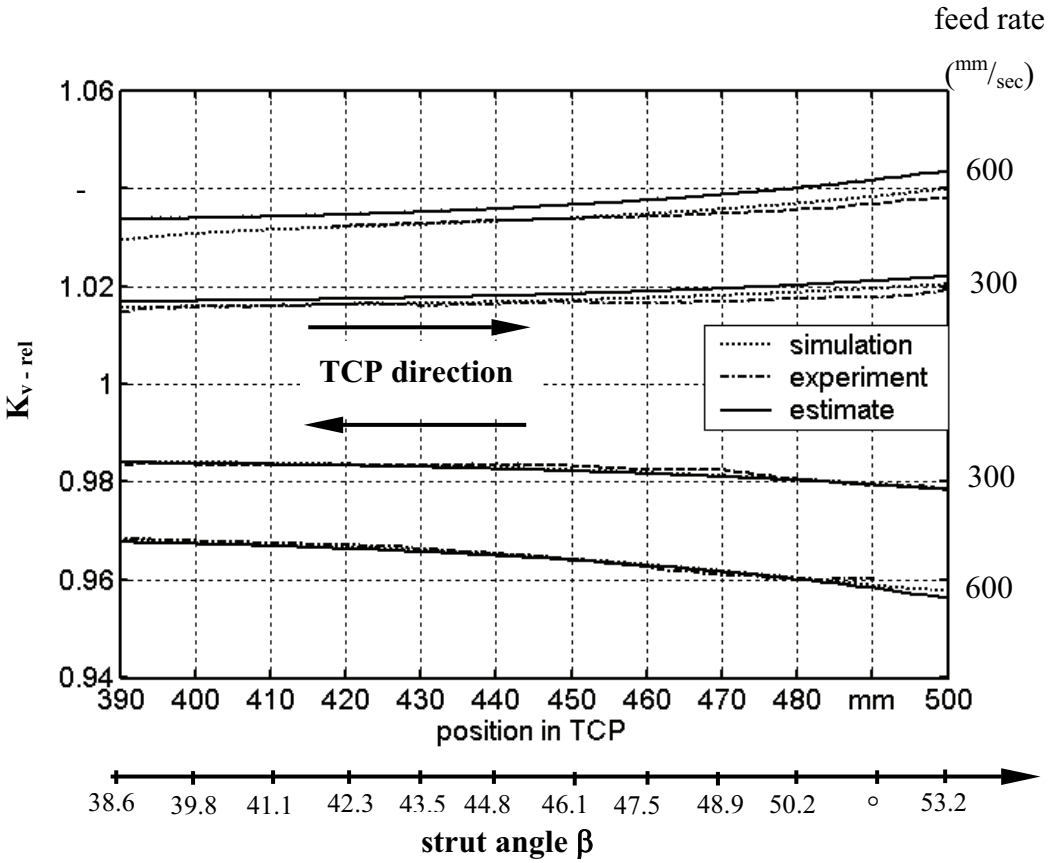

Figure 4-12: Reversal effect of virtual velocity gain

Measured and simulated data show good agreement. Although the estimated model is a rough method in high precision system, in one axis motion the results are close to experimental results. The velocity gain rate is a function of position and feed rate, and is not equal to one. The critical parameter is the strut angle β , that means the virtual velocity gain is a function of the strut inclination and with a more horizontal strut, the factor is more modified.

4.4.3 Effect of direction

According to test results shown in Figure 4-12, the K_{V-rel} is different in forward and backward direction. The K_{V-rel} in backward movement is obtained by taking the mirror image of the forward direction to the unit horizontal line.

This reversal effect is determined by the transform of the Monopod kinematics. Due to the nonlinear transformation in position and velocity for a movement in positive x-direction with constant velocity, the active platform must permanently accelerate and the actual drive velocity is lower than the demanded in the corresponding TCP position.

This becomes obvious when the demanded and actual velocities are plotted against the TCP position, Figure 4-13.

Although the demanded velocity in negative and positive direction in the path are equal, the actual velocity in negative direction, in contrast to positive direction, is higher than the demanded velocity. When the following error in the active platform during acceleration is negative, during deceleration it is positive and its absolute value is higher. In consequence, the transformed following error of the TCP in positive x-direction is higher than the other direction.

The results show the effect of direction dependent amplification and attenuation of the velocity gain.

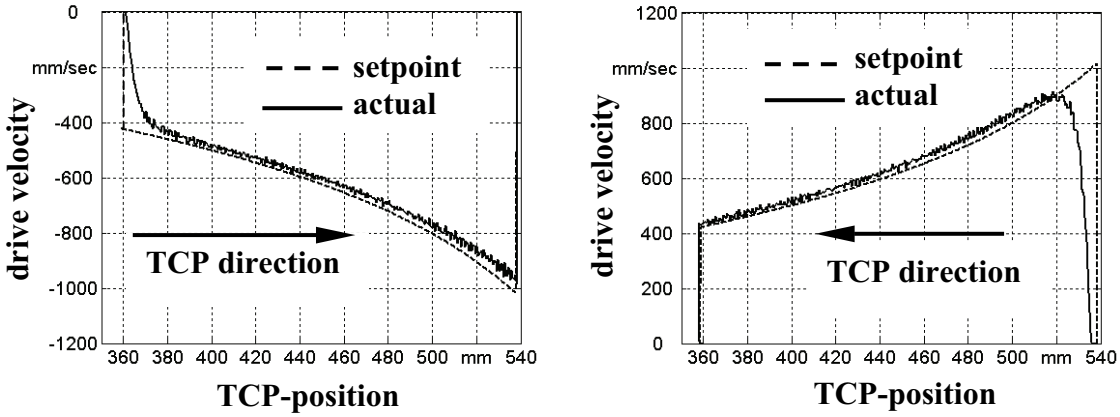

Figure 4-13: Direction bounded acceleration and deceleration, feed rate$_{TCP}$ =300 $^{mm}/_{sec}$

4.4.4 Effect of velocity feed forward control

The virtual velocity gain caused by the position control without and with feed forward control is shown in Figure 4-14.

It becomes clear that, in the system, feed forward control reduces the tracking error, but the virtual velocity gain still varies nonlinearly. As balancing filter in feed forward control, the tracking error cannot be completely compensated.

According to test results, linear feed forward is not sufficient for high precision and high speed motion with PKM. In the study, velocity feed forward control improves dynamic conditioning about 50 percent, but still the relative K_V varies significantly.

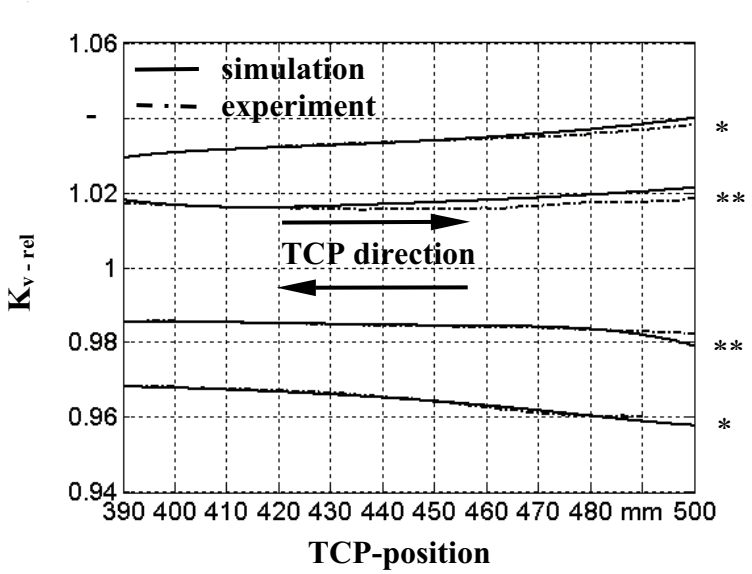

Figure 4-14: Feed forward control effect of virtual velocity gain at feed $rate_{TCP} = 600\ ^{mm}/_{sec}$

(* : without feed forward control, ** : with velocity feed forward control)

5 Effect of Transformed Controller Gain in 2-DOF PKM

5.1 Introduction

The effects of the forward transformation on the tracking errors in parallel kinematic machines are addressed with a simple 1-DOF setup in the previous chapter. Here, the effect on trace accuracy is discussed by contour error in a newly developed test method and radial deviation in circular tests performed by a 2-DOF mechanism.

This chapter presents the contour error algorithms for linear contours and circular trajectories, which calculate the contour errors accurately.

5.2 Design of 2-DOF PKM

The design of the 2-DOF PKM, also known as Bipod, is shown in Figure 5-1. The structure of the Bipod consists of a base plate as reference and two active platforms. The tool center point is connected to the active platforms via struts. Each leg links the active platform and moving plate with revolute joints. The length of struts are constant and active platforms are powered by servo motors in y-direction. The TCP can move in x-y plane when the sliders move in y-direction.

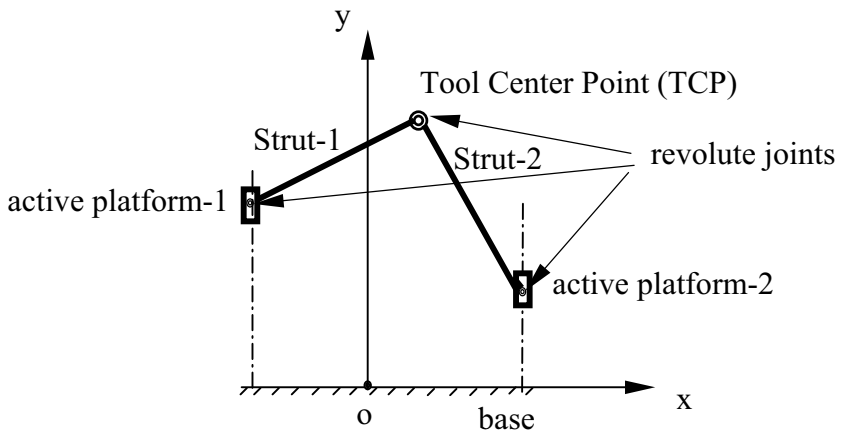

Figure 5-1: Principle of Bipod

5.2.1 Inverse and forward kinematics of Bipod

The kinematic analysis is the essential step for implementing an algorithm to control a manipulator.

Referring to Figure 5-2, a base coordinate system with distance B_1 and B_2 is placed at base plate. Similarly, the TCP with vector P is located at the center of the moving platform.

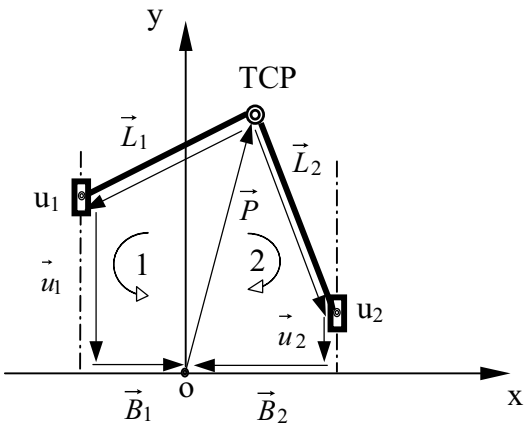

Figure 5-2: Vector loop of Bipod

The coordinates of u_i denote the active platforms displacement and L_i is refered to length of struts. In general, inverse and forward kinematics are carried out with the vector loop approach.

$$\vec{P} + \vec{L}_i + \vec{u}_i + \vec{B}_i = 0 \qquad \text{i : 1, 2} \qquad (5\text{-}1)$$

$$L_{ix}{}^2 + L_{iy}{}^2 = L_i{}^2 \qquad (5\text{-}2)$$

As active sliders are actuated only in y-direction, vector u_i has only y-components and as base plate is horizontal, vector B_i has only x-components, respectively. Here, for system simplification take B_1=B_2=b. With the use of equations (5-1), (5-2), simplified assumption and inverse kinematics relationship, u_i relates to

$$u_1 = P_y - \sqrt{L_1{}^2 - (b - P_x)^2} \qquad (5\text{-}3)$$

$$u_2 = P_y - \sqrt{L_2{}^2 - (b + P_x)^2} \qquad (5\text{-}4)$$

where P_x and P_y are x and y components of TCP-position.

The forward kinematics gives the pose of end effector of the parallel mechanism when given all leg lengths of manipulator. The x and y components of pose of TCP relates to

$$P_x = \frac{m \cdot P_y + n}{4 \cdot b} \qquad (5\text{-}5)$$

$$P_y = \frac{-r}{2 \cdot q} \pm \sqrt{\frac{r^2}{4 \cdot q^2} - \frac{s}{q}} \qquad (5\text{-}6)$$

the parameters m, n, q, r and s can be find

$$m = 2 \cdot (u_2 - u_1)$$

$$n = {u_2}^2 - {u_1}^2$$

$$q = 1 + \frac{m^2}{16 \cdot b^2} \tag{5-7}$$

$$r = -2 \cdot u_1 + \frac{2 \cdot m \cdot n}{16 \cdot b^2} - \frac{m}{2}$$

$$s = {u_1}^2 - {L_1}^2 + b^2 + \frac{n^2}{16 \cdot b^2} - \frac{n}{2}$$

The transmission between the joint space and the platform of a mechanism is described by a set of nonlinear algebraic equations. The Jacobian matrix J, which maps the machine axes velocities to the velocities at the TCP can be derived from this equation.

$$J_i = \frac{\partial f_i}{\partial P} = \begin{bmatrix} \dfrac{P_x - b}{\sqrt{{L_1}^2 - (b - P_x)^2}} & 1 \\ \dfrac{P_x + b}{\sqrt{{L_2}^2 - (b + P_x)^2}} & 1 \end{bmatrix} \tag{5-8}$$

5.2.2 Position and tracking error transformation

The relevant factors that influence the contour error are the nonlinear behaviour of the controller and the controlled system [PRI99-2].

Let $\vec{U}_s$ and $\vec{U}_a$ be the setpoint and actual position vector of the drive on the machine coordinate, and $\vec{X}_s$ and $\vec{X}_a$ be the setpoint and actual position vector on the platform on the Cartesian coordinate, Figure 5-3. $\Delta\vec{U}$ and $\Delta\vec{X}$ be the tracking error vector in the machine coordinates and Cartesian coordinates respectively. The tracking error vector is the difference between the demanded position and actual position value.

$$\Delta\vec{U} = \vec{U}_s - \vec{U}_a, \qquad \Delta\vec{X} = \vec{X}_s - \vec{X}_a \tag{5-9}$$

The $\vec{X}$ vector can be obtained by forward kinematic (FK) transformation matrix of the $\vec{U}$ vector. Then the tracking error vector on the platform is defined as

$$\Delta\vec{X} = \vec{X}_s - \vec{X}_a = FK(\vec{U}_s) - FK(\vec{U}_a) \tag{5-10}$$

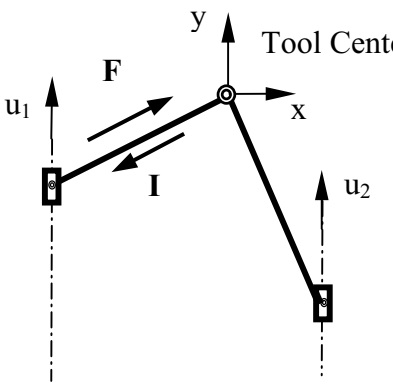

$$\vec{U} = \begin{pmatrix} u_1 \\ u_2 \end{pmatrix}$$

$$\vec{X} = \begin{pmatrix} x \\ y \end{pmatrix}$$

F : Forward transformation

I : Inverse transformation

Figure 5-3: Axes coordinates in Bipod

In the Bipod, the ratio between the drive velocity and Cartesian velocity is not constant. For high speed machining applications, this is an important factor for machine design considerations.

The ratio of drive velocity and Cartesian velocity can be calculated from the Jacobian matrix that relates to the machine coordinates and Cartesian coordinates.

$$\dot{\vec{X}} = J \cdot \dot{\vec{U}} \tag{5-11}$$

In the above equation, $\dot{\vec{X}}$ denotes the velocity vector in platform, $\dot{\vec{U}}$ represents the velocity vector in machine coordinate, J denotes the Jacobian matrix

$$J = \frac{\partial f_i(\vec{U})}{\partial \vec{U}} \qquad \text{that } \vec{X}_i = f_i(\vec{U}) \quad , \quad i = 1, 2 \tag{5-12}$$

Usually, it is difficult to find the analytical function of Cartesian space in TCP over machine coordinate. Therefore, we can use the inverse kinematic function and calculate J^{-1}. J_i is i^{th} row of the Jacobian. The component of velocity in the TCP can be obtained as

$$\dot{\vec{x}} = J_1 \cdot \dot{\vec{U}}, \quad \dot{\vec{y}} = J_2 \cdot \dot{\vec{U}} \tag{5-13}$$

In position control loop in servo control system, the machine velocity vector and the tracking error vector are related by

$$\dot{\vec{U}} = K_V \cdot \Delta\vec{U} \tag{5-14}$$

K_V denotes the actual velocity gain matrix in servo controller.

5.3 Simulation model

The Bipod structure with constant length of struts was modeled to verify the contour error algorithm. In the models, rigid bodies are used for the mechanical parts and for the servo drives a cascade controller is applied. The mechanical model is reduced to the kinematics neglecting the effects of inertia, flexibility, friction and backlash. The motion model of multi axis PKM illustrated in Figure 5-4 contains the inverse kinematics, servo controllers and forward kinematics. In the model, the controller behaviour is significantly studied.

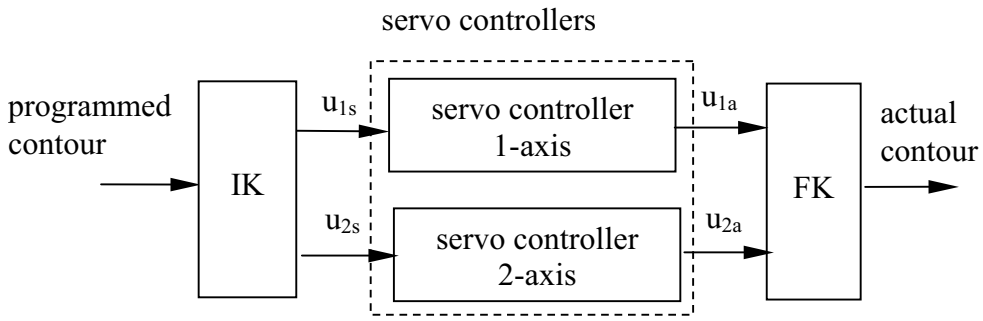

Figure 5-4: Schematic of motion model in Bipod

5.3.1 Star test

In the experimental investigations, the so-called star tests are also performed to understand the effect of transformed tracking errors in workspace. Here the emphasis is placed on linear trajectories with different orientations in the x-y plane.

Contour error model for a linear trajectory

The setpoint linear trajectory in x-y plane is shown in Figure 5-5. The contour error is the distance of the actual point to the trajectory along the normal line direction.

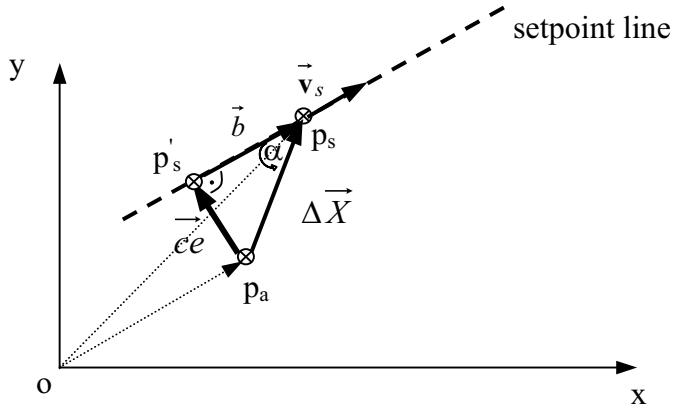

Figure 5-5: Linear trajectory and contour error vector [YEH02]

The contour error is the shortest distance between the generated contour and the programmed contour. Point p_a is the real cutting point away from the setpoint trajectory line, p_s is the setpoint in the same time. $p_s^{'}$ is the point on the setpoint contour that is close to p_a. $\Delta\vec{X}$ is the path tracking error vector in Cartesian coordinates as [YEH02, ZHO02]

$$\Delta\vec{X} = \overrightarrow{op_s} - \overrightarrow{op_a} \tag{5-15}$$

$\vec{b}$ is the projection vector of $\Delta\vec{X}$ on the programmed trajectory and α is the incline angle of the $\Delta\vec{X}$ and the programmed trajectory. $\vec{\mathbf{v}}_s$ represents the setpoint velocity vector.

$$\left|\vec{b}\right| = \left|\Delta\vec{X}\right| \cdot \cos\alpha = \left|\Delta\vec{X}\right| \cdot \frac{\Delta\vec{X} \cdot \vec{\mathbf{v}}_s}{\left|\Delta\vec{X}\right| \cdot \left|\vec{\mathbf{v}}_s\right|} = \frac{\Delta\vec{X} \cdot \vec{\mathbf{v}}_s}{\left|\vec{\mathbf{v}}_s\right|} \tag{5-16}$$

unit vector, $\vec{u}$ in the setpoint trajectory is

$$\vec{u} = \frac{\vec{b}}{\left|\vec{b}\right|} = \frac{\vec{\mathbf{v}}_s}{\left|\vec{\mathbf{v}}_s\right|} \tag{5-17}$$

substitute (5-16) into (5-17) to obtain

$$\vec{b} = \left|\vec{b}\right|\vec{u} = \left|\vec{b}\right| \cdot \frac{\vec{\mathbf{v}}_s}{\left|\vec{\mathbf{v}}_s\right|} = \frac{\Delta\vec{X} \cdot \vec{\mathbf{v}}_s}{\left|\vec{\mathbf{v}}_s\right|} \cdot \frac{\vec{\mathbf{v}}_s}{\left|\vec{\mathbf{v}}_s\right|} = \frac{\Delta\vec{X} \cdot \vec{\mathbf{v}}_s}{\vec{\mathbf{v}}_s \cdot \vec{\mathbf{v}}_s} \cdot \vec{\mathbf{v}}_s \tag{5-18}$$

The contour error is the distance from p_a to the setpoint trajectory line which is denoted as $p_a p_s^{'}$ and $p_a p_s^{'}$ is perpendicular to the setpoint trajectory line.
Finally, the contour error in linear trajectory is

$$\vec{ce} = \Delta\vec{X} - \vec{b} = \Delta\vec{X} - \frac{\Delta\vec{X} \cdot \vec{\mathbf{v}}_s}{\vec{\mathbf{v}}_s \cdot \vec{\mathbf{v}}_s} \cdot \vec{\mathbf{v}}_s \tag{5-19}$$

From $\vec{ce} = \begin{bmatrix} ce_x & ce_y \end{bmatrix} \vec{i}$, the value of contour error can be easily obtained by the equation

$$\left|\vec{ce}\right| = \sqrt{ce_x{}^2 + ce_y{}^2} \tag{5-20}$$

Substitute transformation formula (5-10) and (5-11) into (5-19) to obtain

$$\vec{ce} = \begin{bmatrix} FK_x(\vec{U}_s) - FK_x(\vec{U}_s - \Delta\vec{U}) \\ FK_y(\vec{U}_s) - FK_y(\vec{U}_s - \Delta\vec{U}) \end{bmatrix} - \frac{\begin{bmatrix} FK_x(\vec{U}_s) - FK_x(\vec{U}_s - \Delta\vec{U}) \\ FK_y(\vec{U}_s) - FK_y(\vec{U}_s - \Delta\vec{U}) \end{bmatrix} \cdot \{J \cdot \dot{\vec{U}}_s\}}{\{J \cdot \dot{\vec{U}}_s\}^T \cdot \{J \cdot \dot{\vec{U}}_s\}} \cdot \{J \cdot \dot{\vec{U}}_s\} \tag{5-21}$$

The $\Delta\vec{u}$ is obtained from the joint space tracking error vector that is simulated in control loop over time and calculated in Matlab/Simulink software.

Star tests at two different velocities of the TCP in center of Bipod are modelled. Figure 5-6 indicates the simulated results of star test. θ obtains orientation of constant velocity linear path. The contour error in θ = 90° is cancelled where orientations of struts are stated equal and constant during the straight line motion.

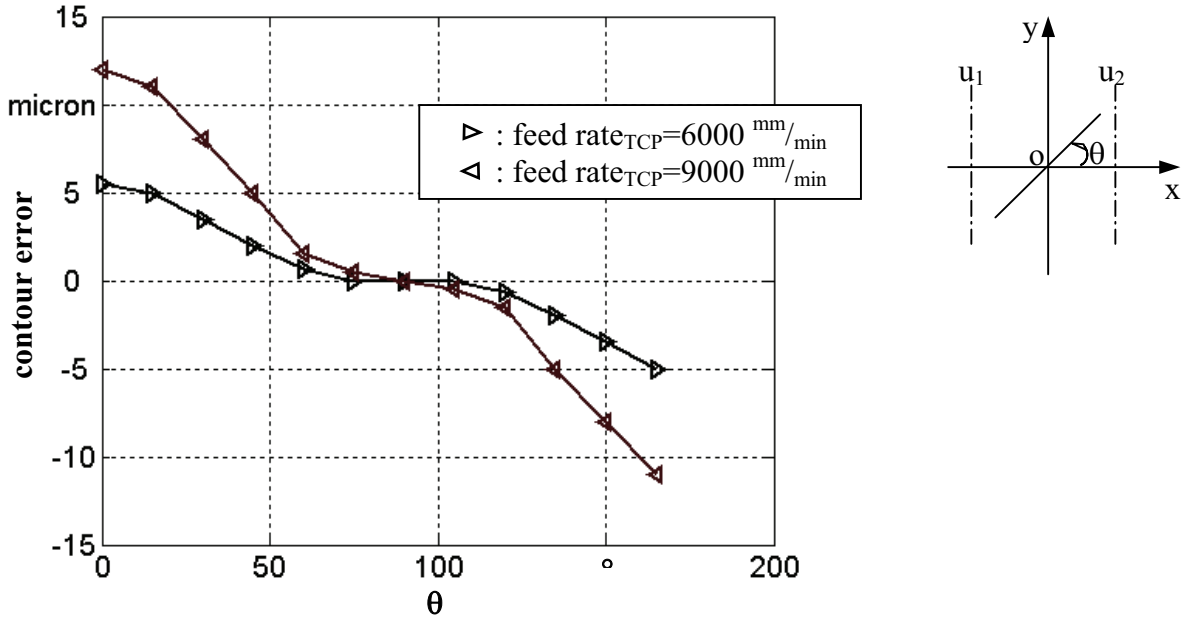

Figure 5-6: Simulated contour error in a planar star test

5.3.2 The proposed contour error model for a circular trajectory

As the contour error is the shortest distance between the generated contour and the programmed contour, the radial deviation is the difference between the produced radius and the programmed radius in circular trajectory. Figure 5-7 depicts the radius error model. Let p_a be the actual position with R_a, p_s be the setpoint position with R_s and α in the same time and p_s' be the position on the setpoint contour that is close to p_a,$C(x_0, y_0)$ be the center point of the circle. R is the radius of the nearest position on programmed contour to actual position and is in every point equal to R_s. Then radius deviation is defined as [KUH07-1].

$$\delta R = R - R_a = R_s - R_a = R_s - \sqrt{(p_{ax} - x_0)^2 + (p_{ay} - y_0)^2} \tag{5-22}$$

p_{ax}, p_{ay}, R_{sx} and R_{sy} are the x and y components of p_a and R_s respectively. v is the setpoint contour velocity vector and v is the tangent on the programmed contour in p_s.The v_x and v_y are the x and y components of v and θ is the incline angle of the contour velocity vector.

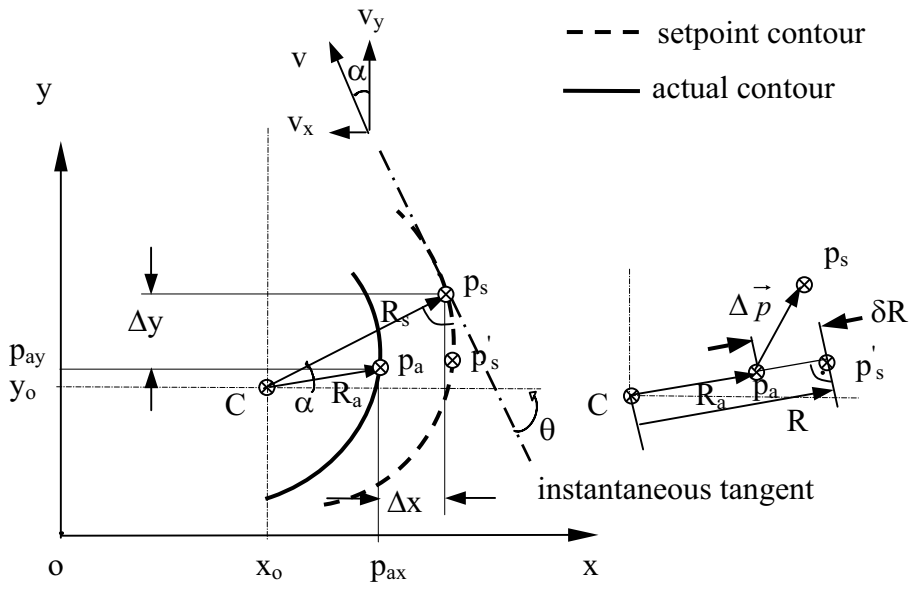

Figure 5-7: Contour error model for a circular trajectory

$$p_{ax} = (R_{sx} - \Delta x) + x_0 \qquad p_{ay} = (R_{sy} - \Delta y) + y_0 \tag{5-23}$$

$$\sin\alpha = \frac{R_{sy}}{R_s} = -\frac{\mathbf{v}_x}{\mathbf{v}} \qquad \cos\alpha = \frac{R_{sx}}{R_s} = \frac{\mathbf{v}_y}{\mathbf{v}} \tag{5-24}$$

substitute (5-23) and (5-24) into (5-22) to obtain

$$\delta R = R_s \cdot \left[1 - \sqrt{(\cos\alpha - \frac{\Delta x}{R_s})^2 + (\sin\alpha - \frac{\Delta y}{R_s})^2}\right] \tag{5-25}$$

Which is not the same as the path tracking error ($\left|\Delta\vec{p}\right| = \sqrt{\Delta x^2 + \Delta y^2}$), and shows that the radial deviation in PKM is dependant on the angular position α.

Substitute (5-10) into (5-25) to obtain

$$\delta R = R_s \cdot \left[1 - \sqrt{\{\cos\alpha - \frac{FK_x(\vec{U}_s) - FK_x(\vec{U}_s - \Delta\vec{U})}{R_s}\}^2 + \{\sin\alpha - \frac{FK_y(\vec{U}_s) - FK_y(\vec{U}_s - \Delta\vec{U})}{R_s}\}^2}\right] \tag{5-26}$$

$\Delta\vec{U}$ is simulated in control loop over time and calculated in Matlab/Simulink software. Finally substitute (5-13), (5-14) and (5-24) into (5-26), yields the radius deviation as a function of the programmed radius, velocity gain and $\Delta\vec{U}$:

$$\delta R = R_s \cdot \left[1 - \sqrt{ \left\{ \frac{J_2 \cdot K_V \cdot \Delta\vec{U}}{\sqrt{[J_1 \cdot K_V \cdot \Delta\vec{U}]^2 + [J_2 \cdot K_V \cdot \Delta\vec{U}]^2}} - \frac{FK_x(\vec{U}_s) - FK_x(\vec{U}_s - \Delta\vec{U})}{R_s} \right\}^2 + \left\{ \frac{J_1 \cdot K_V \cdot \Delta\vec{U}}{\sqrt{[J_1 \cdot K_V \cdot \Delta\vec{U}]^2 + [J_2 \cdot K_V \cdot \Delta\vec{U}]^2}} - \frac{FK_y(\vec{U}_s) - FK_y(\vec{U}_s - \Delta\vec{U})}{R_s} \right\}^2 } \right] \quad (5\text{-}27)$$

Calculation of the proposed radial error algorithm in Bipod

A 2-pod PKM structure with constant length of struts was modeled to verify the radial error algorithm. According to the Figure 5-4, the motion model of Bipod contains the inverse kinematics, servo controller of two active sliders and forward kinematics.

Figure 5-8-a shows schematically the 2-pod model. In the model, u_1 and u_2 are the active sliders, L is the length of each leg.

In the simulation, test parameters are b equal 200 mm, length of struts equal 600 mm, setpoint radius equal 100 mm and feed rate of TCP equal 3000 $^{mm}/_{min}$.

The contour error is calculated using the equation (5-26) and shown in Figure 5-8-b. According to Figure 5-8-b, the radial error during the circle trace is a function of angular position, and significantly observed the reversal points of machine axes, where the individual axes change the direction of their velocity. Maximum and minimum error significantly are related to β, where angle of struts are equal ($\beta_1=\beta_2$), the extremum appears at position B. Figure 5-8-d shows the relationship between the contour error and the velocity in slider u_1 and u_2. An extremum occurs in the contour error, when the axes velocities are near to zero and the velocity changes are highest at position A.

test parameters:

Feed rate = 3000 mm/min
R = 100 mm
b = 200 mm
L = 600 mm

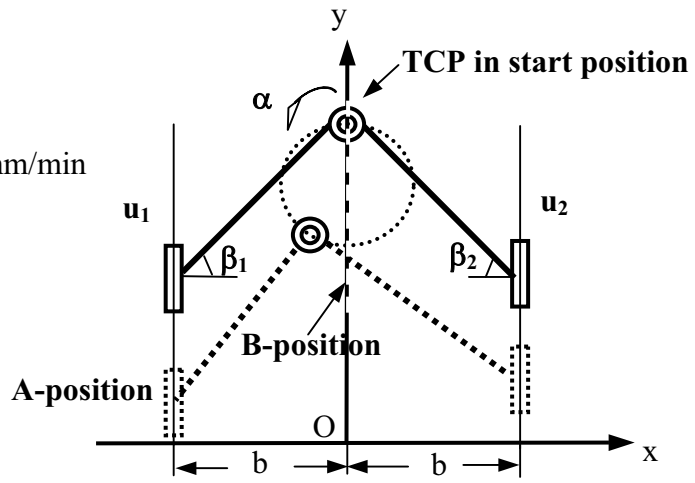

a)

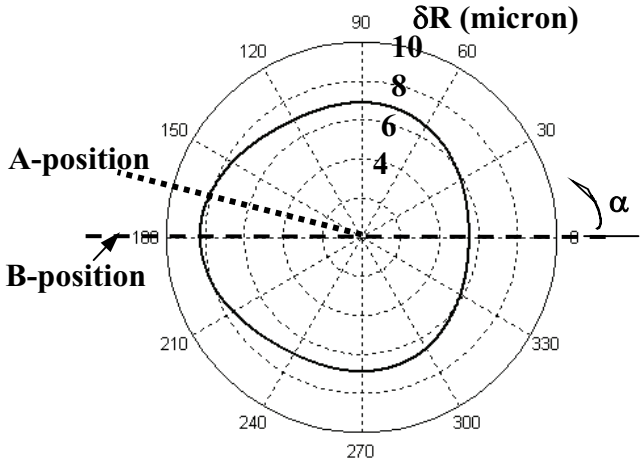

b)

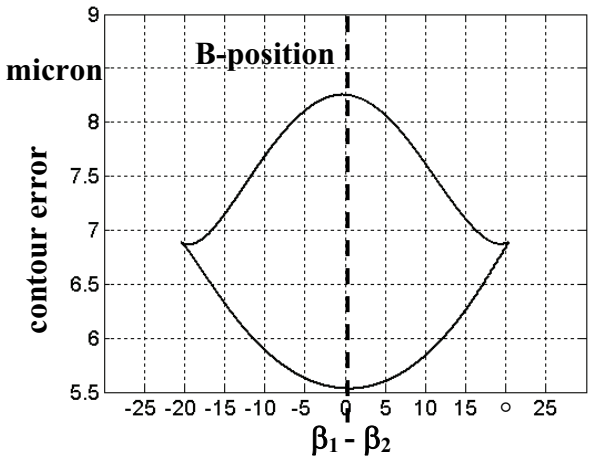

c)

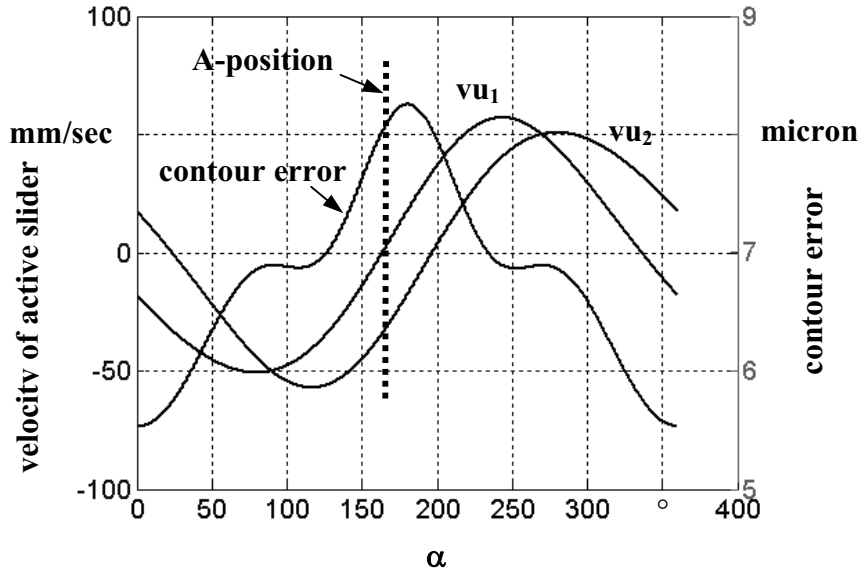

d)

Figure 5-8: a) Principle of Bipod b) Radial error profile c) Contour error profile and β
d) Contour error profile, velocity of active sliders and β

6 Effect of Transformed Controller Gain in a 3-DOF PKM

6.1 Introduction

In contrast to the serial kinematic machines (SKM), in PKM the gear ratio changes in the workspace. In this chapter, the effect on trace accuracy is discussed by contour error in star tests and radial deviations in circular trajectories performed by a Tripod mechanism.

6.2 Tripod configuration

The studies were carried out on a Tripod substructure of an experimental Hybrid Kinematic Milling Machine with two redundant DOF. A conventional cross table carries the workpiece in a horizontal plane (x-y) and the tool is moved with a Tripod in the plane (x-y) and additionally in vertical direction (z) [SCH08]. Figure 6-1 shows the Hybrid Kinematic Machine Tool.

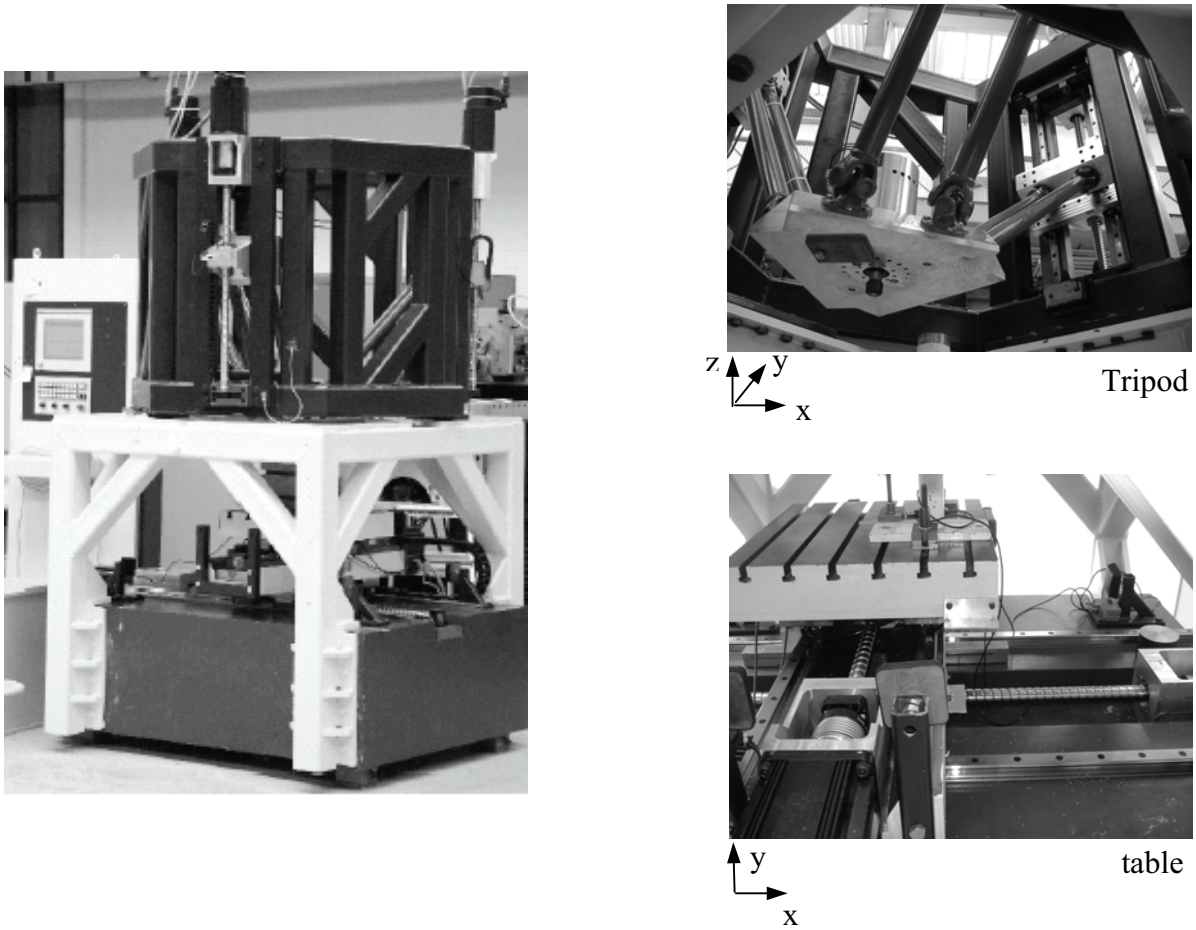

Figure 6-1: Hybrid Kinematic Machine Tool

6.2.1 Structural design

A 3-DOF Tripod is constituted of a moving platform (end effector platform) linked to the base platform. The end effector of the PKM holds the spindle. The spindle drives the cutting tool.

Figure 6-2-a shows the three dimensional CAD model of the Tripod. The base plate (main frame) is formed with hexagonal profiles, at which the 3 vertical transmission ball screws are installed.

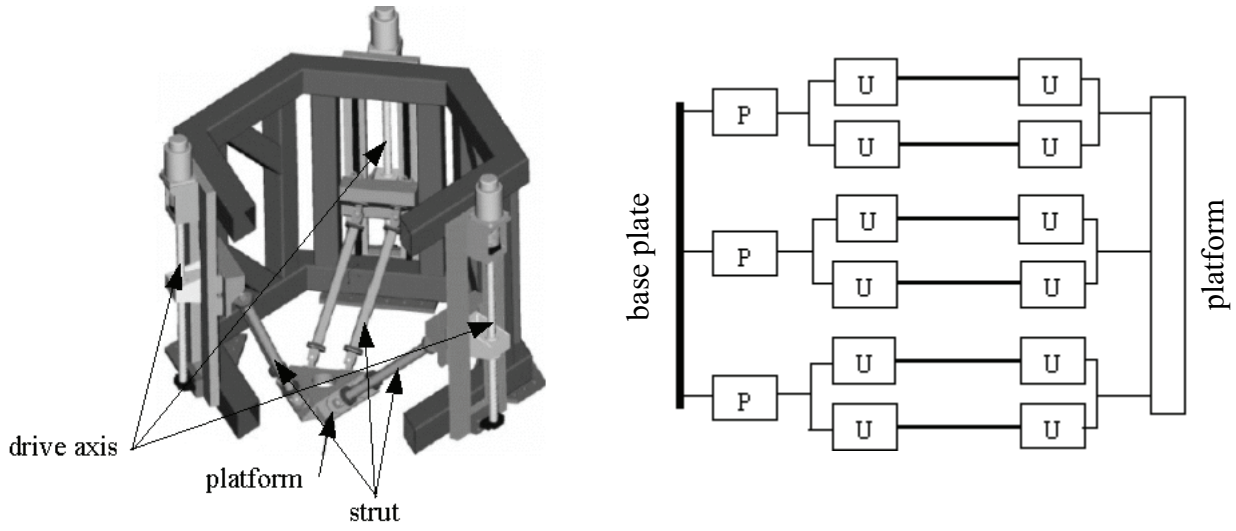

a: CAD-Model [KUH07-1] b: Kinematic architecture

Figure 6-2: Model of the Tripod

The kinematic architecture can be illustrated by a simple scheme, as shown in Figure 6-2-b, where joints are depicted by rectangles (P and U indicate prismatic joints and universal joints, respectively) and links between those joints are represented by lines.

Each strut uses a pair of rods linking a prismatic joint to the moving platform through 2 pairs of universal joints. The movement of the moving platform is generated by the slide of 3 actuators along vertical guideways.

In the Tripod mechanism, all motors move in vertical direction, Figure 6-3. The links to the spindle platform are realized with adjacent struts (L) that are connected with universal joints to the carriers (R_b) and the platform (R_p). With this design three linear DOF (x, y, z) are granted at the TCP. R_p is defined as the distance between the center of the platform and the center of its universal joints. R_b is the distance between the center of the workspace and the center of the base joints in x-y plane. The nominal geometrical values of the Tripod are listed in Table 6-1.

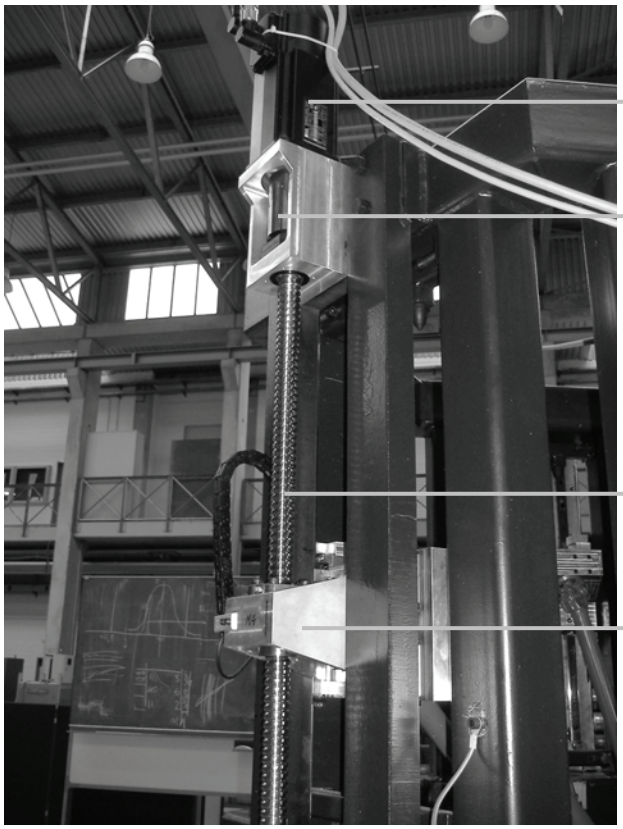

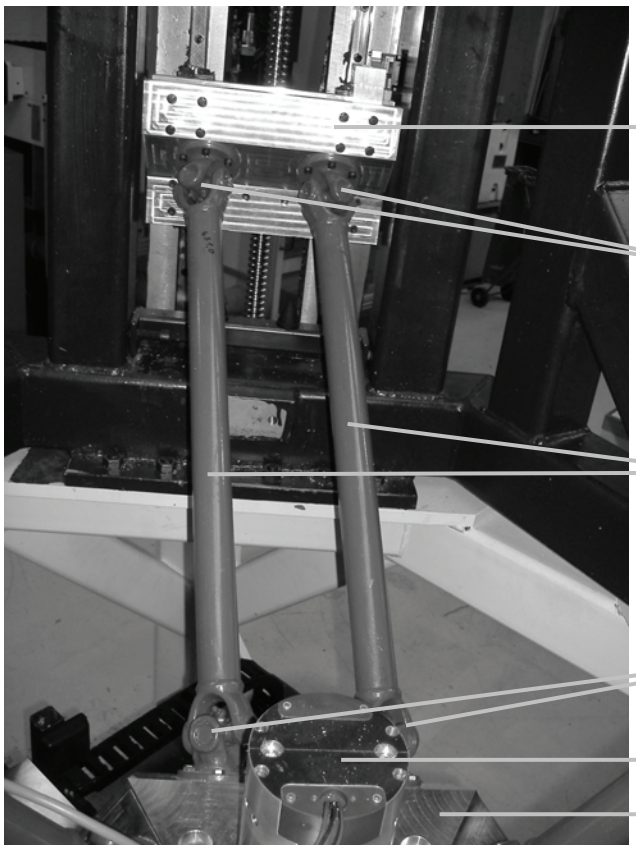

Figure 6-3: Components of the Tripod

Table 6-1: Geometrical values of Tripod

radius of base plate, R_b	513 mm
radius of platform, R_p	150 mm
length of struts, L	600 mm
pitch of ball screw, p	10 mm

6.2.2 Measurement system

A typical ball screw drive system consists of current amplifier, servo motor and ball screw coupling mechanism, Figure 6-4.

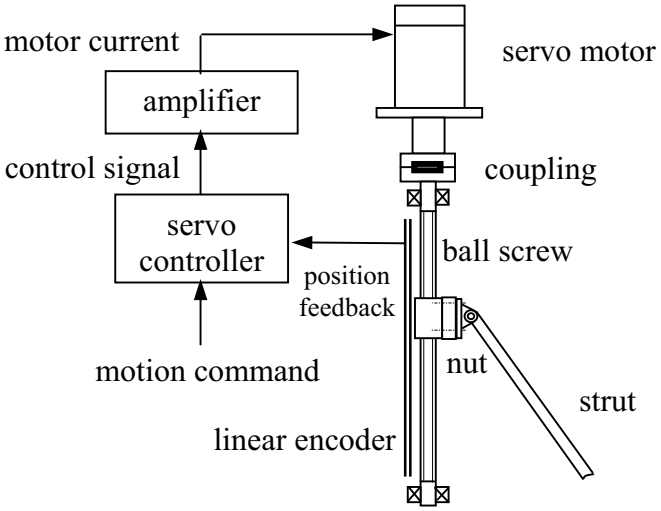

Figure 6-4: Feed drive mechanism with a ball screw in the Tripod

The actual position of each axis of the Tripod is monitored by a non contact linear encoder. A linear encoder with 20 micrometer resolution was selected. The tape scale stationary encoder body was mounted on the fixed main frame, and the moving read head was attached to the base point-plate, Figure 6-5.

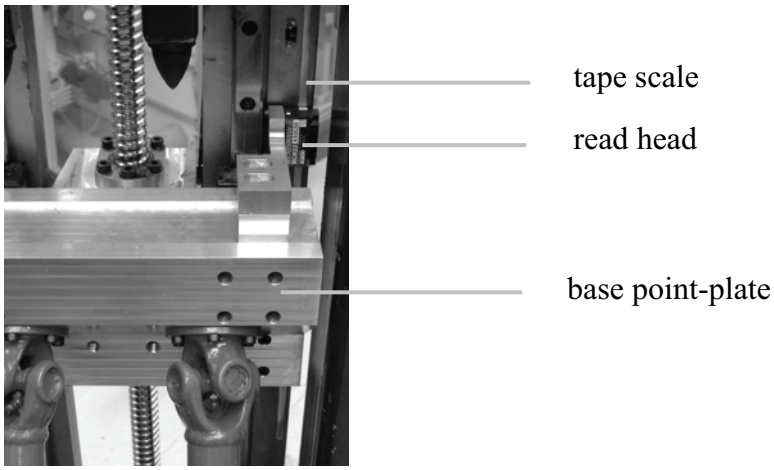

Figure 6-5: Position measuring device in the Tripod

6.2.3 Controller design

The architecture of the Tripod is illustrated in Figure 6-6. The CNC system accepts reference tool path, generated in the form of a standard part program, in CNC format. Each block in the program contains CNC block numbers, tool paths in the form of linear, circular and tool center coordinates, and feed rate for machining a particular part on a CNC machine tool. The trajectory generation algorithm runs for each tool path segment, which creates a 3-D trace series of setpoint positions [SCH08].

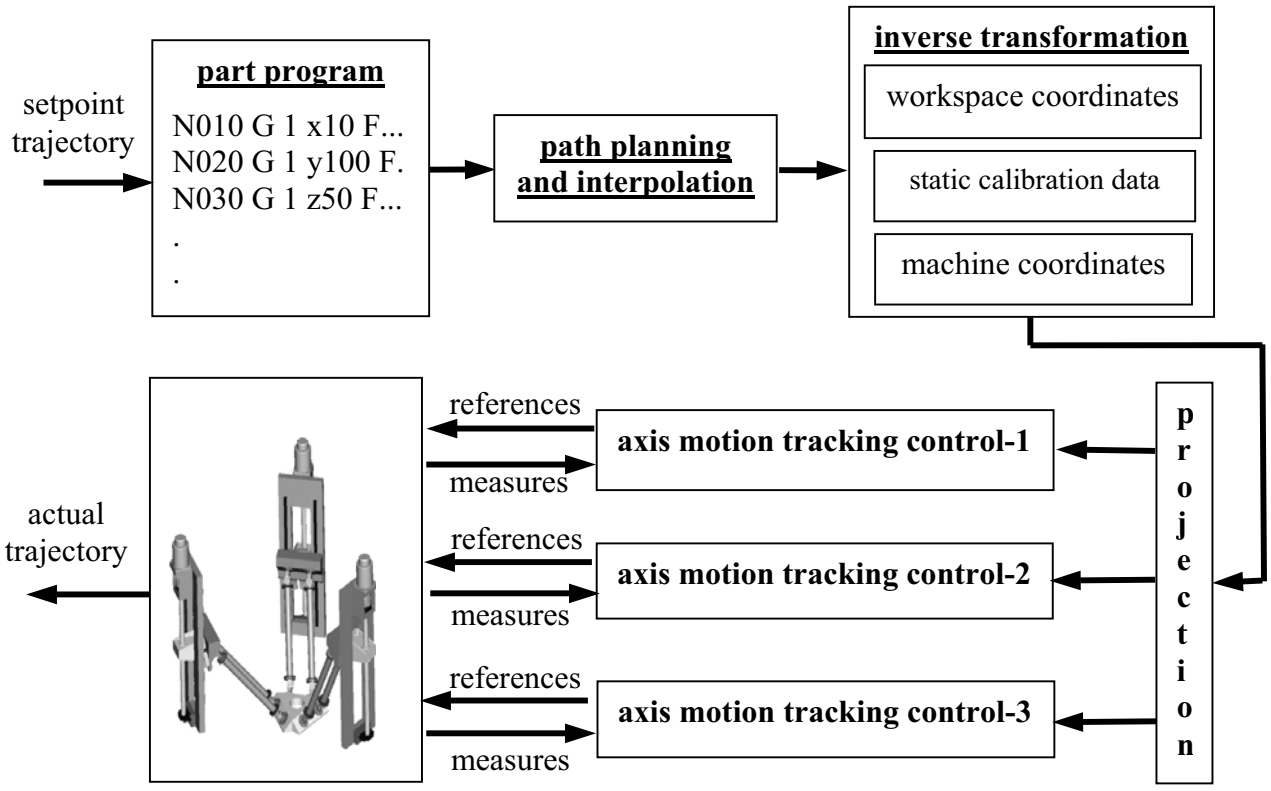

Figure 6-6: Architecture of the Tripod control

The interpolator module is one of the core components in trajectory generation. Therefore, a good and reliable interpolator design is vital to the overall system performance. The interpolator controls the coordinates of the machine axes motion and generates discrete displacement commands for each axis, at every control interval. The main function of the interpolator is to generate coordinated movement of the seperately driven axes of motion, to achieve the setpoint path of the tool. The position error of each axis is evaluated in the feedback.

6.3 Kinematic model

The kinematic model consists of mathematical equations and describes the transformation from the machine coordinates to the Cartesian coordinates and vice versa.
In the following sections, the derivation of the transformation equations is expounded. The kinematic analysis is based on the closed loop vector analysis. Tripod kinematic is analysed and the transformation equations are calculated in [BLE03].

6.3.1 Inverse transformation

These vectors for the first drive axes are represented in Figure 6-7. The arrow in the middle of the illustration indicates the direction in which the vectors were added.
Since the approach must be satisfied for each strut, the index i (1, 2 and 3) indicates each leg of the Tripod.

There are 3 base points in the base plate obtained by $\vec{B}_i$ (i =1, 2, 3). The base points are stated in x-y plane. The value of these vectors is the base plate radius, Table 6-1. The three vectors of machine axes position $\vec{E}_i$ are directed vertical in z-direction. They represent the three ball screw shafts and the value of these vectors correspond to the machine coordinates. The struts are determined by the vectors $\vec{L}_i$, the value of these vectors is the length of struts. Vector $\vec{A}_i$ obtains points on the movable platform and the value of these vectors is the radius of platform.

Allow tool vector, $\vec{W}$ and the vector model is completed with the position vector $\vec{P}$, that describes the position of TCP in Cartesian coordinates.

$$\vec{B}_i + \vec{E}_i + \vec{L}_i - \vec{A}_i + \vec{W} - \vec{P} = 0 \qquad (6\text{-}1)$$

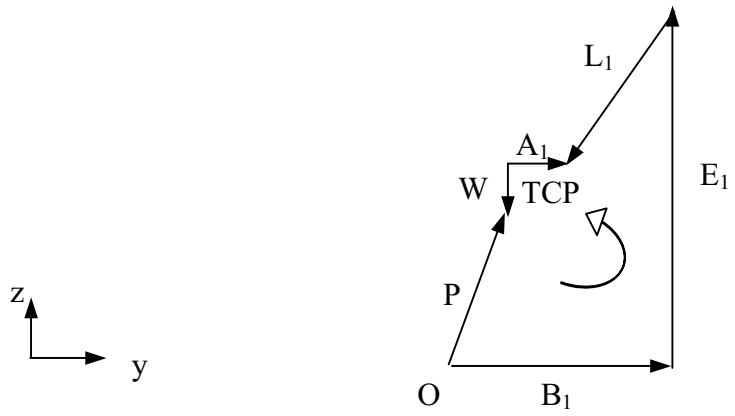

Figure 6-7: The first drive axes vector in y-z plane

The individual vectors are expressed in components to get equation system (6-2). As the ball screws are perpendicular to the x-y plane, the vector $\vec{E}_i$ consists of only one non zero component in z-direction. Furthermore, the base point vectors of the drive axes $\vec{B}_i$ are in x-y plane and, therefore, these z components are zero.

$$\begin{aligned} B_{ix} + 0 + L_{ix} - A_{ix} + W_x - P_x &= 0 \\ B_{iy} + 0 + L_{iy} - A_{iy} + W_y - P_y &= 0 \\ 0 + E_{iz} + L_{iz} - A_{iz} + W_z - P_z &= 0 \end{aligned} \tag{6-2}$$

However, the components of the vectors of L_i are unknown, so they can be expressed in the following equation for L_i and their components.

$$\left|\vec{L}_i\right| = l_i = \sqrt{L^2{}_{ix} + L^2{}_{iy} + L^2{}_{iz}} \tag{6-3}$$

Substituting L_{ix}, L_{iy} and L_{iz} from equation (6-2) into equation (6-3) gives the following relationship between motor displacements and workspace coordinates:

$$E_i = E_{iz} = A_{iz} + P_z - W_z \pm \sqrt{l^2{}_i - \left(A_{ix} + P_x - B_{ix} - W_x\right)^2 - \left(A_{iy} + P_y - B_{iy} - W_y\right)^2} \tag{6-4}$$

The $\pm$ signs of the root testifies that there are two solutions for E_i. In practice, only the solution with the positive root can be hit with the drives.

6.3.2 Forward transformation

The crucial problem of the forward kinematics is the calculation of the moving platform from given strut lenghts. This leads to a system of three nonlinear equations with three variables.
For this kind of the transformation, there are two fundamental methods; one is the analytical solution with direct calculation of the relationship, and the other calculates the coordinates of the TCP by an iterative procedure.

The analytical solution is considerably more extensive in its derivation than the algorithm that is required for the procedure. The following are the equations of the analytical forward transformation:

$$x = z \cdot i + j \tag{6-5}$$

$$y = z \cdot k + l \tag{6-6}$$

$$z = -\frac{i \cdot (j - c_{1x}) + k \cdot (l - c_{1y}) - c_{1z}}{i^2 + k^2 + 1} \pm \sqrt{\frac{\left[i \cdot (j - c_{1x}) + k \cdot (l - c_{1y}) - c_{1z}\right]^2 - (i^2 + k^2 + 1) \cdot \left[(j - c_{1x})^2 + (l - c_{1y})^2 + {c_{1z}}^2 - {L_1}^2\right]}{(i^2 + k^2 + 1)^2}} \tag{6-7}$$

$$i = -\frac{(c_{2z} - c_{1z}) \cdot (c_{3y} - c_{2y}) - (c_{3z} - c_{2z}) \cdot (c_{2y} - c_{1y})}{c_{1x} \cdot (c_{2y} - c_{3y}) + c_{2x} \cdot (c_{3y} - c_{1y}) + c_{3x} \cdot (c_{1y} - c_{2y})} \tag{6-8}$$

$$j = -\left[\frac{(c_{2z} - c_{2y}) \cdot ({c_{1x}}^2 + {c_{1y}}^2 + {c_{1z}}^2 - {L_1}^2 - {c_{2x}}^2 - {c_{2y}}^2 - {c_{2z}}^2 + {L_2}^2)}{2 \cdot (c_{1x} \cdot (c_{2y} - c_{3y}) + c_{2x} \cdot (c_{3y} - c_{1y}) + c_{3x} \cdot (c_{1y} - c_{2y}))}\right] - \left[\frac{(c_{2y} - c_{1y}) \cdot ({c_{2x}}^2 + {c_{2y}}^2 + {c_{2z}}^2 - {L_2}^2 - {c_{3x}}^2 - {c_{3y}}^2 - {c_{3z}}^2 + {L_3}^2)}{2 \cdot (c_{1x} \cdot (c_{2y} - c_{3y}) + c_{2x} \cdot (c_{3y} - c_{1y}) + c_{3x} \cdot (c_{1y} - c_{2y}))}\right] \tag{6-9}$$

$$k = -\frac{(c_{2z} - c_{1z}) \cdot (c_{3x} - c_{1x}) - (c_{3z} - c_{1z}) \cdot (c_{2x} - c_{1x})}{c_{1x} \cdot (c_{3y} - c_{2y}) + c_{2x} \cdot (c_{1y} - c_{3y}) + c_{3x} \cdot (c_{2y} - c_{1y})} \tag{6-10}$$

$$l = -\left[\frac{(c_{3x} - c_{1x}) \cdot ({c_{1x}}^2 + {c_{1y}}^2 + {c_{1z}}^2 - {L_1}^2 - {c_{2x}}^2 - {c_{2y}}^2 - {c_{2z}}^2 + {L_2}^2)}{2 \cdot (c_{1x} \cdot (c_{3y} - c_{2y}) + c_{2x} \cdot (c_{1y} - c_{3y}) + c_{3x} \cdot (c_{2y} - c_{1y}))}\right] - \left[\frac{(c_{2x} - c_{1x}) \cdot ({c_{1x}}^2 + {c_{1y}}^2 + {c_{1z}}^2 - {L_1}^2 - {c_{3x}}^2 - {c_{3y}}^2 - {c_{3z}}^2 + {L_3}^2)}{2 \cdot (c_{1x} \cdot (c_{3y} - c_{2y}) + c_{2x} \cdot (c_{1y} - c_{3y}) + c_{3x} \cdot (c_{2y} - c_{1y}))}\right] \tag{6-11}$$

$$c_{ix} = B_{ix} - A_{ix} \tag{6-12}$$

$$c_{iy} = B_{iy} - A_{iy} \tag{6-13}$$

$$c_{iz} = E_i - B_{iz} - A_{iz} \tag{6-14}$$

With these equations, the x, y and z coordinates of the TCP in the workspace of the machine are calculated. The machine coordinates, besides the numerous geometry parameters, are the input parameters for these equations.

The approximation procedures is the standard procedure for the solution of multi dimensional nonlinear equation systems. The Jacobi Matrix is required for it, which is obtained by the partial differential equation. The iteration rule of the method is to calculate the value for the next iteration step:

$$P_{s+1} = P_s - J^{-1}(P_s) \cdot f(P_s) \tag{6-15}$$

In this formula, J^{-1} (P_s) is the Inverse of the Jacobi matrix. The Jacobi matrix contains the partial equation of the polynomial form of the transformation equation for the inverse transformation, which is given in equation 6-4. P_s marks the current point and the point of the next iteration step is P_{s+1}. The Jacobi matrix is fully written out as follows:

$$J = \begin{pmatrix} f_1'(P_x, P_y, P_z) \\ f_2'(P_x, P_y, P_z) \\ f_3'(P_x, P_y, P_z) \end{pmatrix} = \begin{pmatrix} \frac{\partial f_1}{\partial P_x} & \frac{\partial f_1}{\partial P_y} & \frac{\partial f_1}{\partial P_z} \\ \frac{\partial f_2}{\partial P_x} & \frac{\partial f_2}{\partial P_y} & \frac{\partial f_2}{\partial P_z} \\ \frac{\partial f_3}{\partial P_x} & \frac{\partial f_3}{\partial P_y} & \frac{\partial f_3}{\partial P_z} \end{pmatrix} = \tag{6-16}$$

$$2.\begin{pmatrix} P_x + (A_{1x} - B_{1x})^2 & P_y + (A_{1y} - B_{1y})^2 & P_z + A_{1z} - E_1 \\ P_x + (A_{2x} - B_{2x})^2 & P_y + (A_{2y} - B_{2y})^2 & P_z + A_{2z} - E_2 \\ P_x + (A_{3x} - B_{3x})^2 & P_y + (A_{3y} - B_{3y})^2 & P_z + A_{3z} - E_3 \end{pmatrix}$$

6.4 Experimental tests

In order to study the response of position controlled feed drives, the contour error must be measured. In addition to the characteristics of transfer elements, their steady state and dynamic response is responsible for the accuracy performance of the machine.

6.4.1 Star test

The experimental measurement of star contours consists of two items: orientations and straight line motions with which servo dynamic effects in varying orientations are measured.

6.4.1.1 Measurement device

A schematic of the linear measurement instrument in x-y plane is shown in Figure 6-8. This instrument consists of a straightedge, a displacement sensor adapted to the end effector, display and PC. The contour error can be measured by positioning a rotary table carrying the straightedge at different angles.

The measuring sensor is one of the main sensitive component of the measuring system. It is a precision transducer (Millimar Inductive Probe 1318 Mahr-LVDT) whose displacement can be measured over a travel of approximately ± 1 mm around its nominal state. The digital reading can be set to 0.1 μm resolution.

The transducer provides electrical signals and then transforms the analog signal to the digital form over time. The results are converted electronically into a form which can be read by

computer software. This allows minute changes in the transducer's nominal state to be measured and analysed.

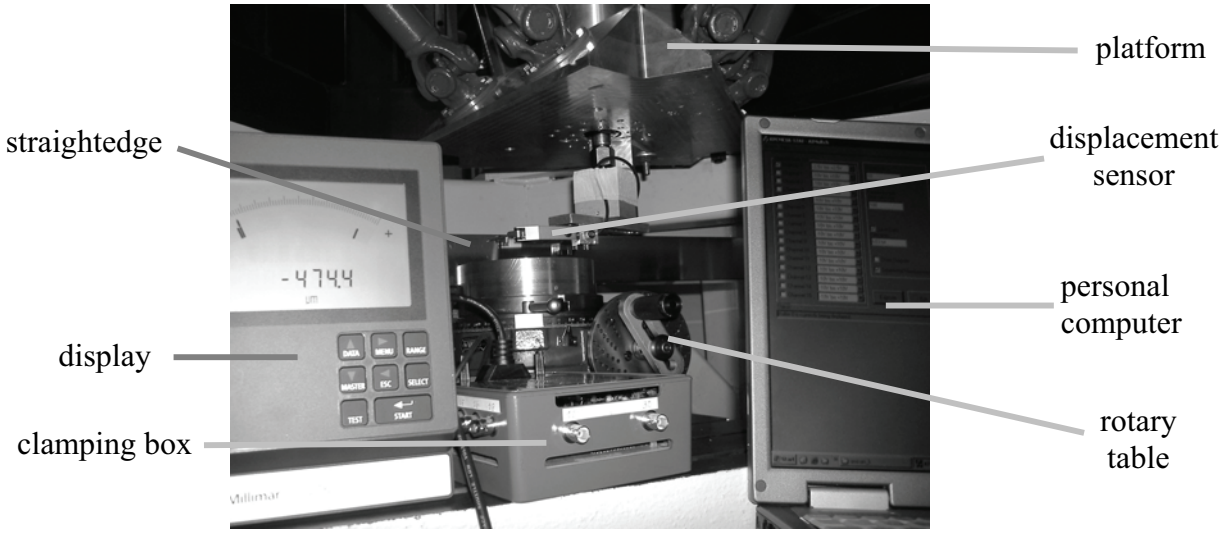

Figure 6-8: Details of star measuring system

The sensor interface contains an electronic card, which tracks the transducer changes and then transfers data readings to the computer.

The software samples the data readings from the sensor interface with a maximum of 100 readings per second.

The measuring sensor touches the straightedge, which is fixed, and the sensor moves with the TCP, Figure 6-9.

As the straightedge is a linear reference for straight line trajectory in different orientations, the path is referred to the setpoint contour.

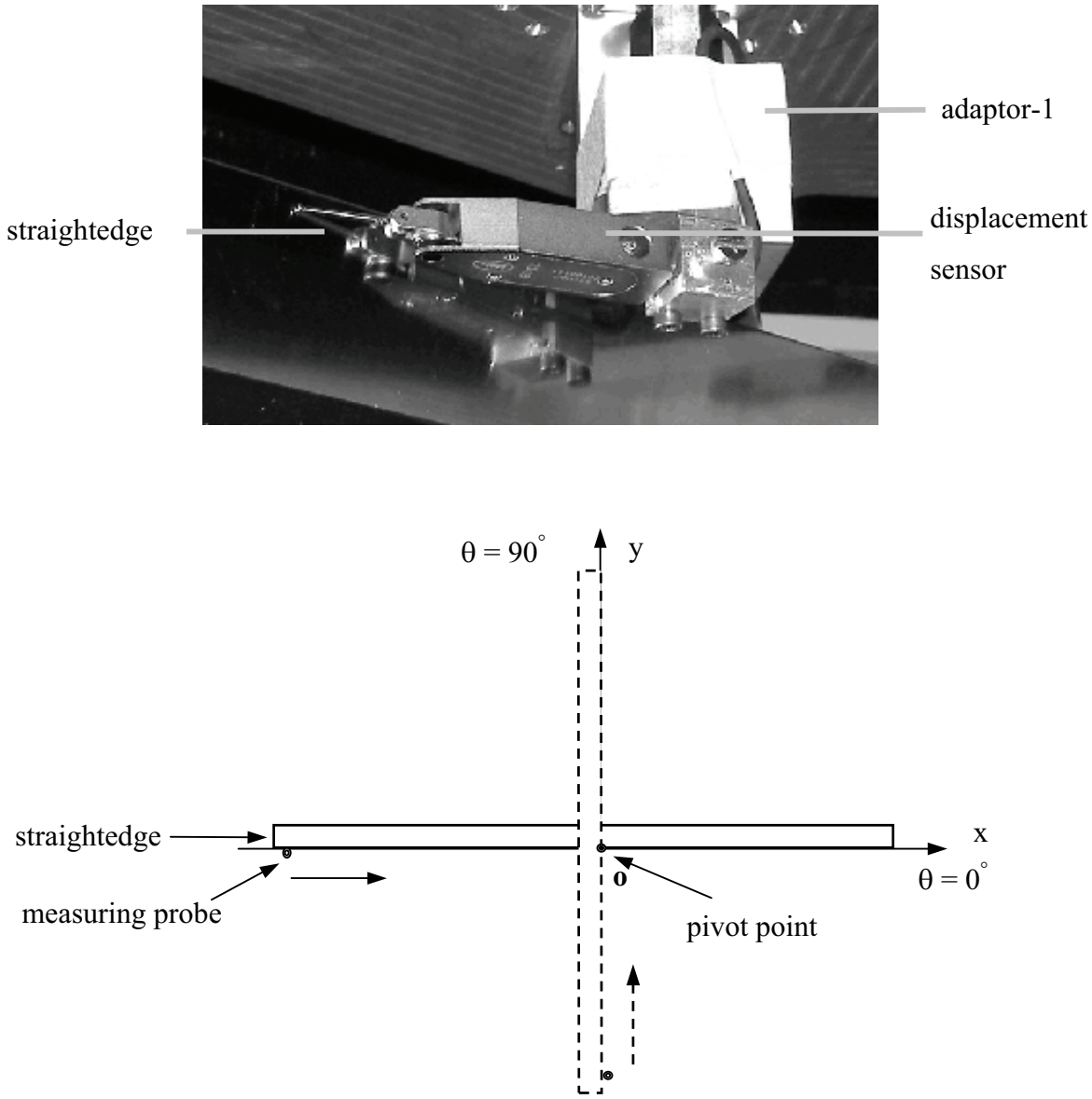

Figure 6-9: Measuring sensor and straightedge

Adaptor-1 is designed as a holder of measuring sensor and fixed to the platform. With the rotary table mounted on the machine table, the holder of straightedge is centered around the axis of the rotary table, which in turn is centered around the cutting tool's axis or TCP. The rotary table and TCP are aligned the axes of rotation. Figure 6-10 shows the schematic of alignment setting.

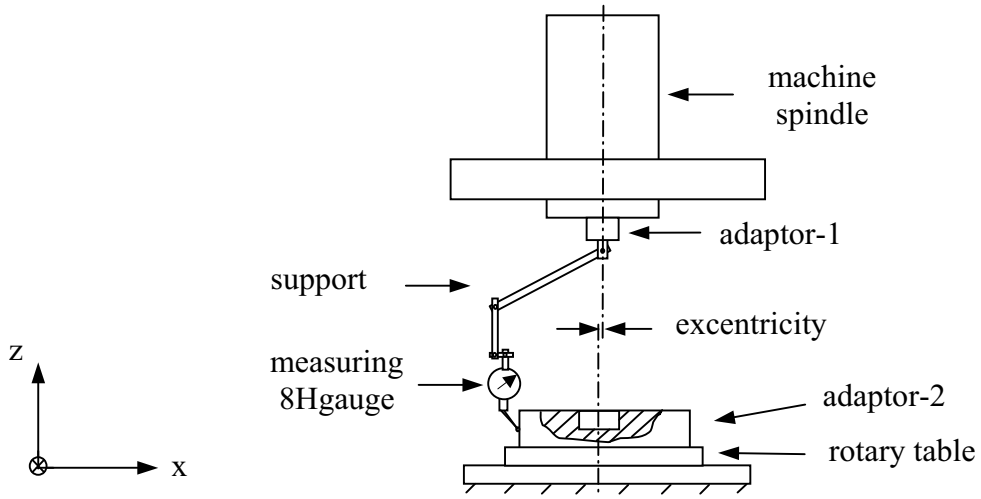

Figure 6-10: Rotary table and TCP settings

This setting consists of a support and measuring indicator. The alignment can be achieved using trial and error approach.

This allows concentric measuring operations during the star test and then obtains dynamic measuring contour error with the alignment of the rotational axes in different orientations.

6.4.1.2 Measuring strategy

Dynamic deviation, known as contour error, is measured by the above described principle. Dynamic measurements, especially at high traverse speeds, provide information on contouring behavior that permits conclusions on the conditions of the control loop.

As the straightedge is the trajectory reference, the measurement is completed with consideration of geometry and assembly errors. Static measurements are deviations of the straightedge reference and static position errors in TCP and due to assembly, permitting conclusions exclusively on the geometric accuracy of the trajectory.

The difference between indicator value in high and slow speed motion indicates how much the generated contour value lags behind the setpoint value.

To evaluate the measured data effectively, the setpoint path is divided into four intervals, from start to stop point, which are termed as intervals a, b, c and d, respectively, as indicated in Figure 6-11. In the Figure, x and y are measuring coordinates and x denotes direction of TCP motion.

The main part intervals on machine response is b and only in this part the sensor can measure the deviations. The path length is 200 mm from –100 mm to +100 mm. In each measurement, servo tracking error is calculated by comparing the dynamic and static deviations.

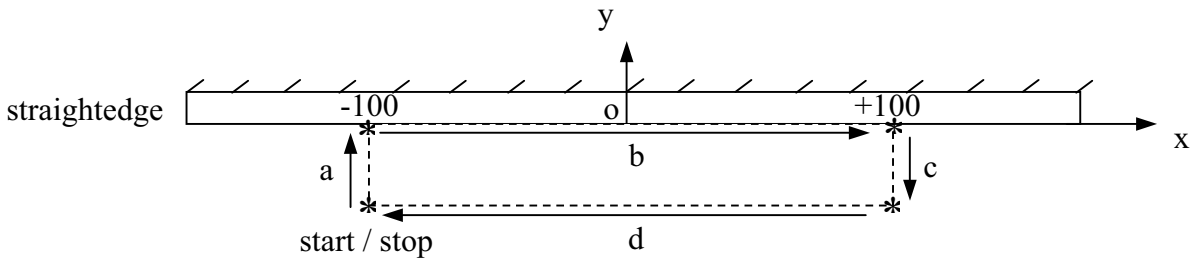

Figure 6-11: Setpoint trajectory, top view

The measuring method is illustrated in Figure 6-12, that contains static and dynamic errors. The static error occurs at a low feed rate of operation.

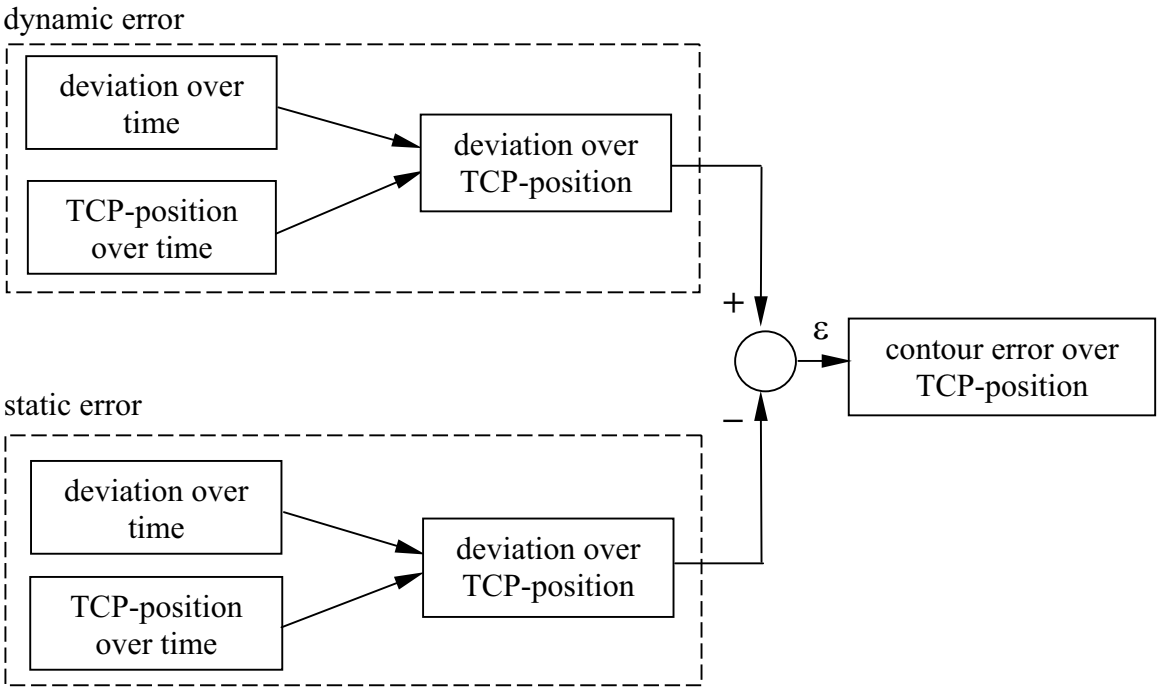

Figure 6-12: Measuring strategy of contour error in straightline path of the Tripod

The deviation over time is measured and TCP-position over time is measured by external laser interferometer device. Within the measuring results and resampling, the deviation over TCP-position is obtained.

Figure 6-13 shows the difference between dynamic and static measurement over TCP-position that means actual contour error originated from servo tracking error in orientation $\theta=0°$ of TCP at feed rate 9000 $^{mm}/_{min}$.

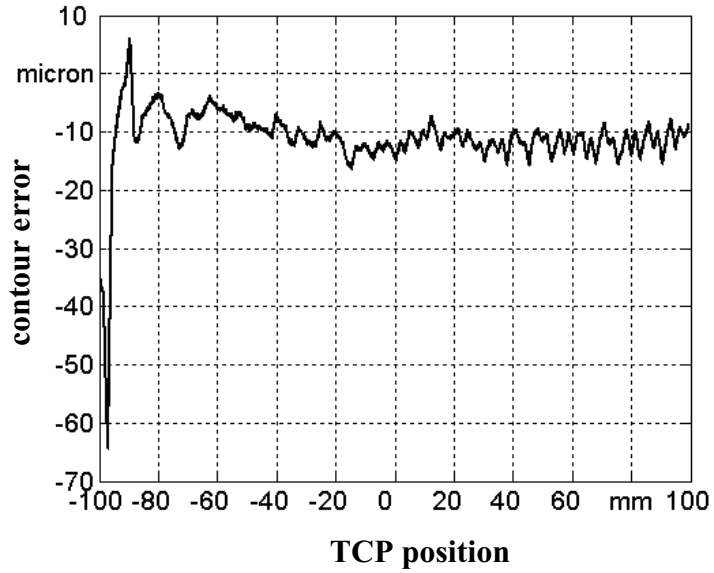

Figure 6-13: Servo contour error at feed rate$_{TCP}$=9000 $^{mm}/_{min}$

In the measurement results at start and stop, there are effects of acceleration, decceleration and vibration. After neglecting the start and stop area, contour error is mean value of remaining data.

Straight lines in the workspace are traced with varying orientations, where pivot points positioned in the center of TCP, Figure 6-14. When this test is performed with a SKM the setpoint trace is perfectly fitted as the velocity gains are equal in the interpolating axes x and y. With the Tripod, this behavior can only be observed when the straight line motion is performed in the directions where the drive axes are positioned (45°, 165° and 285°). In all other directions, the distance between the setpoint and the TCP is almost constant indicating different K_V values in x- and y-direction, Figure 6-14. Although velocity gains are constant in the drive controllers, they are transformed by the machine kinematics resulting in nonconstant values in the Cartesian space.

Furthermore, in perpendicular axes with different K_V values, the deviations straight line motion occur on both sides of the path depending on the travel direction. In contrast, there is no hysteresis in the Tripod motion when the direction of motion is inverted. The hysteresis is converted to a one sided deviation by the reversal gain transform effect described above.

As shown in the measured results, the deviations in -15° to 45° appear right sided and in 45° to 105° appear left sided, Figure 6-14.

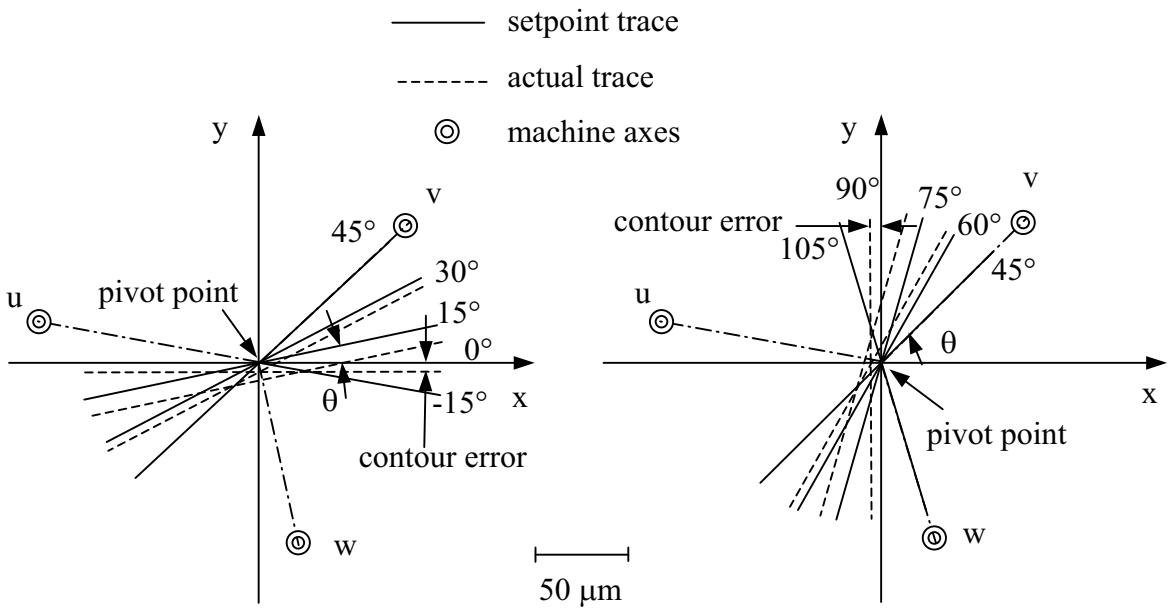

Figure 6-14: Zoom of top view on simulated and measured actual traces in a planar star test

The results at TCP feed rates of 6000 $^{mm}/_{min}$ and 9000 $^{mm}/_{min}$ are compared in figure 6-15. This represents mean values and standard deviations of contour error in a planar star test from five measurement data. As there is vibration in 15° and 90° at 9000 $^{mm}/_{min}$ feed rate, it is not possible to measure the error. The results clearly show that the deviations are a function of orientation and feed rate [KUH08-1].

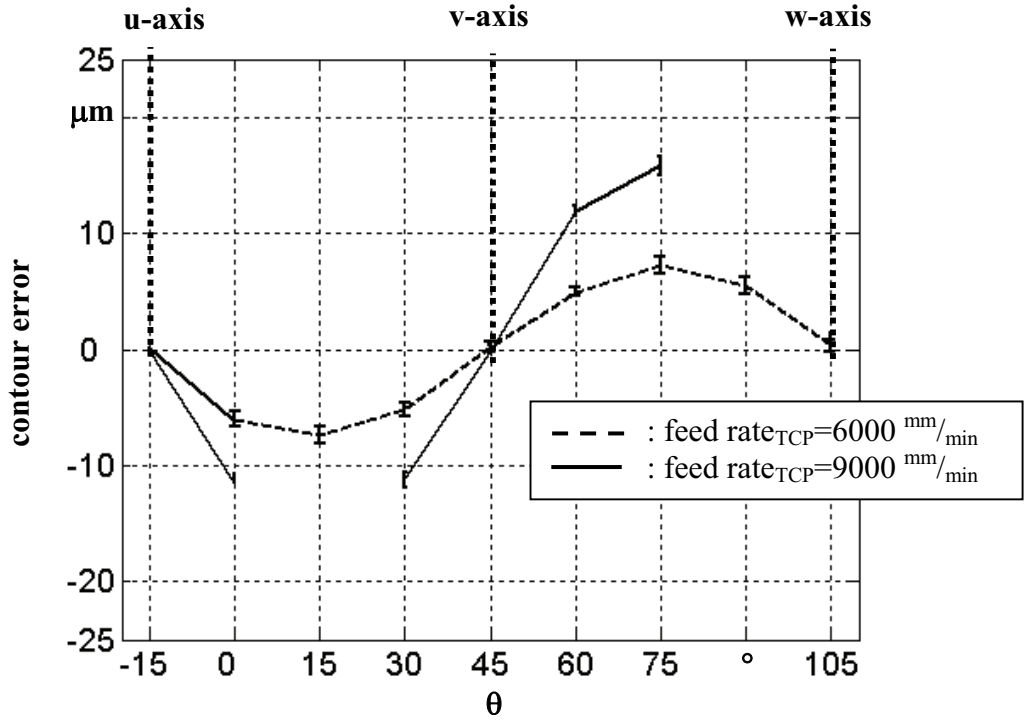

Figure 6-15: Measured contour error in a planar star test

In the following star tests with different pivot points are compared, Figure 6-16.

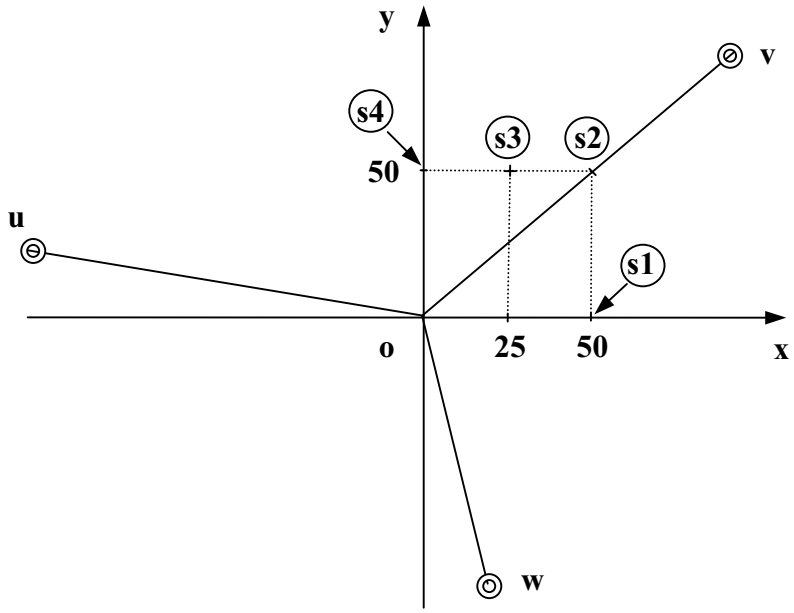

Figure 6-16: Different center points in workspace

Figure 6-17 and 6-18 show the measured results of star tests with different pivot points at feed rates of TCP of 6000 $^{mm}/_{min}$ and 9000 $^{mm}/_{min}$ respectively.

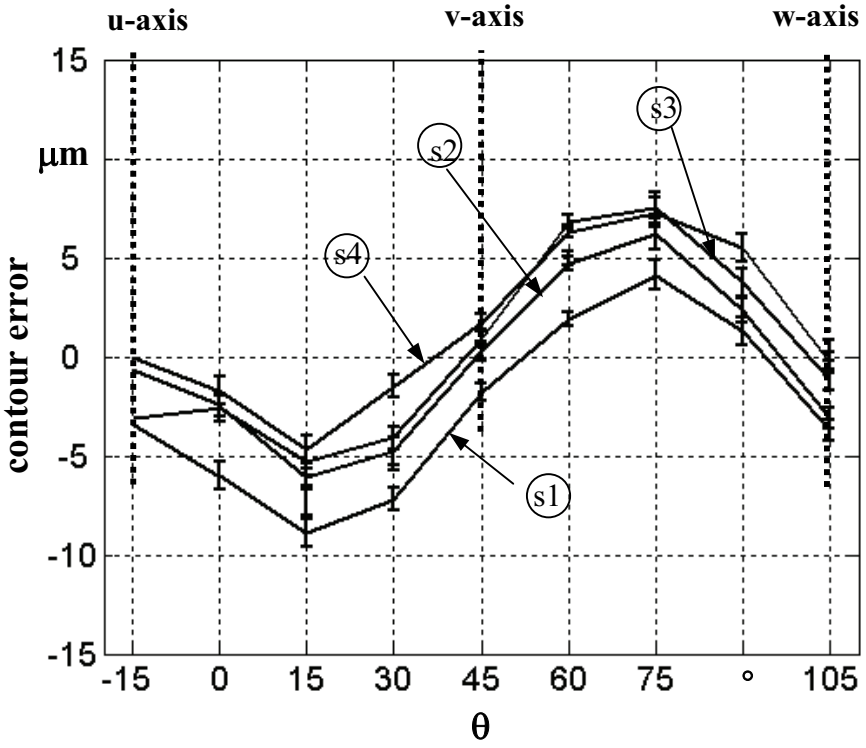

Figure 6-17: Measured contour error at feed rate$_{TCP}$=6000 $^{mm}/_{min}$

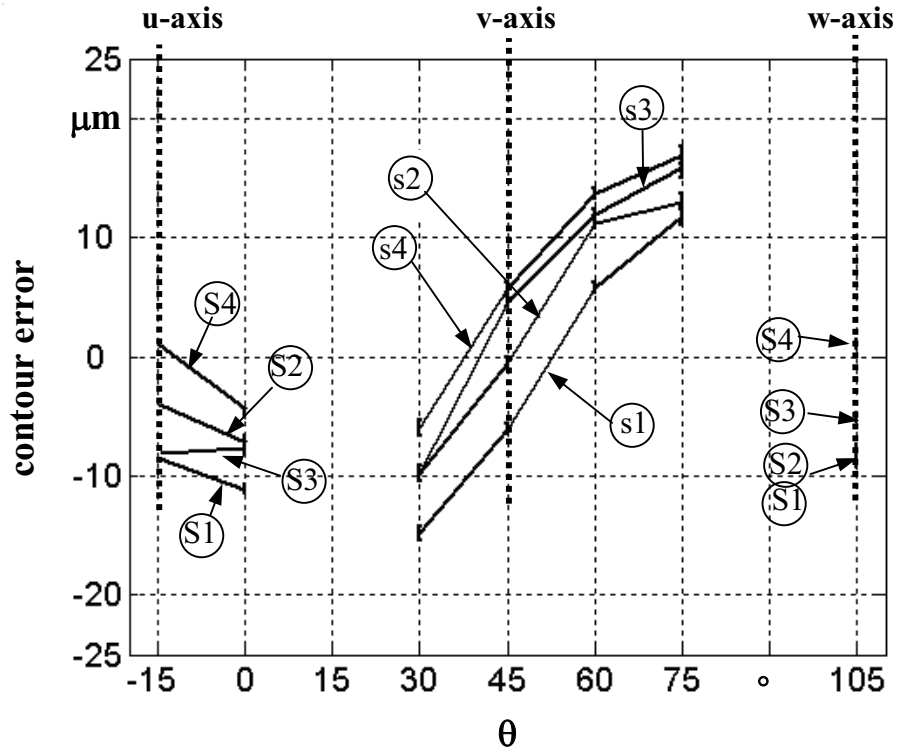

Figure 6-18: Measured contour error at feed rate$_{TCP}$=9000 $^{mm}/_{min}$

6.4.2 Circular test

Measurements were carried out tracking a 100 mm circular radius centered on the machine at a feed rate of 3000 $^{mm}/_{min}$, in both clockwise and counter clockwise directions. The circularity error plot resulting from the experiment, as shown in Figure 6-19, indicates that the shape of the plot exhibits 3 prominent buckles with opposite direction to the drive axis locations at 105°, 225° and 345°.

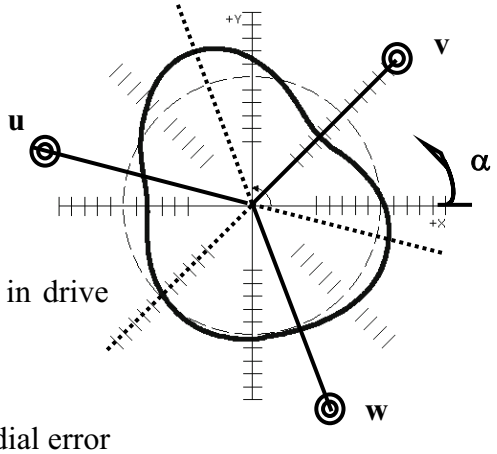

◎: top view of position in drive

100 μm/div

Figure 6-19: Measuring radial error

When a circular shape is commanded, the radius of the actual path becomes smaller than the commanded one because of a delay in the servo response of each axis. As in SKM, radial deviation is defined as the difference between the programmed radius and actual radius. A smaller radial reduction represents a higher tracking ability.

6.5 Simulation model

The motion of each axis is generated by the inverse transform of workspace coordinates. Actual trajectory is obtained from forward transformation of actual position of the drive. Here, the simulated results of linear trajectory in different orientations (star test) and circular trajectory are presented.

6.5.1 Star test

Simulation of the star test, centered with respect to the Tripod, is performed for a given two axis linear trajectory in x-y plane, with a length of ± 100 mm along workspace of the machine, and with varying orientations and feed rates.

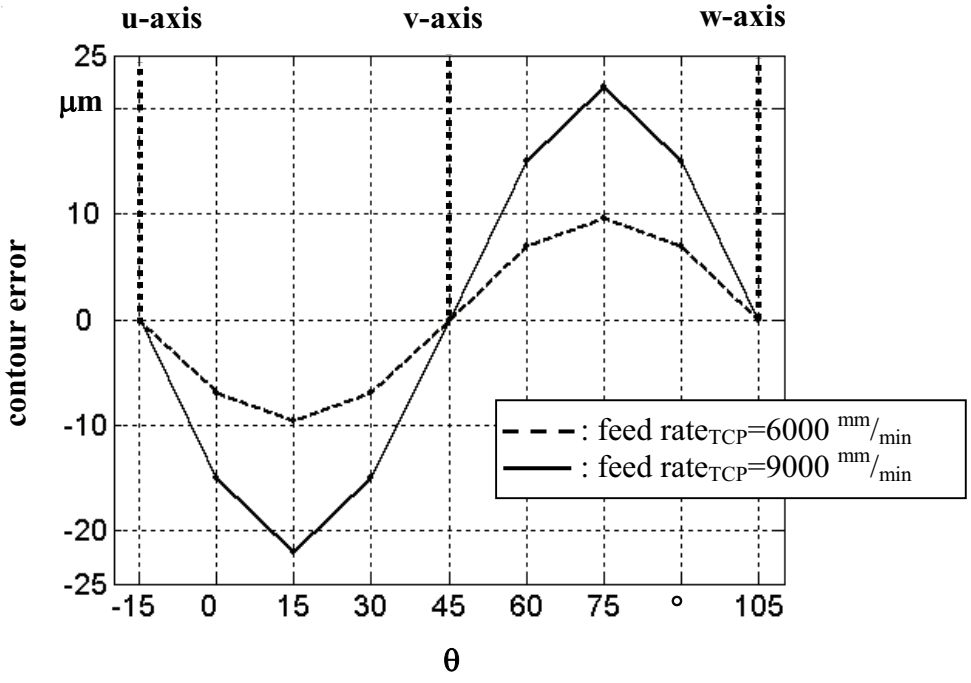

Figure 6-20: Simulated contour error in a planar star test

Contour error is calculated by formula (5-20) and (5-21) and results are presented in Figure 6-20. Simulated contour erorr of star tests, virtually performed with a Tripod with constant velocity gain in the drive controllers as parameter are faced to measured ones.

In the following, star tests with different pivot points are compared. Figure 6-21 and 6-22 show the simulated results at feed rates of TCP of 6000 $^{mm}/_{min}$ and 9000 $^{mm}/_{min}$, respectively.

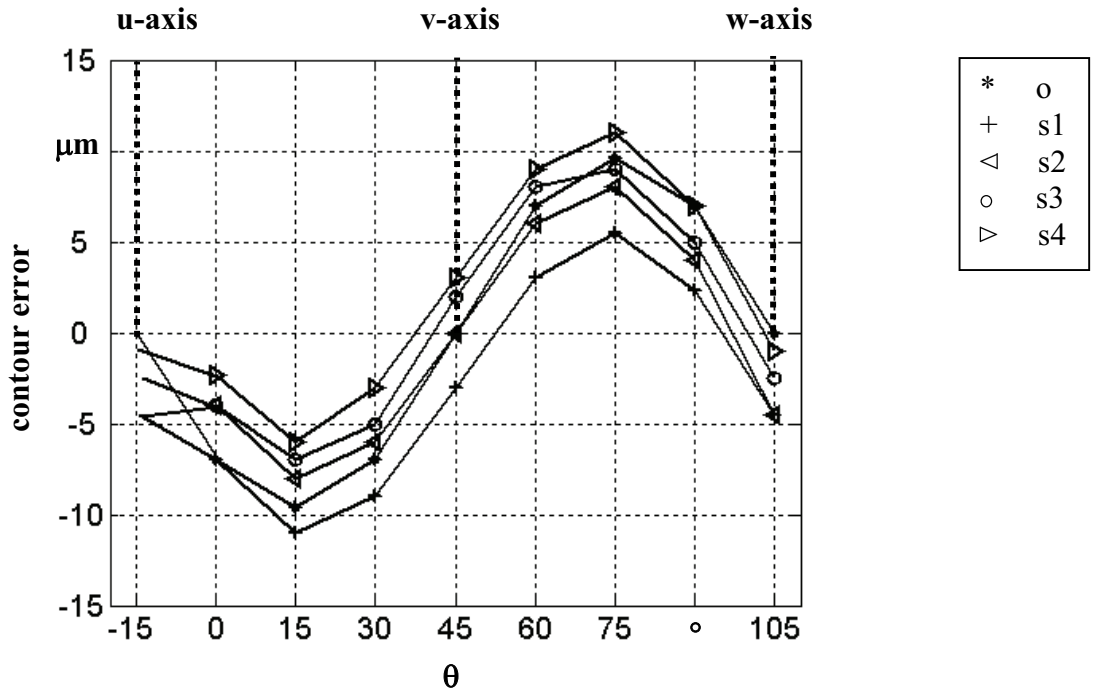

Figure 6-21: Simulated contour error feed rate$_{TCP}$=6000 $^{mm}/_{min}$

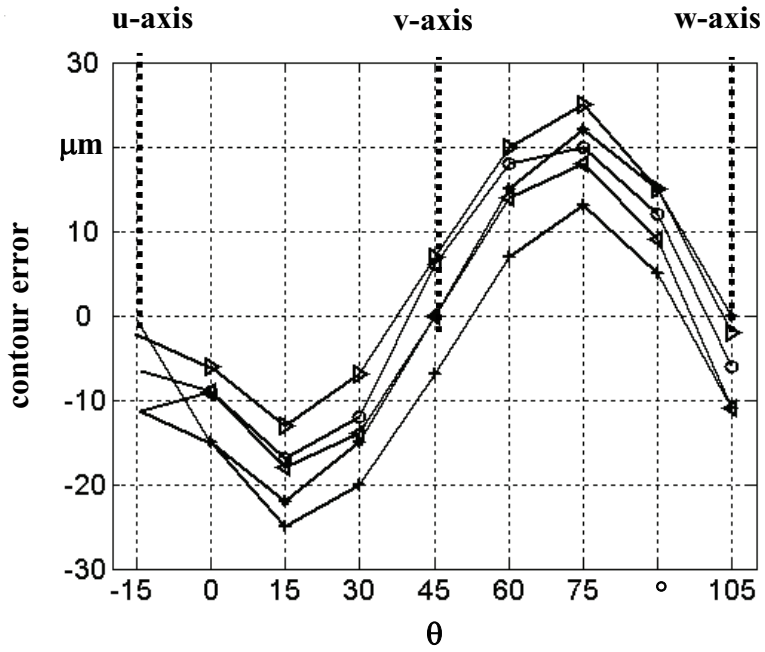

Figure 6-22: Simulated contour error feed rate$_{TCP}$=9000 $^{mm}/_{min}$

The results illustrate that the contour error in star test with pivot point o at 45° is zero, but it occurs for pivot point s1 at the orientation 52° and for pivot point s4 at the orientation 38°.

6.5.2 Circular contour

Simulation is carried out for a circle with a radius of 100 mm, centered with respect to the Tripod, at a feed rate of 3000 $^{mm}/_{min}$.

The radial deviation is calculated with Equation (5-26) using a geometric approach, Figure 6-23.

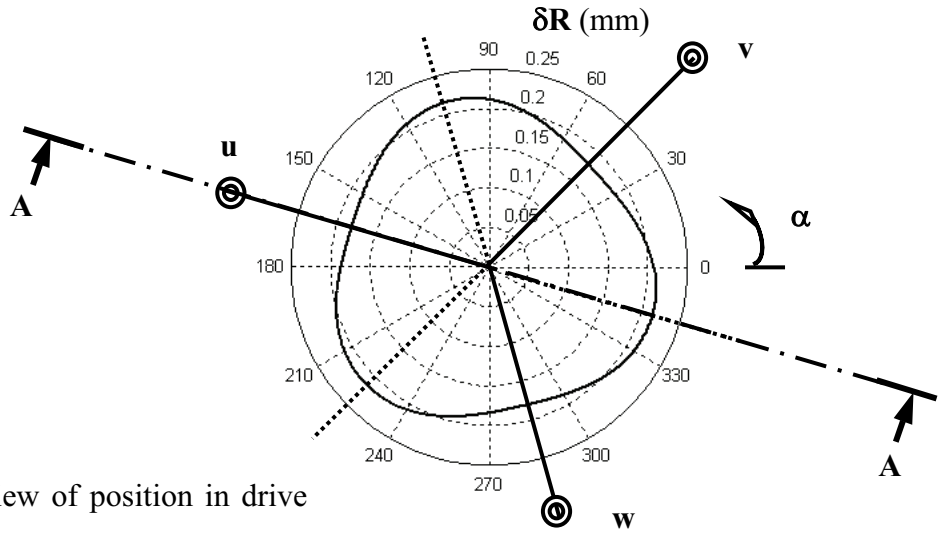

Figure 6-23: Simulated radial deviation in Tripod

In SKM, the performed radius is always smaller than the nominal radius but constant with constant feed rate along the whole circular path. In contrast, in Tripod, the actual radius is smaller than the nominal radius but not constant. During the circle trace the radial error is a function of angular position.

δR shows three prominent extrema, Figure 6-23. This deviation occurs in opposite direction to each machine axis at 105°, 225° and 345° of circle path. Figure 6-24 shows the view A-A from Figure 6-23, indicating positioning of strut u in extremum radial deviation of circle contour.

When the strut changs direction (Figure 6-24-b) in these positions, the velocity of the strut is zero (Figure 6-24-c). On the other hand, when the constant length strut is most horizontal ($\beta_2 > \beta_1$), (Figure 6-24-d), the generated radius at this point is shortest and the resulting radius error is highest.

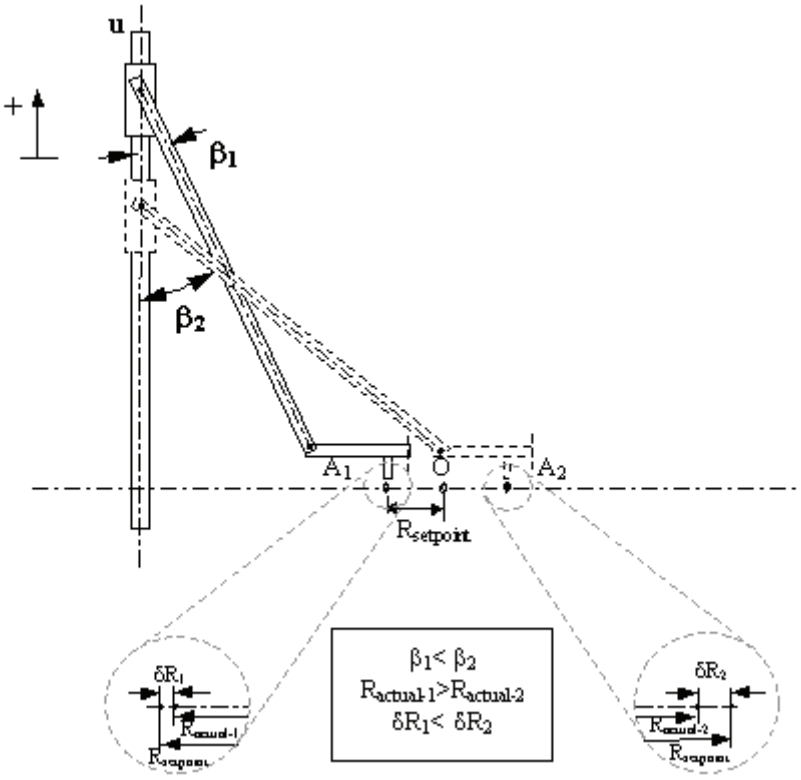

a) view A-A

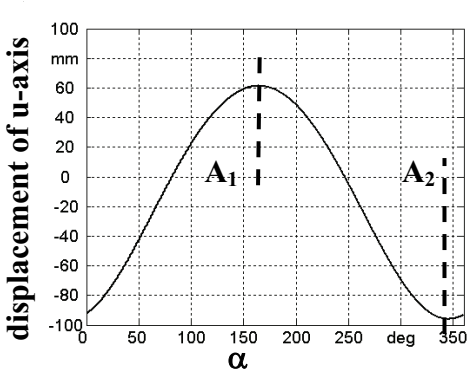

b) position of u-axis

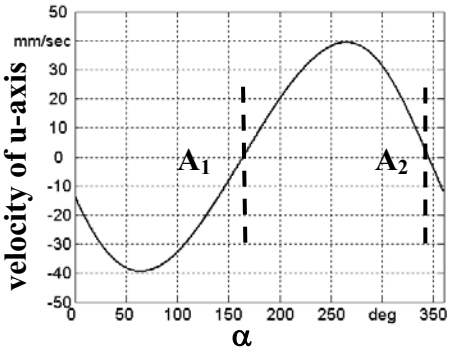

c) velocity of u-axis

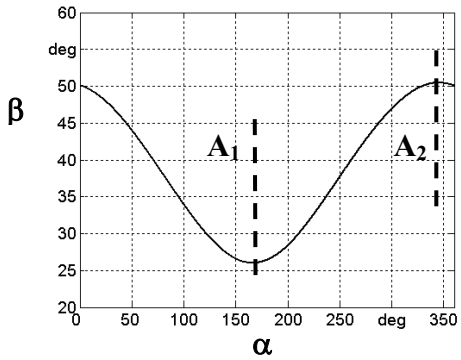

d) angle of strut jointed in u-axis

Figure 6-24: Status of u-axis in circular trajectory in Tripod

The effect of β in each strut on contour error is indicated in Figure 6-25. Maximum and minimum radial deviation are significantly related to β on each machine axis.

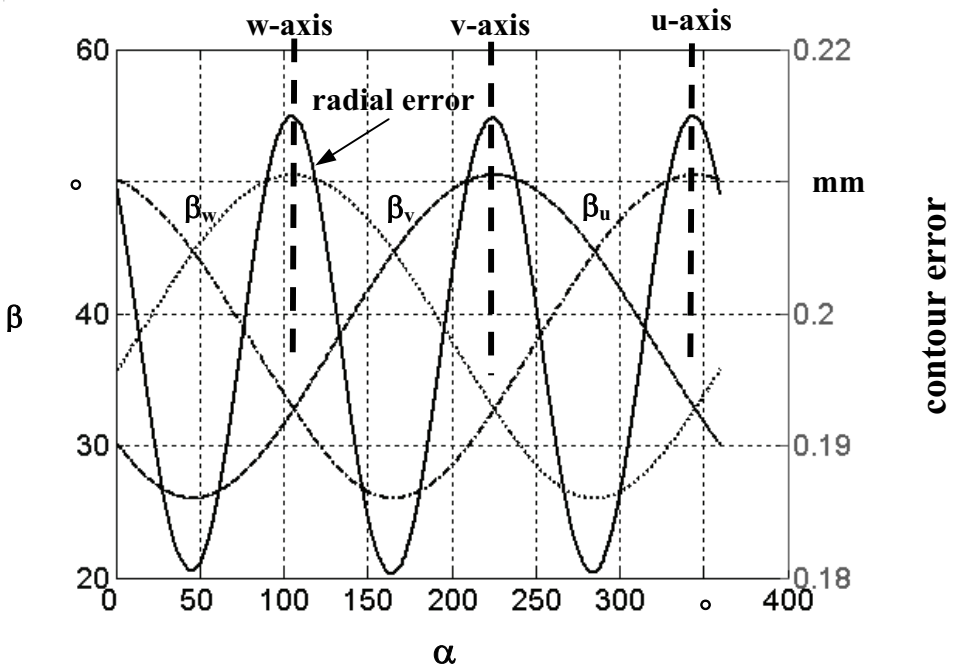

Figure 6-25: Relationship between contour error and angle struts

Figure 6-26 shows the relationship between contour error and velocity in joint space. An extremum occurs in the contour error when the axes velocities are near to zero and the velocity changes are highest.

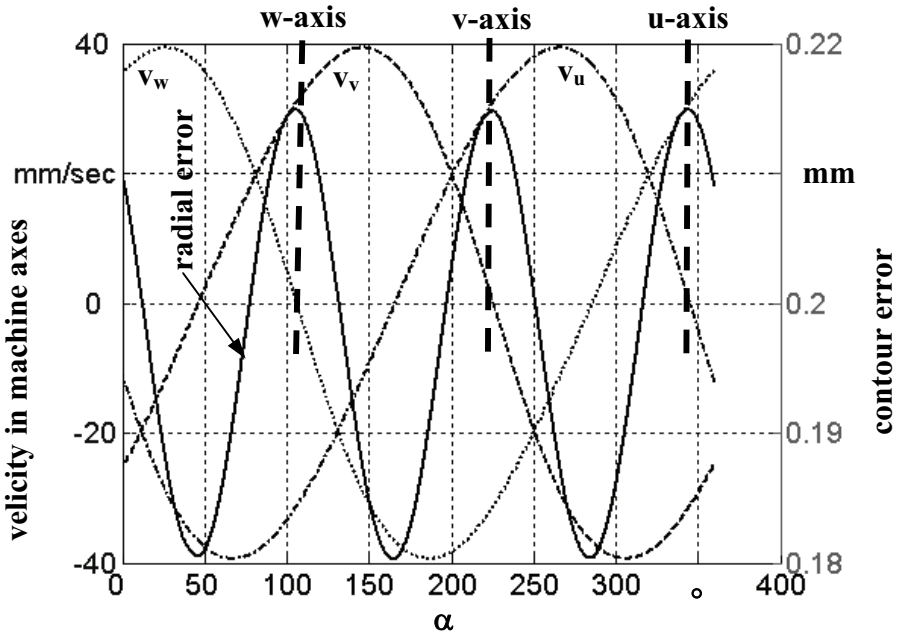

Figure 6-26: Relationship between contour error and velocity in joint space in circular

A schematic of center points of simulated circle trajectories are demonstrated in Figure 6-27.

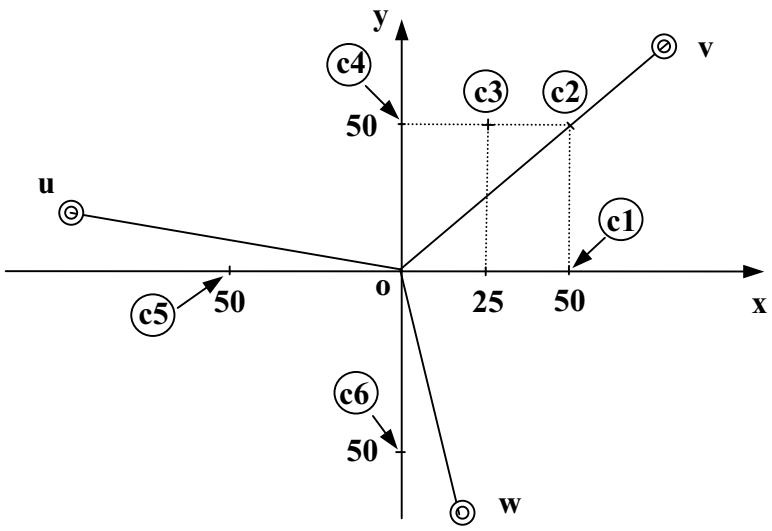

Figure 6-27: Different center point in workspace

Circularity is defined as the difference between the largest and smallest radius. Circularity at different radius and center points at a feed rate of TCP =3000 $^{mm}/_{min}$ is illustrated in Figure 6-28. An increase in the circle radius results in reduction of the extremum (both maximum and minimum deviation) and also increase the circularity.

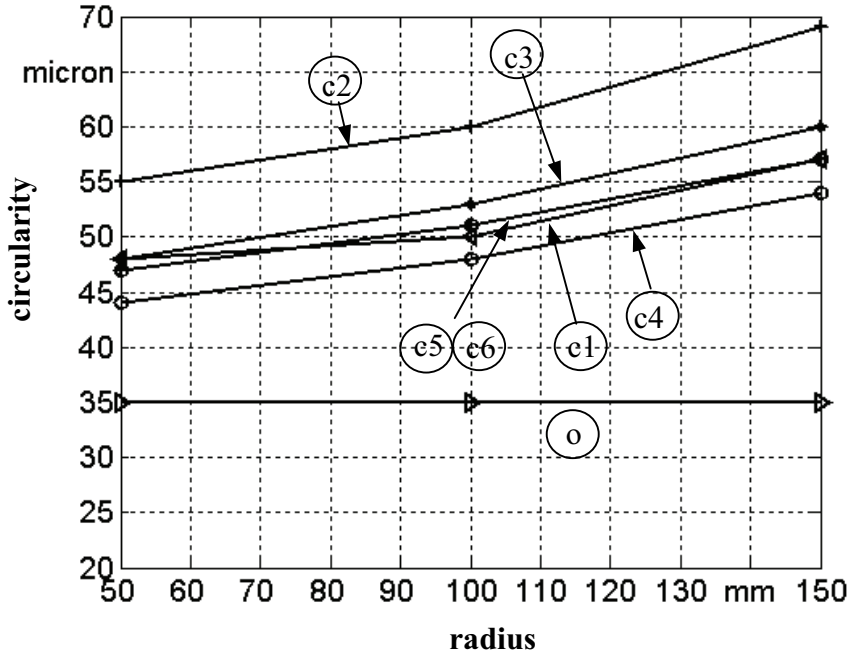

Figure 6-28: Circular test in different radius

Results of circular test with radius=100 mm at different velocities and center points are illustrated in Figure 6-29.

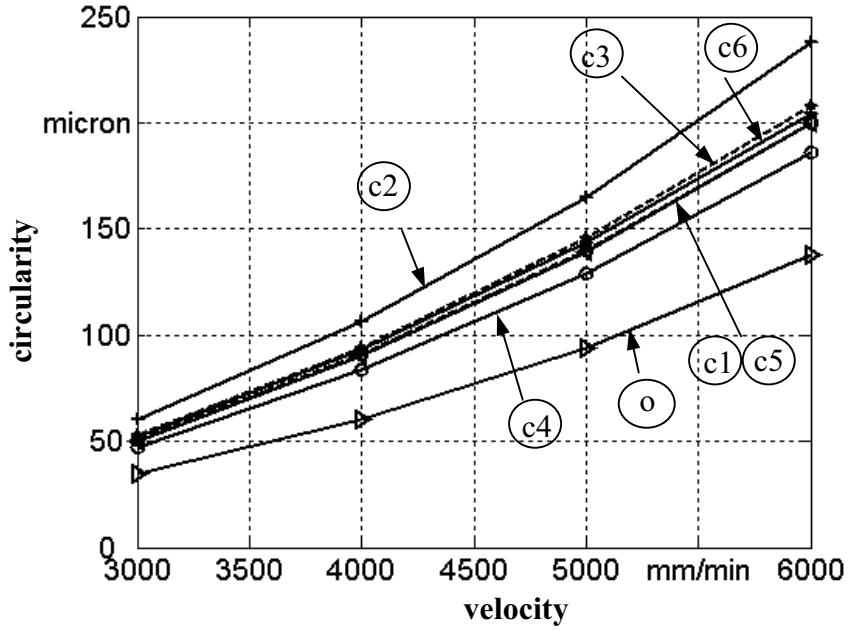

Figure 6-29: Circular test in different velocities

Figure 6-28 and Figure 6-29 indicate that the accuracy of circle contour is a non linear function of β for each machine axes and velocity.

In Figure 6-30, a comparison of the measured and simulated radial deviation is shown and this reveals a high degree of similarity. The differences are determined by a tilting effect of the end effector platform.

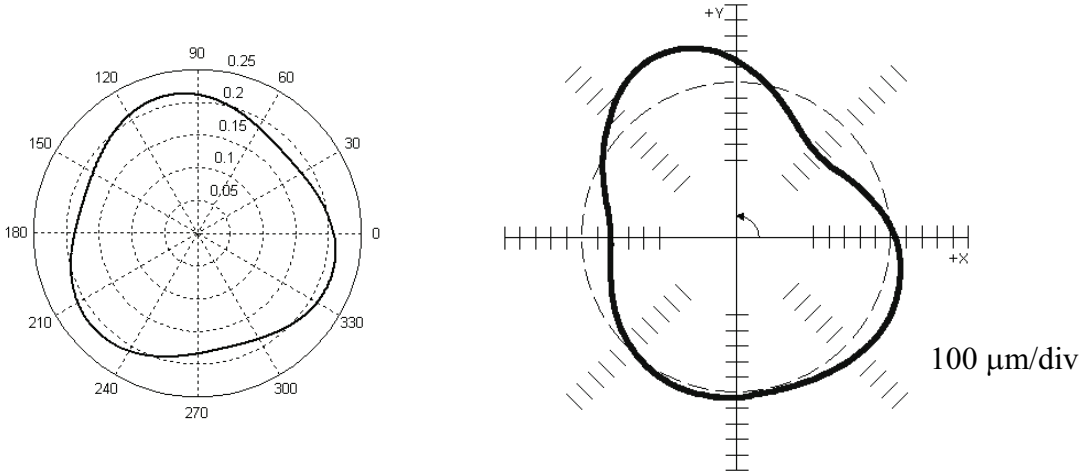

Figure 6-30: Radial deviation, simulation (left), measurement (right)

The tilting of actual platform in x- and y-direction is measured, Figure 6-31. The measured results show that the tilting angle of platform during motion in x-direction over y-axis is positive, and the angle during motion in y-direction over x-axis is negative. With comparison

of platform motion in x- and y-direction that is $R_{actual\text{-}x} > R_{actual\text{-}y}$ and consequently $\delta R_x < \delta R_y$. Thus, the measured radial deviation in x-direction is smaller than y-direction.

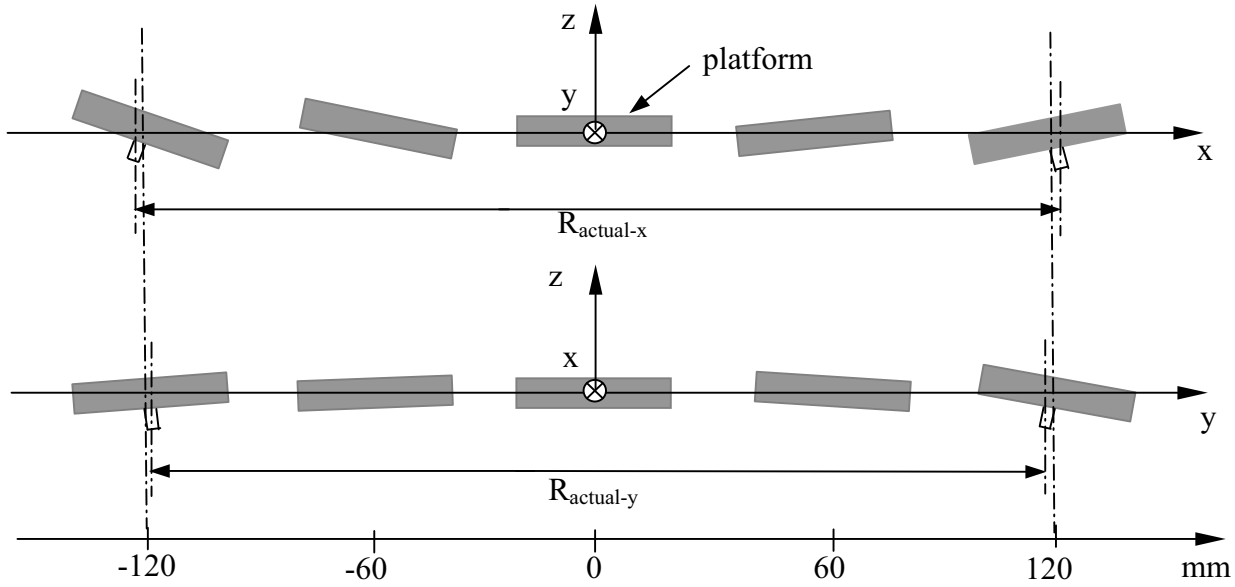

Figure 6-31: Tilting of platform in x- and y-direction

6.6 The effect of mismatches the K_V factors

The main precondition for a setpoint accurate contouring is that both the feed axes must have the same command response characteristics. Not only the K_V factors and the setpoint delays must be the same, but also the dynamic characteristic values such as response time, settling time as well as the command frequency response with amplitude and phase response in the position and the speed control loop must match. In case that drives with different size of axes are used, some difficulties may occur which must be reduced by appropriate controller parameter settings. In straight line motion, if the velocity gains are not equal, a deviation arises due to parallel offset of the actual path in comparison to the commanded path. Curved contours are always prone to dimensional errors, whose value is inversely proportional to the K_V factor. Different K_V factors or different dynamic characteristics of the axes involved in the motion cause additional errors, which increase as the contouring feed rate increases.

Indeed, to follow a straight line in a plane, the motion of the two requested axes must be coordinated to avoid any contour error.

The contour error is expressed according to Figure 6-32 notations in the form

$$ce = \Delta y \cdot \cos\theta - \Delta x \cdot \sin\theta \tag{6-17}$$

In straight line with constant velocity, with using the correlation between tracking error and

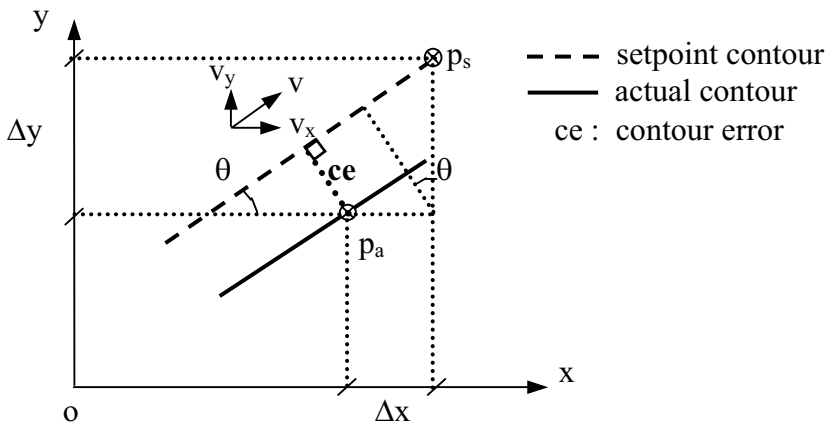

Figure 6-32: Contouring error in straight line interpolation [BEA04]

velocity gain in each axes:

$$\Delta x = \frac{\mathbf{v}_x}{K_{Vx}} = \frac{\mathbf{v} \cdot \cos\theta}{K_{Vx}} \tag{6-18}$$

$$\Delta y = \frac{\mathbf{v}_y}{K_{Vy}} = \frac{\mathbf{v} \cdot \sin\theta}{K_{Vy}} \tag{6-19}$$

Substitute (6-18) and (6-19) into (6-17) to obtain

$$ce = \frac{\mathbf{v} \cdot \sin\theta}{K_{Vy}} \cdot \cos\theta - \frac{\mathbf{v} \cdot \cos\theta}{K_{Vx}} \cdot \sin\theta \tag{6-20}$$

or

$$ce = \mathbf{v} \cdot \frac{\sin(2\theta)}{2} \cdot \left(\frac{1}{K_{Vy}} - \frac{1}{K_{Vx}}\right) = \mathbf{v} \cdot \frac{\sin(2\theta)}{2} \cdot \frac{(K_{Vx} - K_{Vy})}{K_{Vx}.K_{Vy}} \tag{6-21}$$

Obviously, the contouring error on a straight line is cancelled if the dynamic characteristics of each axis are identical [BEA04]. Radial error was tested with the Tripod in experiment and simulation model, in both radial error results, the contour error is function of position and is not constant. This is different to the observed behavior in the horizontal star test performed by a Tripod with constant length struts, where the path deviations appear with varying orientations. According to the plotted results and formula (6-21), the deviations can be explained. Although velocity gains are constant in the drive controllers with the nonlinear transform, they are not constant and not equal in the Cartesian space ($K_{Vx} \neq K_{Vy}$). This explains the deviations in experiment and simulated model. A straight lines trajectory produces a parallel offset to setpoint trajectory. The magnitude and side of the deviation depend on the value of the difference between K_{Vx} and K_{Vy}. To obtain high contouring accuracy at high speed machining the K_V factors must be the same in work coordinates, and not in machine coordinates.

7 Compensation algorithm in Tripod

7.1 Introduction

Contour error is an important aspect which needs to be effectively addressed in order to maintain and enhance the dynamic performance of Tripod.

In this chapter, the contouring performance of conventonial position controllers is improved by generating new motion commands in order to eliminate the contour error in Tripod.

7.2 Compensation algorithm

To improve contouring performance, contour error must be reduced by considering the motions of all axes relative to each other, and by controlling the movement of each individual axis based on the movement data of the other axes.

Concerning this control strategy, the control systems for multi axis control are coupled into a multi variable control system. The objective of these systems is to decrease contour error directly, rather than decreasing the tracking error of each individual axis. The proposed control system is called a direct system due to the relative movements produced by the contour error controller design.

In the proposed system, the controller consists of two parts. The first part of the controller calculates the contour error due to tracking error of each individual axis. The position loop of each individual axis must have a dedicated controller, which is the position loop controller, in order to control the position of each axis. The second part is a compensation controller, which is used to offset common contour to reduce the contour error of the system.

Typically, the improved control system for a multi axis Tripod cascaded controller is multi variable, nonlinear and time varying.

ε: error vector

c: compensation vector

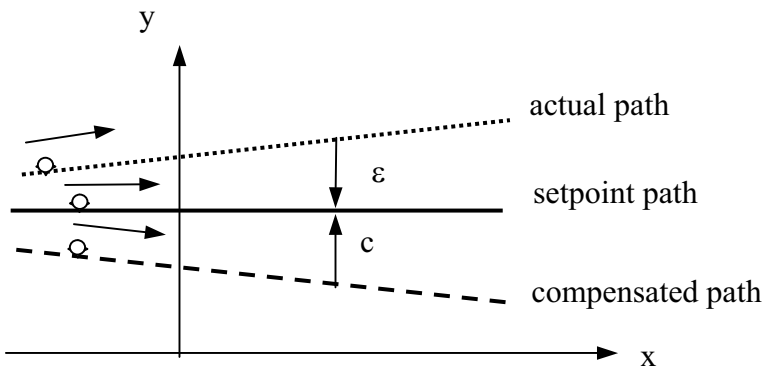

Figure 7-1: Feature error compensation

In Figure 7-1, the basic principle of compensation errors on a straight line trajectory is illustrated. The horizontal solid line represents the setpoint linear path of the part.

As it is shown in the same figure, the actual path which is deviated from this setpoint path in PKM machining results from contour errors in the process. The compensation trajectory is the modified tool path to generate an actual path that coincides with the setpoint path. From the figure, it is seen that the tendency to deviate from a setpoint by a certain amount is compensated by determining a path, which contains a point that deviates from the setpoint by the same amount, in the opposite direction.

The actual location of the tool when it should be at any given point along the setpoint path can be found in a direction perpendicular to the setpoint path, by projecting a vector from that point. ε is the error vector, defined as extension of any setpoint to the corresponding actual path. The compensation vector c is obtained by reflecting the error vector with respect to the setpoint surface.

The compensation curve is the locus of compensation vectors for all points on the setpoint path. Although it is obvious in case of an error curve, the same principle which is applied for a typical nonlinear biaxial contour machining, is depicted in Figure 7-2. The actual tool path does not coincide with the setpoint path, and consequently, causes a contour error.

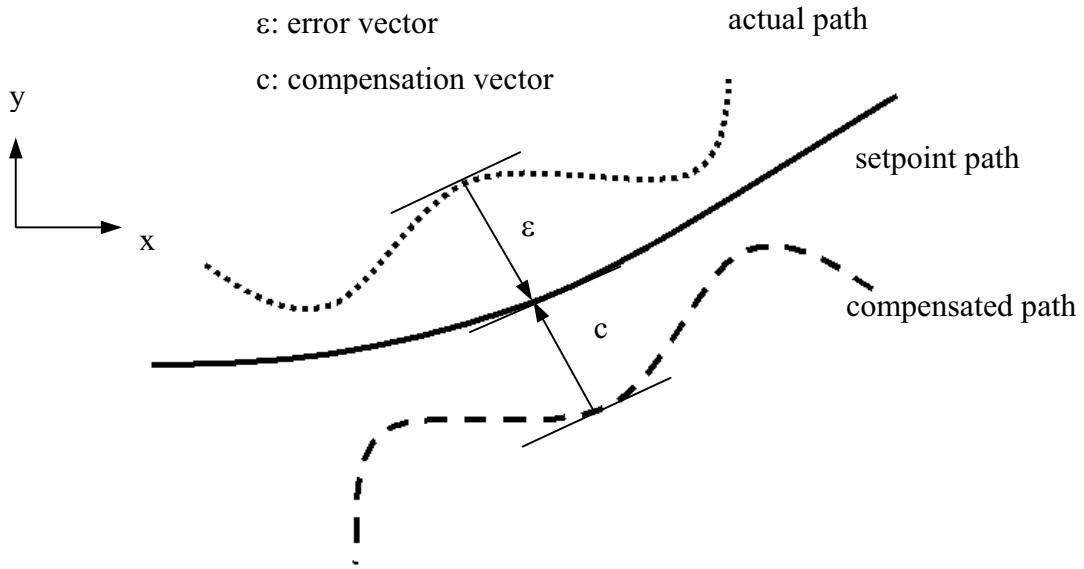

Figure 7-2: Biaxial contour machining and the compensation strategy

As is shown in the figure, the idea of the proposed method is to generate a compensated path, for which the contour error is opposite to the contour error for the actual path, and then to perform the compensated path as the new reference tool path for the subsequent contour machining. With the proposed tool path compensation algorithm, the contour error in the subsequent action is expected to be reduced.

The concept of the compensation strategy is forward in path processing. However, a prior problem to be coped with is described as follows.

7.3 Tool path compensation strategy

The idea of the compensated path is to influence the transfer error of the proportional position control loop with suitable actual controller parameters. Figure 7-3 shows the compensation control block diagram where G_a is the actual transfer function of Tripod, G_a^{-1} the inverse transfer function, G_c is the transfer function of the servo controller system and G_m denotes the mechanical transfer function. This method estimates the error between the actual contouring path and the programmed contouring path in normal direction, and uses an appropriate compensated contour to correct the error.

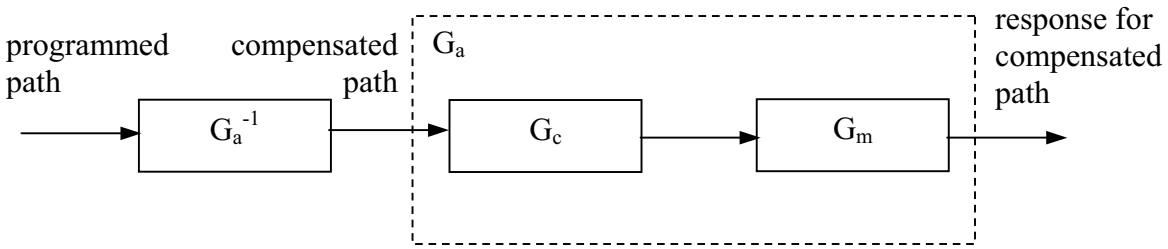

Figure 7-3: Compensation block diagram

7.4 Modelling of Tripod motion

A functional representation of the Tripod mechanism system is depicted in Figure 7-4. The system consists of inverse transformation, servo controller system of each axes and forward kinematics by the Tripod.

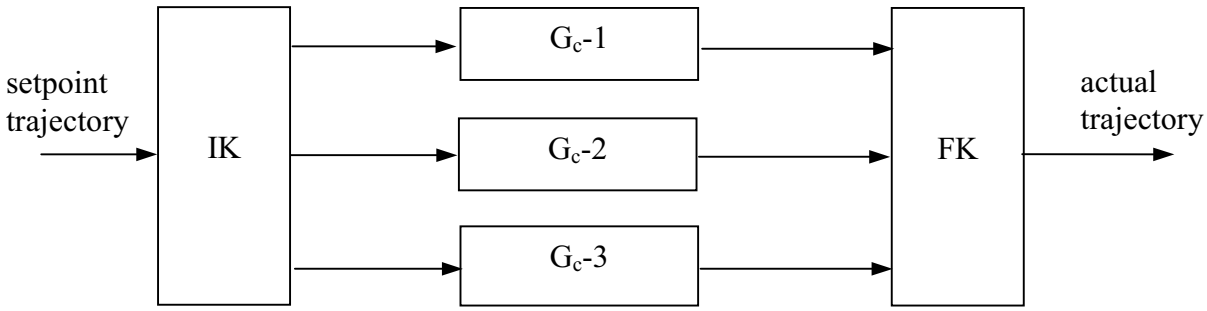

Figure 7-4: Functional representation of the Tripod

Figure 7-5 shows the servo controller block diagram of the u-axis as a PI cascaded controller.

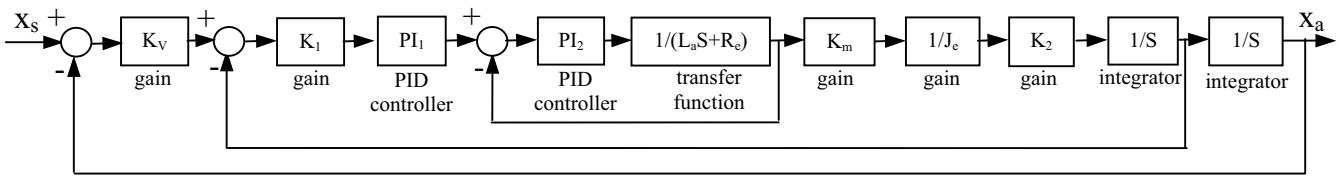

Figure 7-5: Servo controller block diagram

The transfer function block in each axes of the Tripod implements a transfer function, where the input (X_s) and output (X_a) can be expressed in transfer function as the following equation:

$$G_c=\frac{X_a}{X_s}=\frac{N_1S^2+N_2S+N_3}{D_1S^5+D_2S^4+D_3S^3+D_4S^2+D_5S+D_6} \quad (7\text{-}1)$$

$$\Delta X = X_s - X_a = X_s(1-G_c)$$

N and D contain the coefficients of the numerator and denominator in descending powers of S respectively.

That the coefficients of the numerator:

$$N_1= K_V \cdot K_1 \cdot K_2 \cdot K_m \cdot K_p \cdot K_{pi}$$

$$N_2= K_V \cdot K_1 \cdot K_2 \cdot K_m \cdot K_p \cdot T_{pi} + K_V \cdot K_1 \cdot K_2 \cdot K_m \cdot K_{pi} \cdot T_p \quad (7\text{-}2)$$

$$N_3= K_V \cdot K_1 \cdot K_2 \cdot K_m \cdot T_p \cdot T_{pi}$$

and the coefficients of the denominator as:

$$D_1= L_a \cdot J_e$$

$$D_2= (R_e + K_{pi}) \cdot J_e$$

$$D_3= T_{pi} \cdot J_e + K_1 \cdot K_2 \cdot K_m \cdot K_p \cdot K_{pi}$$

$$D_4= K_1 \cdot K_2 \cdot K_m \cdot K_p \cdot T_{pi} + K_1 \cdot K_2 \cdot K_m \cdot K_{pi} \cdot T_p + K_V \cdot K_1 \cdot K_2 \cdot K_m \cdot K_p \cdot K_{pi} \quad (7\text{-}3)$$

$$D_5= K_1 \cdot K_2 \cdot K_m \cdot T_p \cdot T_{pi} + K_V \cdot K_1 \cdot K_2 \cdot K_m \cdot K_p \cdot T_{pi} + K_V \cdot K_1 \cdot K_2 \cdot K_m \cdot K_{pi} \cdot T_p$$

$$D_6= K_V \cdot K_1 \cdot K_2 \cdot K_m \cdot T_p \cdot T_{pi}$$

where $K_V = 1.2\ {}^{1000}/_{min}$, $Kp = 2.4\ {}^{Asec}/_{rad}$, $T_p = .002$ sec, $K_{pi} = 15\ {}^{V}/_{A}$, $T_{pi} = .003$ sec, $L_a = .0072$ H, $R_e = 1.45\ \Omega$, $K_m = .77\ {}^{Nm}/_{A}$, $J_e = .087\ kgm^2$, $K_1 = 2\Omega/10\ {}^{rad}/_{mm}$ and $K_2 = 10\ {}^{mm}/_{rev}$.

The derivative of a function with respect to the variable is defined as

$$Sx_i = \frac{d}{dt}x_i = \lim_{\Delta t_i \to 0}\frac{\Delta x_i}{\Delta t_i} = \frac{x_i - x_{i-1}}{t_i - t_{i-1}} \qquad i = 2,3,.....,n \quad (7\text{-}4)$$

that n is the number of samples that $n=T \cdot f$, where T is whole time and f is frequency.

when $\Delta t = \Delta t_i$;

$$Sx_i = \frac{x_i - x_{i-1}}{\Delta t} \qquad S^2x_i = \frac{x_i - 2x_{i-1} + x_{i-2}}{\Delta t^2}$$

$$S^3x_i = \frac{x_i - 3x_{i-1} + 3x_{i-2} - x_{i-3}}{\Delta t^3} \qquad S^4x_i = \frac{x_i - 4x_{i-1} + 6x_{i-2} - 4x_{i-3} + x_{i-4}}{\Delta t^4} \quad (7\text{-}5)$$

$$S^5x_i = \frac{x_i - 5x_{i-1} + 10x_{i-2} - 10x_{i-3} + 5x_{i-4} - x_{i-5}}{\Delta t^5}$$

From Eq. (7-1), take following equation;

$$(N_1S^2+N_2S+N_3)X_s=(D_1S^5+D_2S^4+D_3S^3+D_4S^2+D_5S+D_6)X_a \quad (7\text{-}6)$$

Substitution of (7-5) into (7-6) yields

$$A_0\cdot X_{si}+A_1\cdot X_{si-1}+A_2\cdot X_{si-2}=B_0\cdot X_{ai}+B_1\cdot X_{ai-1}+B_2\cdot X_{ai-2}+B_3\cdot X_{ai-3}+B_4\cdot X_{ai-4}+B_5\cdot X_{ai-5} \quad (7\text{-}7)$$

With rewriting Eq. (7-7), and simplify about X_{ai};

$$X_{ai} = [A_0\cdot X_{si}+A_1\cdot X_{si-1}+A_2\cdot X_{si-2}-(B_1\cdot X_{ai-1}+B_2\cdot X_{ai-2}+B_3\cdot X_{ai-3}+B_4\cdot X_{ai-4}+B_5\cdot X_{ai-5})]/B_0$$

$$i= 6, 7, 8,....., n \quad (7\text{-}8)$$

Where

$$A_0=\frac{N_1}{\Delta t^2}+\frac{N_2}{\Delta t}+N_3$$

$$A_1=\frac{-2N_1}{\Delta t^2}+\frac{-N_2}{\Delta t}$$

$$A_2=\frac{N_1}{\Delta t^2}$$

$$B_0=\frac{D_1}{\Delta t^5}+\frac{D_2}{\Delta t^4}+\frac{D_3}{\Delta t^3}+\frac{D_4}{\Delta t^2}+\frac{D_5}{\Delta t}+D_6 \quad (7\text{-}9)$$

$$B_1=\frac{-5D_1}{\Delta t^5}+\frac{-4D_2}{\Delta t^4}+\frac{-3D_3}{\Delta t^3}+\frac{-2D_4}{\Delta t^2}+\frac{-D_5}{\Delta t}$$

$$B_2=\frac{10D_1}{\Delta t^5}+\frac{6D_2}{\Delta t^4}+\frac{3D_3}{\Delta t^3}+\frac{D_4}{\Delta t^2}$$

$$B_3=\frac{-10D_1}{\Delta t^5}+\frac{-4D_2}{\Delta t^4}+\frac{-D_3}{\Delta t^3}$$

$$B_4=\frac{5D_1}{\Delta t^5}+\frac{D_2}{\Delta t^4}$$

$$B_5=\frac{-D_1}{\Delta t^5}$$

Response of the system for unit ramp, step and impulse as input is given in Figure 7-6. These responses show that, in the system, there is not any overshoot and delay time is 0.035 sec.

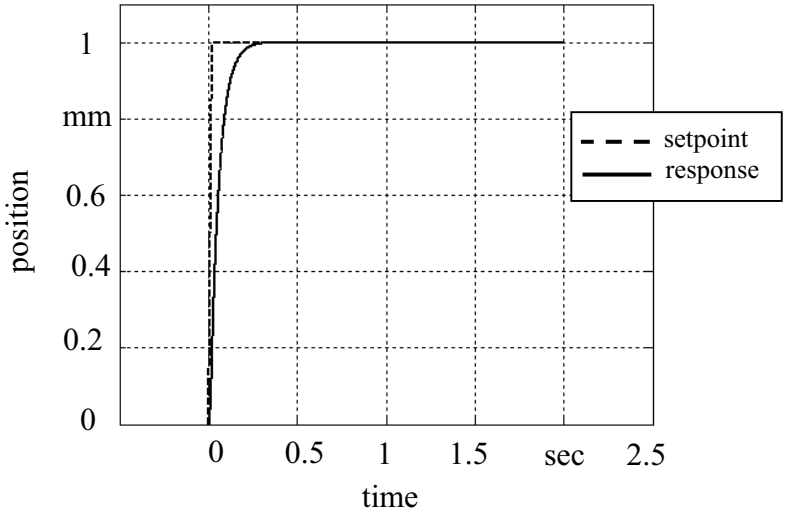

a: Step

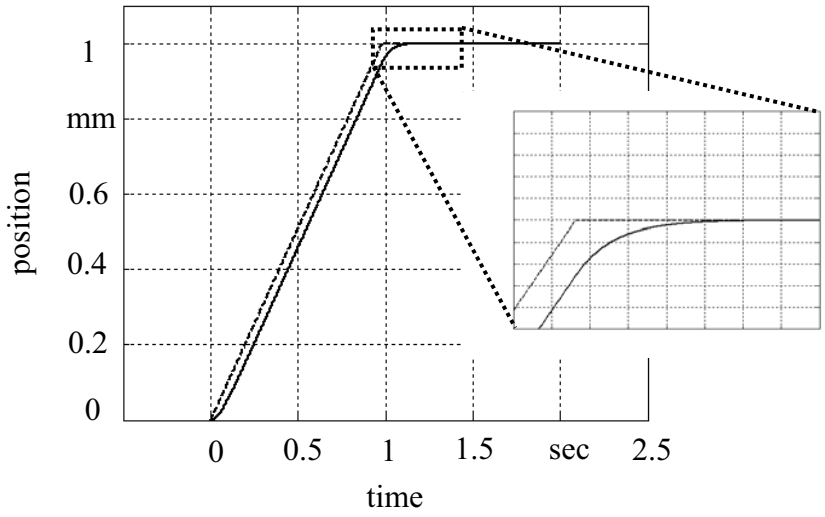

b: Ramp

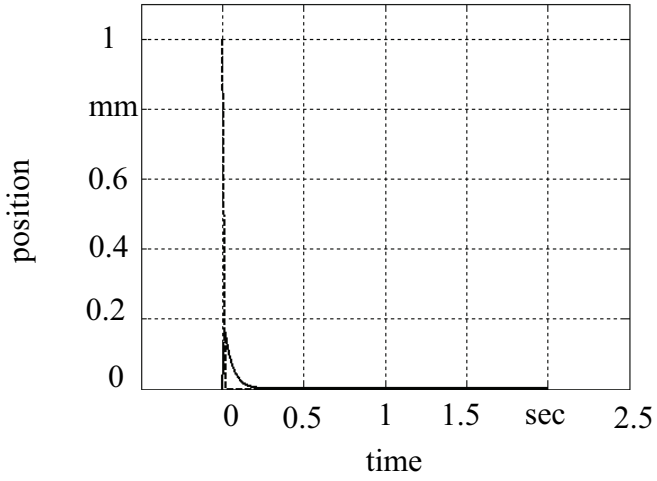

c: Impulse

Figure 7-6: Response of the system

7.5 Results of the compensated trajectory method

With some practical tests on the Tripod, the efficiency of the proposed method, introduced in the study of the contour error compensation is illustrated especially with high constant contour velocity. In PKM, relationship among the contour error, the drive axis positions and the complex contour error model make the contouring controllers difficult to design. Hence, the proposed method is to generate a compensated path, equal in amount and negative in direction of the expected contour error.

Thereby, in the case of a modified linear trajectory, the contour error could be reduced. In order to verify the proposed method, experiments of the Tripod were performed and the test results are shown in Figure 7-7 and Figure 7-8. The actual contour error of multi axis 3-DOF PKM are compared in tracking planar star test with different angles with and without compensation. A comparison of the results at TCP feed rate of 6000 $^{mm}/_{min}$ and 9000 $^{mm}/_{min}$ are shown in the Figure.

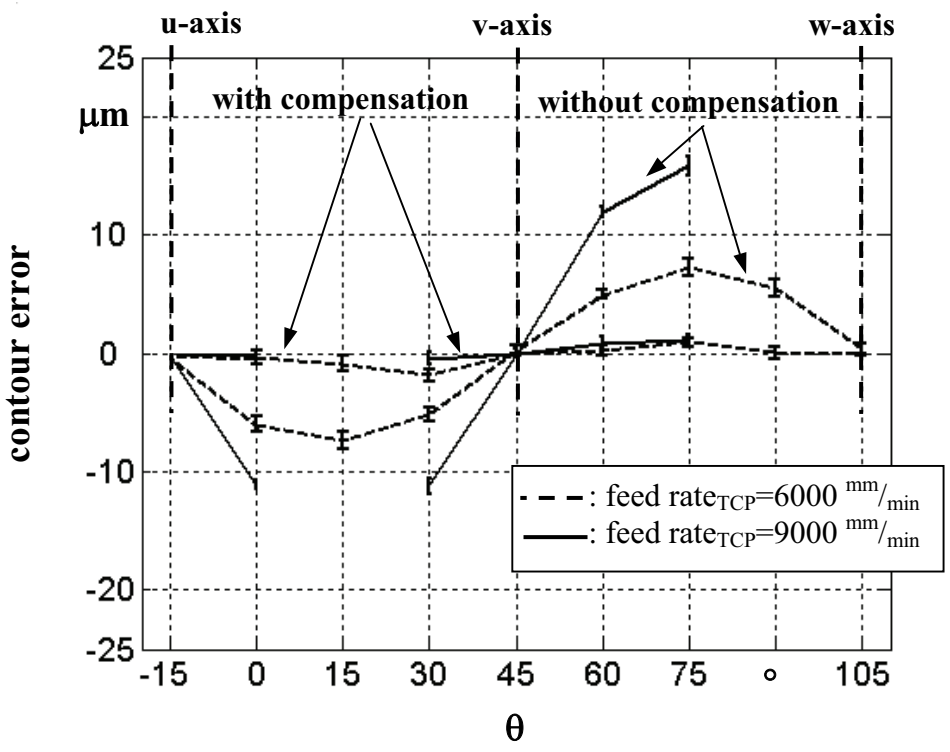

Figure 7-7: Comparison of measuring contour error in planar star test with compensation based on measured contour

As there is vibration at 15° and 90° at 9000 $^{mm}/_{min}$ feed rate, it is not possible to measure the error. The results demonstrate the effectiveness of the compensated path method in reducing error. Reducing the contour errors to almost zero, with compensated path, could become

possible due to the fact that the proposed trajectory could be improved when using the modified path [KUH08-2].

Figure 7-7 shows the experimental results in compensation strategy when using measured contour errors, and Figure 7-8 shows the measurement results with compensated path based on simulated contour errors.

A comparison of Figure 7-7 and Figure 7-8 reveals that although the simulated modified contour reduces the error, it cannot be completely compensated. This is in contrast to the simulation results where the contour error completely vanishes. The reason is that the simulated model and experimental setup is not completely the same. One possible solution for this is to employ the real contour errors estimated by actual transfer function.

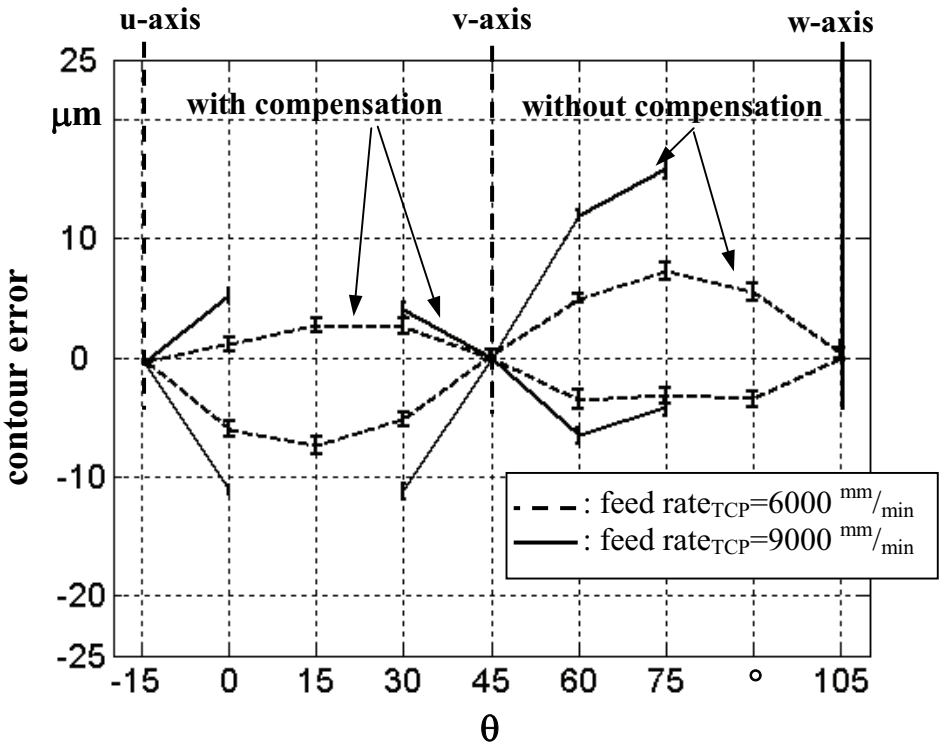

Figure 7-8: Comparison of measuring contour error in planar star test with compensation based on simulated modified contour

7.6 Machine parameter identification principle

With a good approximation, the order of the numerator and denominator in the transfer function of the system can be taken like the order in the servo controller transfer function because the form of simulated and measured contour errors are similar. There are two sections with respect to the modelling. First, the order of the transfer function is obtained and then the

actual coefficients of the numerator and denominator are quantified by parameter identification.

Real modeling and identification of the whole machine system is an important step in design and modelling of a high performance PKM. A method is suggested to identify the coefficients of transfer function as well as the dynamic effects of machine tool drives.

The prerequisite for the described concept is that the system models of the individual machine axes are available in the form of a mathematical description as in Formula 7-1. In the following, the actual model design is discussed with respect to the experimental acquisition by means of parameter identification methods. The information about the system is used to compensate contour errors.

Hence, it is difficult to select the actual machine parameters. Although a trial and error approach for controller parameter selection is adopted in some applications, to obtain the actual controller parameters, neuron algorithms can be applied to find the parameters of the system, considering stability.

Identification is realized in two consecutive steps. The first step of NN is trained by simulated contour errors using transfer function where [N], [D] are filled with matrix of variety arbitrary coefficients of the numerator and denominator respectively, Figure 7-9.

The system is identified with individual training trajectory. The contours are star contour and circular trajectory with different radius, different center point and feed rates. The identification is realized when the NN is trained in each coefficients of [N] and [D].

The simulated trajectory is obtained by the action of transfer function with random variety of coefficients on the setpoint trajectory. The simulated contour errors are calculated by the proposed algorithms in the thesis.

For the initialization of the system, [N] and [D] contain the coefficients of the numerator and denominator in descending powers of S of servo controller system with a suitable tolerance band i.e. the tolerance band must converge.

The resulting net is fed with measured contour errors. Therefore a new set of $[N]_{real}$ and $[D]_{real}$ is created by the process.

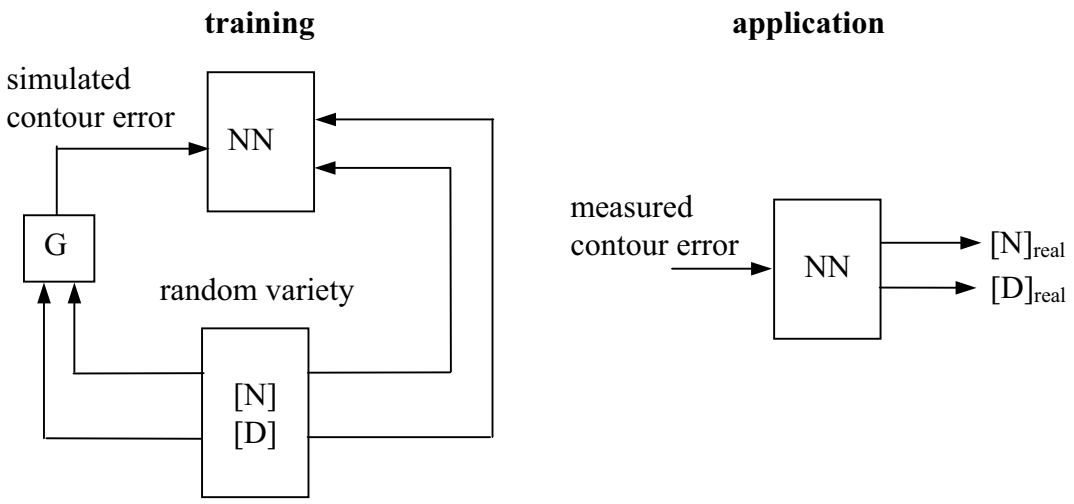

Figure 7-9: Parameter quantification procedure

In the following, there is an example to identify the coefficients of transfer function. The coefficients of servo control system are:

N1 =3.483e+003 N2 =3.599 N3 =5.805e-004
D1 =6.264e-005 D2 =0.143 D3 =1.741e+002
D4 =3.483e+003 D5 =3.599 D6 =5.805e-004

After first iteration with the following coefficients, the compensation results are shown in Figure 7-10.

N1 =4.1e+003 N2 =3.99 N3 =6.01e-004
D1 =6.265e-005 D2 =0.154 D3 =1.734e+002
D4 =4.02e+003 D5 =4.01 D6 =6.021e-004

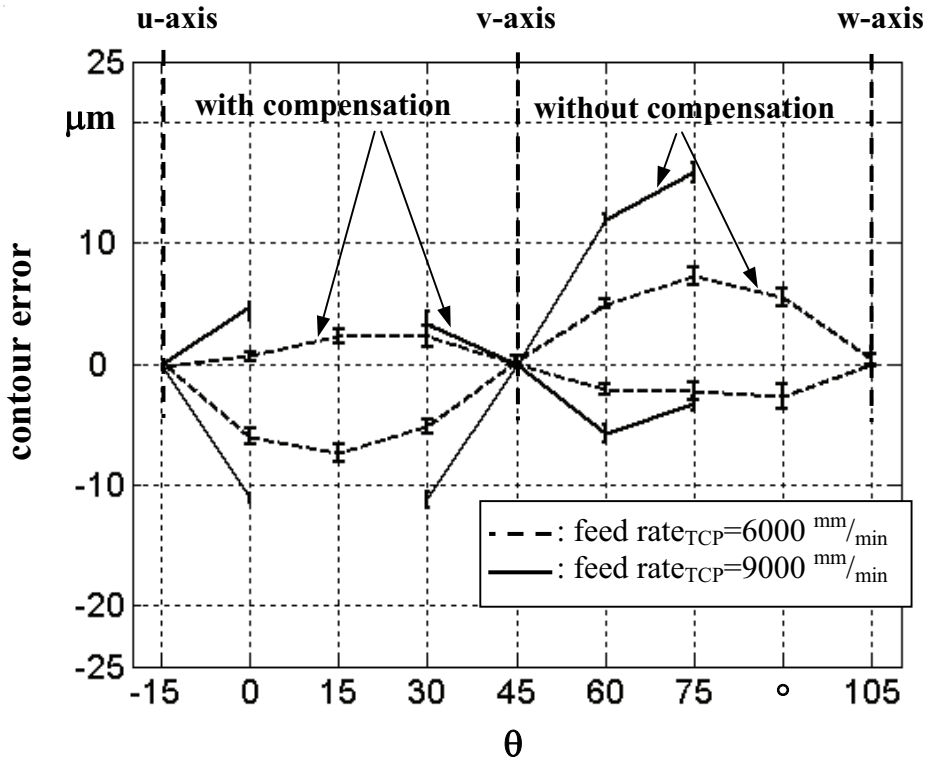

Figure 7-10: Comparison of measued contour error in planar star test with compensation based on identified contour error after first iteration

Figure 7-11 shows a comparison of the compensated contour with using the simulated contour error and identified contour error after first iteration.

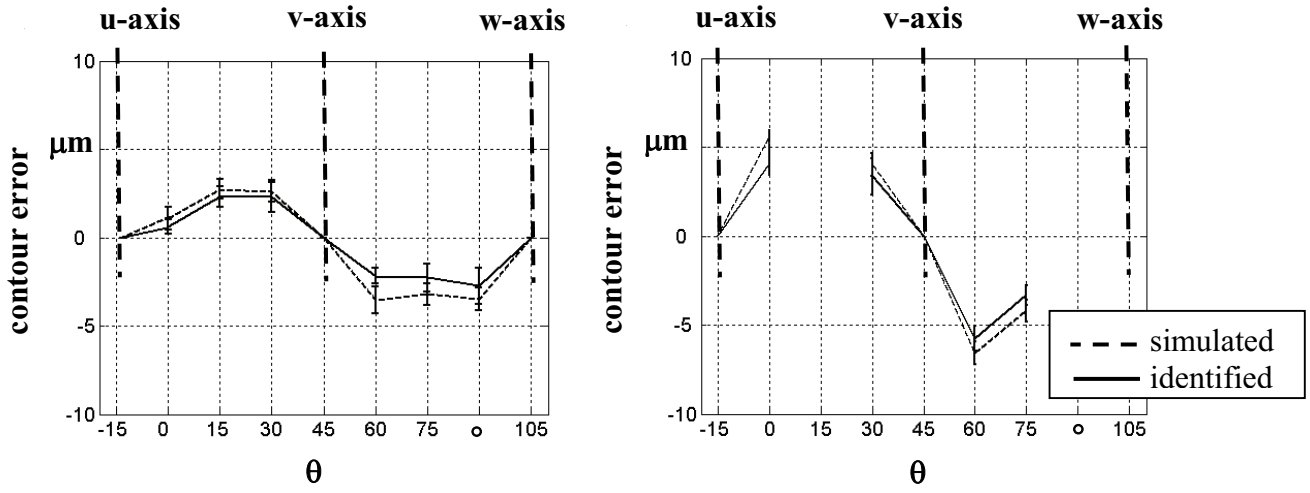

a: feed rate$_{TCP}$=6000 $^{mm}/_{min}$ b: feed rate$_{TCP}$=9000 $^{mm}/_{min}$

Figure 7-11: Comparison of measured contour error in planar star test with compensation based on simulated and identified contour error after first iteration

Results of contour error in compensated path in different centers of star trajectories show in Figure 7-12.

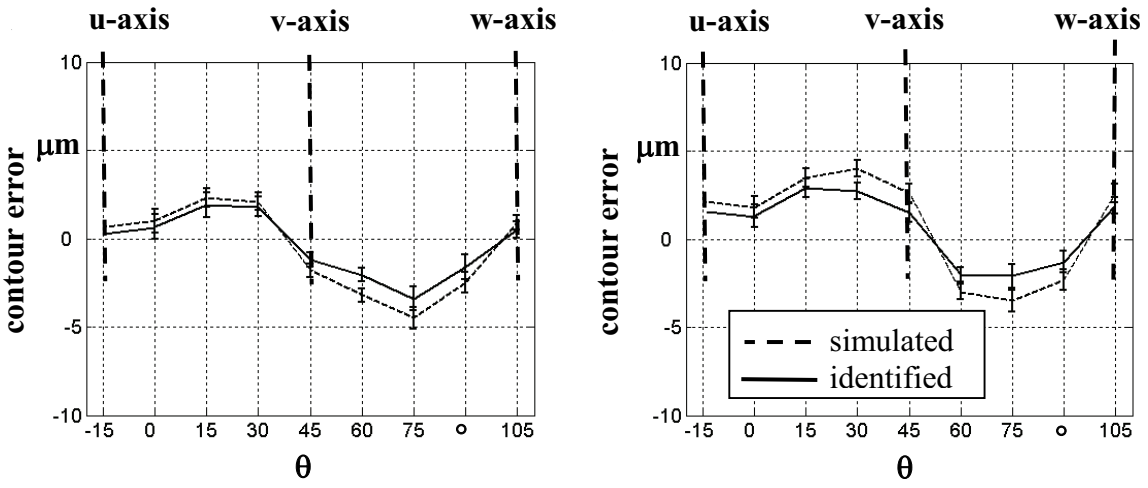

a: center of star contour: (0, 50) b: center of star contour: (50, 0)

Figure 7-12: Comparison of measuring contour error in planar star test with compensation based on simulated and modified contour after first iteration at $f_{TCP}=6000\ ^{mm}/_{min}$

Figure 7-11 and 7-12 show contour error after first iteration at different velocities, orientations and pivot points of star contours. The contour errors are improved and the compensated method is approved, however, the contour error cannot be completely compensated.

Development of the NN method in dynamic compensation could be required to eliminate the contour errors completely.

8 Conclusions and suggestions for future work

In this thesis, the effects of the forward transformation of the tracking errors in parallel kinematics machines are addressed with experiments and simulations. The general problem is illustrated with a simple 1-DOF setup, and the effect on trace accuracy is discussed by contour deviations in circular and star tests performed by a Tripod mechanism.

In Cartesian machine tools, motion properties such as velocity and acceleration of the individual drives are directly transferred to the tool center point. With PKM, the axes motions are transformed by nonlinear transfer functions as a general rule. Like positions and velocities, the controller parameters are transformed from joint to work coordinates. To study the transformation of the velocity gain, the relative gain K_{V-rel} is defined as the ratio of the actual values of both active and passive axes. The K_{V-rel} is a nonlinear function of TCP position and feed rate and is particularly not equal to one. The K_{V-rel} in backward movement occurs as the mirror image of the forward direction to the unit horizontal line. This reversal effect is determined by the transform of the Monopod kinematics. Due to the nonlinear transformation of a movement in positive x-direction with constant velocity, the active platform must permanently accelerate and the actual drive velocity should be lower than the demanded in the corresponding TCP position. Hence, by the nonlinear transform controller, settings must be adjusted to the most critical positions. In the exemplary Monopod, this is the region of minimum strut-inclination. In this region, small deviations in active platform are transformed to large deviations in TCP, and the tiny vibrations in the drive cause unacceptable vibrations in the TCP. These are the conditions for which the controller settings must be tuned. For a more horizontal strut position (maximum strut-inclination), a higher gain is possible in the controller concerning stability in the TCP. It is necessary to provide a constant tracking error in working coordinates, because the tracking error is higher for the higher velocity needed for constant feed rate.

For the Monopod setup, constant feed rate at TCP is considered and, therefore, a constant deviation in TCP is transformed by inverse kinematics to joint space. The magnitudes of the resulting deviations in drive depend on the position. The deviations depend not only on absolute position but also on the relative position and direction. According to the present study, the relative tracking error in active platform cannot be linearized, and it is a nonlinear function of TCP-position. The feed forward control improves the dynamics of servo system in Monopod, but the virtual velocity gain varies nonlinearly with the position, like a system

without feed forward control. Although servo control with feed forward improves the motion, it is not sufficient for high precision and high speed motion with PKM and depends on balancing filter.

The effect on trace accuracy is discussed as the basis of multi axis PKM such as Bipod and Tripod. When looking at the actual paths of the curves that machine tools carry out, tracking errors are the most influencing factors on accuracy, besides geometric machine errors, tool errors and temperature changes. It involves a divergence of the target and actual position of each axis and causes contour error. The contour error is defined as the orthogonal deviation from the desired tool path. The existence of inherent tracking error in each active axis and consideration of the nonlinear transformation to TCP lead to new aspects in PKM in comparison to conventional serial mechanisms.

To study the effects of transformation tracking error in workspace coordinates, the actual contour is approved in star contour and circular trajectory by simulation model and experiment setup. When a star test is performed with a SKM, the setpoint trace is perfectly fitted as the velocity gains are equal in the interpolating axes x and y. In Bipod, the contour error depends on workspace position, but vanishes in similar orientation of struts ($\beta_1 = \beta_2$). With the Tripod, this behavior can only be observed when the straight line motion is performed in the directions where the drive axes are positioned (45°, 165° and 285°). In all other directions, the distance between the setpoint and the TCP is almost constant indicating different K_V values in x- and y-direction. Although velocity gains are constant in the drive controllers, they are transformed by the machine kinematics resulting in nonconstant values in the Cartesian space ($K_{Vx} \neq K_{Vy}$). The results indicate that the contour error is a nonlinear function of TCP-position, feed rate and pivot point.

Furthermore, in perpendicular axes with different K_V values, the deviations from straight line motion occur on both sides of the path depending on the travel direction. In contrast, there is no hysteresis in the Tripod motion when the direction of motion is inverted. The hysteresis is converted to a one sided deviation by the reversal gain transform effect described above. To obtain high contouring accuracy at high speed machining, the system gains should be matched well in workspace. A K_V adaption could equalize the error. To keep them equal in the Cartesian space, they must be adapted in process in the drive controllers.

The radius deviation in a serial Cartesian machine is constant in a circular path, which is not valid for PKM machine tools. The radius deviation is calculated with the simulated model of Bipod. The radial error is a function of angular position, with an extremum positioned at $\beta_1 = \beta_2$. An extremum occurs where the axes velocities are near to zero and the velocity changes

are highest. Circular tests are performed with the experimental Tripod milling machine and a simulated model. The characteristic shape is dominated by three prominent buckles positioned opposite to each machine axis in the areas where the constant length struts are most horizontal (maximum β) and change their direction. At these points, the produced radii are smallest and the radial deviations are highest. These two different contours in PKMs indicate that the errors in different radius and center of circles are related to orientation of struts.

Improving the overall control performance of a multi axis machine tool is not necessarily ensured only by improving the tracking performance of each individual axis. Contour error, which is a typical performance index for the evaluation of multi axis servo control systems, also needs to be effectively minimized. In this study, the model based compensation is introduced in order to address the issue of contour errors in servo systems. The compensation algorithm is applied according to the preprocessor principle. The method, however, requires accurate model of the kinematic configuration of the machine tool since different axis controllers have to be coupled among themselves. The adequacy of the method is proven by the Tripod.

Although the tracking error transformation in the research is performed on Monopod, Bipod and Tripod, continued investigations in other structures such as 5-axes milling machine could be interesting in future work.

In the test machine, linear encoders are used as measurement systems in the control closed loop. The major work that can be done in this respect is to develop an optimization measuring device that can measure TCP position directly and give the feedback to controller algorithm. The direct measurement systems normally increase the accuracy of PKM machine tools. With rearranging the measurement system for the TCP, geometric and assembly errors of the mechanical structure can be considered in the control system. Although this effort is not sufficient but could be useful.

In order to improve the contouring accuracy and dynamic performance of the positioning, the actual inverse transfer function can be identified by means of neural networks.

In the future work, the transformation problem will be addressed by online adapted velocity gain parameters to realize constant velocity gains in workpiece coordinates, which may improve dynamic accuracy and exploit full dynamic capacities of PKM.

Such efforts to reduce or eliminate tracking and contouring errors are reflected directly on the system performance and quality of machined parts.

9 References

[ABD06] Abdelatif, H.; Heimann, B.; Learning Control for Accuracy Enhancement of Parallel Kinematic Machines. 5th Chemnitz Parallel Kinematics Seminar, Chemnitz 2006, proceedings pp. 443-456.

[ALT00] Altintas, Y.; Manufacturing Automation, metal cutting mechanics, machine tool vibrations and CNC design; Cambridge University Press 2000.

[ALT00-1] Altintas , Y., Erkorkmaz, K., Zhu, W.-H.; Sliding mode controller design for high speed drives, Annals of CIRP 49 (1) (2000) 265-270.

[AST06] Ast, A.; Eberhard, P.; Flatness-based control of parallel kinematics using multibody system-simulation and experimental results ; Arch Appl Mech 76 (2006), pp. 181-197.

[BEA04] Bearee, R.; Barre, P.; Bloch, S.; Influence of High-Speed Machine Tool Control Parameters on the Contouring Accuracy. Application to Linear and Circular Interpolation; Journal of Intelligent and Robotic Systems 40 (2004), pp. 321-342.

[BLE03] Bleicher, F.; Parallelkinematische Werkzeugmaschinen. Neuer Wissenschaftlicher Verlag GmbH. Wien 2003.

[BRE06] Brecher, C.; Ostermann, T.; Friedrich, D. A.: Control Concept for PKM Considering the Mechanical Coupling between Actuators. 5th Chemnitz Parallel Kinematics Seminar, Chemnitz 2006, proceedings pp. 413-427.

[BRE06-1] Brecher, C.; Hoffmann, F.; Multi-Criteria Comparison of Standardised Kinematic Structures for Machine Tools; 5th Chemnitz Parallel Kinematics Seminar, Chemnitz 2006, proceedings pp. 65-82.

[BRU02] Bruzzone, L. E.; Molfino, R. M.; Zoppi, M.; A Cost-Effective Purely Translational Parallel Robot for Rapid Assembly Tasks. 2nd Chemnitz Parallel Kinematics Seminar. Chemnitz 2002, proceedings pp. 429-440.

[CAM06] Campos, A.; Budde, C.; Hesselbach, J.; A Synthesis Method for Hybrid Robots; 5th Chemnitz Parallel Kinematics Seminar, Chemnitz 2006, proceedings pp. 839-842.

[CHE99] Chen, J. S.; Kou, T. W.; Chiou, S. H.; Geometric error calibration of multi-axis machines using an auto-alignment laser interferometer; Precision Engineering, ELSEVIER, 23 (1999), pp. 243-252.

[CHE02] Chen, S. L.; Liu, H. L.; Ting, S. C.; Contouring Control of Biaxial System Based on Polar; ASME Transactions on Mechatronics, VOL. 7, NO. 3, 2002, pp. 329-345.

[CHE04] Chen, J. S.; Hsu, W. Y.; Design and analysis of a tripod machine tool with an integrated Cartesian guiding and metrology mechanism; Precision Engineering, ELSEVIER, 28 (2004), pp. 46-57.

[CHE06] Chen, J. S.; Hsu, W. Y.; Dynamics and Compliant Characteristics of a Cartesian-Guided Tripod Machine; International Journal of Manufacturing Science and Engineering ASME Vol.128 (2006), pp. 494-502.

[CHO06] Cho, M. W.; Kim, G. H.; Seo, T. I.; Hong, Y. C.; Cheng, H. C.; Integrated machining error compensation method using OMM data and modified PNN algorithm; International Journal of Machine Tools & Manufacture 46 (2006), pp. 1417-1427.

[COB02] Cobet, M.; Designing PKMs: Working Volume, Stiffeness, Frequencies. 2nd Chemnitz Parallel Kinematics Seminar. Chemnitz 2002, proceedings pp. 83-103.

[COL04] Collado, V.; Herranz, S.; Space 5H - A new Machine Concept for 5-Axis Milling of Aeronautic Structural Components; 4th Chemnitz Parallel Kinematics Seminar, Chemnitz 2004, proceedings pp. 611-624.

[DEL06] Delbressine, F. L. M.; Florussen, G. H. J.; Schijvenaars, L. A.; Schellekens, P. H. J.; Modelling thermomechanical behaviour of multi-axis machine tools; Precision Engineering, ELSEVIER, 30 (2006), pp. 47-53.

[DEN04] Denkena, B; Holz, C.; Grendel, H.; State Control through Linearization of the Linear Direct Driven Parallel Kinematics PaLiDA; Production Engineering Vol. XI/2 (2004), pp. 189-194.

[DEN06] Denkena, B.; Holz, C.; Advanced Position and Force Control Concepts for the Linear Direct Driven Hexapod PaLiDA. 5th Chemnitz Parallel Kinematics Seminar, Chemnitz 2006, proceedings pp.359-378.

[DON04] Dong, J.; Yuan, C.; Stori, J. A.; Ferreira, P. M.; Development of a high-speed 3-axis machine tool using a novel parallel-kinematics X-Y table; International Journal of Machine Tools & Manufacture 44 (2004), pp. 1355-1371.

[ERK01-1] Erkorkmaz, K.; Altintas, Y.; High speed CNC system design. Part II: modelling and identification of feed drives; International Journal of Machine Tools & Manufacture 41 (2001), pp. 1487-1509.

[ERK01-2] Erkorkmaz, K.; Altintas, Y.; High speed CNC system design. Part III: high speed tracking and contouring control of feed drives; International Journal of Machine Tools & Manufacture 41 (2001), pp. 1637-1658.

[ERK06-1] Erkorkmaz, K.; Yeung, C.; Altintas, Y.; Virtual CNC system. Part II: High speed contouring application; International Journal of Machine Tools & Manufacture 46 (2006), pp. 1124-1138.

[ERK06-2] Erkorkmaz, K.; Wong, W.; Rapid identification technique for virtual CNC drives; International Journal of Machine Tools & Manufacture (2006).

[EST06] Esteban, I.; Heisel, U.; Analysis of the Component Requirements and the Feasible Mechanical Properties of Hexapod Machine Tools; 5th Chemnitz Parallel Kinematics Seminar, Chemnitz 2006, proceedings pp. 97-113.

[FLE06-1] Fleischer, J.; Schmidt-Ewig, J. P.; Combination of a Parallel and a Serial Kinematics for the Integrated Handling and Machining of Lightweight Extrusion; The 5th Chemnitz Parallel Kinematics Seminar Chemnitz 2006, proceedings pp. 289-306.

[FLE06-2] Fleischer, J.; Munzinger, C.; Kipfmüller, M.; Investigation on the Increase of Accuracy by the Use of Direct Pose Measurement; 5th Chemnitz Parallel Kinematics Seminar, Chemnitz 2006, proceedings pp. 851-854.

[GRE04] Grendel, H.; Entwurf und Regelung einer parallelkinematischen Maschine mit hoher Dynamik; Dissertation. IFW, Universität Hannover, 2004.

[GRO01] Gross, H.; Wiegärtner, G.; Electrical Feed Drives in Automation, Basics, Computation, Dimensioning; Publics MCD Werbeagentur GmbH, Munich, 2001.

[GRO02] Gronbach, H.; TriCenter - A Universal Milling Machine With Hybrid Kinematic, 3rd Chemnitz Parallel Kinematics Seminar, Chemnitz 2002, proceedings pp. 595-608.

[HEI04] Heimpel, W.; Schwaar, M.; Wagner, R.: Industrial Experience in Application of Hybrid Kinematics Machines with Overlayed Axes. 4th Chemnitz Parallel Kinematics Seminar, Chemnitz 2004, proceedings pp. 313-328.

[HEI06] Heisel, U.; Maier, W.; DFG SPP 1099– Production Machines with Parallel Kinematics; 5th Chemnitz Parallel Kinematics Seminar, Chemnitz 2006, proceedings pp. 13-37.

[HES02] Hesselbach, J.; Helm, M. B.; Soetebier, S.; Workspace-Optimised Parallel Robot for Placing Tasks. 2nd Chemnitz Parallel Kinematics Seminar. Chemnitz 2002, proceedings pp. 697-713.

[KOR91] Koren, Y.; Lo, C.-C.; Variable-gain cross coupling controller for contouring, Annals of CIRP 40 (1) (1991) 371-374.

[KOR92] Koren, Y.; Lo, C.-C.; Advanced controllers for feed drives, Annals CIRP, 41(2), pp. 689-697, 1992.

[KRA04] Krabbes, M.; Neugebauer, R.; Ihlenfeldt, S.; Schroeder, T.; Reactive Splitting into Dynamic Components for Overlayed Drive structures. 4th Chemnitz Parallel Kinematics Seminar, Chemnitz 2004, proceedings pp. 247-256.

[KRÜ00] Krüger, P.; Weck, M.; Adaptive Regelung für Maschinen mit paralleler Kinematik. 2. Chemnitzer Parallelkinematik Seminar, Chemnitz 2000, Tagungsband, S. 369-377.

[KWO96] Kwon, H. D.; Burdekin, M.; Development and application of a system for evaluating the feed-drive errors on computer numerically controlled machine tools; Precision Engineering 19 (1996), pp. 133-140.

[KWO97] Kwon, H. D.; Burdekin, M.; Adjustment of CNC machine tool controller setting values by an experimental method; International Journal of Machine Tools & Manufacture 38 (1998), pp. 1045-1065.

[KUH04] Kuhfuss, B.; Schenck, C.; Estimated Process Time Saving by PKM and HKM Machining. 4th Chemnitz Parallel Kinematics Seminar, Chemnitz 2004, proceedings pp. 277-290.

[KUH04-1] Kuhfuss, B.; Recent Development and Manufacture of Machine Tools in Germany, Keynote - Paper, 11th International Machine Tool Engineers Conference, Tokyo, Japan 01 - 08.11.2004.

[KUH06] Kuhfuss, B.; Schenck, C.; Allers, S.; Static Calibration of a Tripod by Neural Network Error Identification. 5th Chemnitz Parallel Kinematics Seminar, Chemnitz 2006, proceedings pp. 603-616.

[KUH07] Kuhfuss, B.; Schenck, C.; Productivity Increase in Aircraft Component Machining by Hybrid Kinematic Structures; International Conference on Applied Production Technology (APT'07), Bremen, Germany, 2007, pp. 219-230.

[KUH07-1] Kuhfuss, B.; Schenck, C.; Amirian, G.; Comparison of Radial Deviation in Serial and Parallel Kinematic Machining; The second International Conference on Manufacturing Engineering (TICME 2007), Tehran, IRAN, 2007.

[KUH07-2] Kuhfuss, B.; Schenck, C.; Amirian, G.; Contour error in circular trajectory in parallel kinematic machining (PKM); Modern Technologies, Quality and Restructuring (TMCR 2007), Kishinev/Moldawien, May 31st-June 3rd, 2007, proceedings pp. 21-27.

[KUH08] Kuhfuss, B.; Schenck, C. ; Einsatzmöglichkeiten von Hybridkinematiken für die Hochgeschwindigkeitsbearbeitung von Großbauteilen; In: Fertigungsmaschinen mit Parallelkinematiken - Forschung in Deutschland / Hrsg.: Heisel, U. ; Weule, H. - Aachen: Shaker-Verlag; 2008.-409-430S. ; ISSN 978-3-8322-7203-6.

[KUH08-1] Kuhfuss, B.; Schenck, C.; Amirian, G.; Contour Error in Parallel Kinematics Machining by Tracking Error; 13th International Conference on Machine Design and Production (UMTIK 2008), September 3rd - 5th, 2008, Istanbul/Türkei.

[KUH08-2] Kuhfuss, B.; Schenck, C.; Amirian, G.; Influence of Tracking Servo Control on the Contouring Accuracy in Parallel Kinematics Machining; The 2nd International Conference on Computing and Solutions in Manufacturing Engineering (CoSME 08); Brasov/Romania, September 25 –27, 2008.

[LAC00] Lacerda, H. B.; A Modified Contour Error Controller for a High Speed XY Table; Journal of the Brazilian Society of Mechanical Sciences, 22 (2000).

[LIU05] Liu, H. L.; Shi, H. M.; Li, B. Li, X.; A new method and instrument for measuring circular motion error of NC machine tools ; International Journal of Machine Tools & Manufacture 45 (2005), pp. 1347-1351.

[LO02] Lo, C. C.; A tool-path control scheme for five-axis machine tools; International Journal of Machine Tools & Manufacture 42 (2002), pp. 79-88.

[MAR06] Marek, J; Kolibal, Z.; Application Fields of Machine Tools with Parallel Kinematics. 5th Chemnitz Parallel Kinematics Seminar, Chemnitz 2006, proceedings pp. 863-866.

[MER06] Merlet, J.-P.; Computing the Worst Case Accuracy of a PKM over a Workspace or a Trajectory; 5th Chemnitz Parallel Kinematics Seminar, Chemnitz 2006, proceedings pp. 83-96.

[MUN06] Munzinger, C.; Kipfmüller, M.; Konzept einer genauen Parallelkinematik; VDI-Z 148 (2006), Nr. 11/12 – November/ Dezember pp. 30-33.

[NAK04] Nakamura, Y.; Murai, A.; Evaluation of Designed Closed Kinematic Chains Based on Constraints and Deformation Analysis. 4th Chemnitz Parallel Kinematics Seminar. Chemnitz 2004, proceedings pp. 347-364.

[NEU02] Neugebauer, R.; Weidermann, F.; Structure Optimization of Machine Tools with Parallel Kinematics. 3rd Chemnitz Parallel Kinematics Seminar. Chemnitz 2002, proceedings pp. 105-118.

[NEU06] Neumann, K.-E.; Exechon Concept; 5th Chemnitz Parallel Kinematics Seminar, Chemnitz 2006, proceedings pp. 787-802.

[ÖZE06] Özel, T.; Precision tracking control of a horizontal arm coordinate measuring machine in the presence of dynamic flexibilities; Int Adv. Manuf. Technol. 27 (2006) 1 pp. 960-968.

[OGA02] OGATA, K.; Modern Control Engineering; Fourth Edition; Prentice Hall, 2002.

[PRI92] Pritschow, G.; Philipp, W.; Research on the efficiency of feed forward controllers in M direct drives; Annals of CIRP 41 (1) (1992) 411-415.

[PRI96] Pritschow, G.; On the influence of the velocity gain factor on the path deviation; Annals of the CIRP 45 (1996) 1 pp. 367-371.

[PRI97] Pritschow, G.; Wurst, K.-H.; Systematic Design of Hexapods and other Parallel Link; Annals of the CIRP 46 (1997) 1 pp. 291-295.

[PRI97-1] Pritschow, G.; Kosiedowski, U.; Optimization strategies for adaptive feed forward control, production engineering research and development. (2), 1997- 69-72.

[PRI99-1] Pritschow, G.; Überlegungen zur Armgesteltung von Parallelstab - kinematiken; wt Werkstattstechnik 89 (1999) H.5 pp. 244-246.

[PRI99-2] Pritschow, G.; Bretschneider, J.; A Self -Tuning Controller for Digitally Controlled Electromechanical Servo Drives in Machine Tools; Annals of the CIRP 48 (1999) 1 pp. 307-312.

[PRI00] Pritschow, G.; Parallel Kinematic Machines (PKM) - Limitations and New Solutions; Annals of the CIRP 49 (2000) 1 pp. 275-280.

[PRI02] Pritschow, G.; Eppler, C.; Garber, T.; Influence of the Dynamic Stiffness on the Accuracy of PKM; The 4th Chemnitz Parallel Kinematics Seminar, Chemnitz 2002, proceedings pp. 313-334.

[RAH00] Rahman, M.; Heikkala, J.; Lappalainen, K.; Modeling, Measurement and error compensation of multi-axis machine tools. Part I: theory; International Journal of Machine Tools & Manufacture 40 (2000), pp.1535-1546.

[RAM00] Ramesh, R.; Mannan, M. A.; Poo, A. N.; Error compensation in machine tools- a review Part I: geometric, cutting-force induced and fixture- dependent errors; International Journal of Machine Tools & Manufacture 40 (2000), pp. 1235-1256.

[RAM05] Ramesh, R.; Mannan, M. A.; Poo, A. N.; Tracking and contour error control in CNC servo systems; International Journal of Machine Tools & Manufacture 45 (2005), pp. 301-326.

[REN--] Renishaw Quick-Check-Handbuch; H/8014/0289/01/A.

[REN00] Renton, D.; Elbestawi, M. A.; High speed servo control of multi-axis machine tools; International Journal of Machine Tools & Manufacture 40 (2000), pp. 539-559.

[SAE02] Saenz, A. J.; Collado, V.; Gimenez, M.; San Sebastian, I.; New Automation Solutions in Aeronautics Through Parallel Kinematic Systems. 2nd Chemnitz Parallel Kinematics Seminar. Chemnitz 2002, proceedings pp. 563-578.

[SCH99] Schulz, H.; Pandilov, Z.; Gao, H.; Bork, B.; Dynamic Stiffness and Contouring Accuracy of a HSC Linear Motor Machine, 2nd International Conference on High Speed Machining, 1999, PTW TU Darmstadt.

[SCH07] Schmitz, T. L.; Ziegert, J. C.; Canning, J. S.; Zapata, R.; Case study: A comparison of error sources in high-speed milling; Precision Engineering, ELSEVIER, 2007.

[SCH08] Schenck, C.; Einsatz bewegungsredundanter Hybridkinematiken für die Hochgeschwindigkeits- Fräsbearbeitung; Dissertation, Universität Bremen, 2008.

[SHE96] Shen, Y.; Moon, S.; Error Compensation of Coordinate Measurements in Computer-Integrated Manufacturing Using Neural Networks, Journal of Materials Processing Technology 61 (1996) 12-17.

[SHI02] Shih, Yi.-Ti.; Chen, C.-S.; Lee, A. -C.; A novel cross-coupling control design for Bi-axis motion; International Journal of Machine Tools & Manufacture 42 (2002), pp. 1539-1548.

[STE02] Stengele, G.; Cross Hueller Specht Xperimental, a Machining Center with New Hybrid Kinematics. 2nd Chemnitz Parallel Kinematics Seminar. Chemnitz 2002, proceedings pp. 609-627.

[SUH02] Suh, J. D.; Lee, D. G.; Composite Machine Tool Structures for High Speed Milling Machines; Annals of the CIRP, Vol. 51/1 (2002), pp. 285-288.

[SUN04] Sungchul, J.; Koren, Y.; Adaptive fuzzy logic controller for feed drives of a CNC machine tool; Mechatronics, ELSEVIER, 14 (2004), pp. 299-326.

[TAR99] Tarng, Y. S.; Chuang, H. Y.; Hsu, W. T.; Intelligent cross-coupled fuzzy feed rate controller design for CNC machine tools based on genetic algorithms; International Journal of Machine Tools & Manufacture 39 (1999), pp.1673-1692.

[TSA87] Tsao, T. C.; Tomizuka. M.; Adaptive zero phase error tracking algorithm for digital control, Journal of Dynamic Systems, Measurement, and Control 109 (1987) 349-354.

[VAL02] Valasek, M.; Bauma, V.; Silka, Z.; Vampola, T.; Redundantly Actuated Parallel Structures Principle, Exampls, Advantages. 2nd Chemnitz Parallel Kinematics Seminar. Chemnitz 2002, proceedings pp. 993-1010.

[VER06] Verl, A.; Croon, N.; Kramer, C.; Garber, T.; Force Free Add-on Position Measurement Device for the TCP of Parallel Kinematic Manipulators, Annals of CIRP 55 (1) (2006).

[WAN04] Wang, J.; Robust tracking controller design with application to the motion control of an x-y feed table for high-speed; Dissertation, Katholieke Universiteit Leuven, 2004.

[WEC90] Weck, M.; Ye .G.; Sharp corner tracking using the IKF control strategy, Annals of CIRP 39 (1) (1990) 437-441.

[WEC01] Weck, M.; Werkzeugmaschinen Fertigungssysteme 3, Mechatronische Systeme: Vorschubantriebe und Prozessdiagnose; 5., neu bearbeitete, Auflage Springer-Verlag Berlin 2001.

[WEC02] Weck, M.; Staimer, D.; Parallel Kinematic Machine Tools – Current State and Future Potentials; Annals of the CIRP, Keynote Papers, Vol. 51/2 (2002), pp. 671-682.

[WEC03] Weck, M.; Queins, M.; Brecher, C.; Coupled Simulation of Control Loop and Structural Dynamics; Production Engineering Vol. X/2 (2003), pp. 105-110.

[WEC06] Weck, M.; Brecher, C.; Werkzeugmaschinen Fertigungssysteme 5; Messtechnische Untersuchung und Beurteilung, dynamische Stabilität ; 7., neu bearbeitete Auflage Springer-Verlag Berlin 2006.

[WEI04] Weinert, K.; Surmann, T.; Du, S.; Integrated Process and Machine Simulation for the Five-Axis Milling of Sculptured Surfaces on Parallel Kinematic Machines. 4th Chemnitz Parallel Kinematics Seminar, Chemnitz 2004, proceedings pp. 625-639.

[WEN02] Wen-jia, C.; Ming-yang; Z. Ling, Y.; A Six-leg, Four-DOF Parallel Manipulator. 3rd Chemnitz Parallel Kinematics Seminar, Chemnitz 2002, proceedings pp. 227-240.

[XIU98] Xiu, D.; Trajectory Control of a New Class of CNC Machine Tools; Dissertation, Florida Atlantic University, 1998.

[YE92] Ye, G.; Erhöhung der Bahngenauigkeit NC-gesteuerter Vorschubachsen mit Hilfe eines Kompensationsfilters; Dissertation. WZL, Universität Aachen, 1992.

[YEH02] Yeh, S. S.; Hsu, P. L.; Estimation of the Contouring Error Vector for the Cross-Coupled Control Design; ASME Transactions on Mechatronics, VOL. 7, NO. 1, 2002, pp. 44-51.

[YEU06] Yeung, C.; Altintas, Y.; Erkorkmaz, K.; Virtual CNC system. Part I: System architecture; International Journal of Machine Tools & Manufacture 46 (2006), pp. 1107-1123.

[ZAE05] Zaeh, M. F.; Englberger, G.; Robust Speed Control of Feed Drive System with Ball Screw for Machine Tools; Production Engineering Vol. XII/1 (2005), pp. 209-212.

[ZHA04] Zhang, D.; Land, S. Y. T.; An Enhanced 5-Axis PKM System for Light Finishing Operations. 4th Chemnitz Parallel Kinematics Seminar. Chemnitz 2004, proceedings pp. 449-465.

[ZHO02] Zhong, Q.; Shi, Y.; Mo, J.; Huang, S.; A Linear Cross-Coupled Control System for High-Speed; Int J. Adv. Manuf. Technol. 19 (2002) 1 pp. 558-563.